Master Thesis of Science

Pumping Kites Wind Farm

Faggiani Pietro

19-12-2014

TU Delft Delft University of Technology
TU/e Technische Universiteit Eindhoven University of Technology
DUWIND DELFT UNIVERSITY WIND ENERGY RESEARCH INSTITUTE

Pumping Kites Wind Farm

Master of Science Thesis

For obtaining the degree of Master of Science in Sustainable Energy Technology in the 3TU framework at Delft University of Technology Eindhoven University of Technology and University of Twente.

Faggiani Pietro

19-12-2014

SET Master Program
DUWIND - Delft University of Technology
TU/e, - Eindhoven University of Technology

SET Master Program
Of
DUWIND - Delft University of Technology

The undersigned hereby certify that they have read and recommend to the SET Master Program for acceptance a thesis entitled **"Pumping Kites Wind Farm"** by **Faggiani Pietro** in partial fulfillment of the requirements for the degree of **Master of Science**.

Dated: 19-12-2014

Supervisor: _____
Dr.-Ing. Roland Schmehl of TU Delft

Supervisor: _____
Prof. Dr. Gerard van Bussel of TU Delft

Reader: _____
Ing. William Anderson of University TU Delft

Summary

The mainstream of harvesting energy is about to change. Not only has the impact on the environment of human polluting activities been proven by several studies, but the fossil resources that are being exploited to fulfill our energy needs are becoming progressively scarcer and more expensive. Environmental concern is forcing the shift towards renewable sources at remarkably increasing rate.

Among the renewable sources, wind power, with its potential and large availability, is playing an important role. A new and promising way to harvest wind energy with airborne devices tethered to the ground is gaining global attentions. Those concepts are commonly described as airborne wind energy (AWE).
The AWE concept studied at Delft University of Technology consists of an leading edge inflatable (LEI) kite tethered to a ground station. The flight of the kite is controlled by a kite control unit (KCU) which is hanging beneath it. At the ground station the traction that the kite exerts on the tether is converted into electrical power by reeling out the tether winded on a drum. When a predefined altitude is reached, the tether must be reeled back in using a fraction of the energy produced in the previous reeling out phase.

The object of the present work is to calculate the levelized cost of energy (LCOE) of a farm of pumping kite systems. To achieve this objective the unit is designed starting from the choice of the kite area. The most important operational parameters are optimized to obtain the maximum power output at every wind speed and the annual energy production is predicted. For the optimization of the parameters and the prediction of power production of the unit a fast and nevertheless reliable computational algorithm has been used. This algorithm has been developed within the research group at TU Delft and it is based on a quasi-steady model. In this model, the flying states of the kite, considered as a point mass, are approximated in quasi steady equilibrium, taking also into account the effects of the gravitational force on the kite and on the tether. The results obtained have been validated with experimental data and by comparison with another more accurate four-point mass dynamic model, also used for the prediction of power production

of the unit. This latter comparison has led to small improvements in the quasi-steady algorithm. A model for the energy conversion at the ground then computes the efficiency of the conversion process from mechanical power into electricity.

Some effort is put in studying the farm operation and layout, such as spatial distribution of the units, necessary infrastructure to connect them and simultaneous production of several units. Finally, after setting up a cost model, the cost of energy is obtained. At this point the initial design choice of kite size is checked and the sensibility of the cost of energy on this initial parameter is studied.

The reasons of this work is to assess whether a pumping kite system will be capable of economically competing with wind turbines; whether the efforts and resources that many research institutes, companies and universities are justified ,and finally, whether there is any economical and/or physical advantage in connecting several units in clusters.

Acknowledgements

In those last years I received help from many people. I will try not to forget anyone by following a chronological order.
It all begun in Eindhoven, there good friends, who shared my same studies, helped me to understand my interest for the wind energy, which brought me to Delft.
Unluckily, few months after I begun my work, my daily supervisor PhD Rolf Van der Vlugt left the academic environment. Thank to Rolf I was put in the right direction, but the path to the final result was still long. Dr.-Ing. Roland Schmehl guided me from then on, to the best that his busy daily schedule as head of the kite power group allowed him. His wise guidance, the freedom he left me and his care for the details improved significantly the quality of my work. I also received good academic support from Prof. Dr. Gerard van Bussel who followed and approved my work.
A big thank goes to the entire kite power group, in particular to the friends of the study room 6.08. They were not only the first to help me with any kind of thesis related problems, but also good friends outside the university. We shared passions, interests and adventures during my stay in Delft. Thanks to them this period has been cheerful and fun.
Good luck to the KitePower2.0 present and future team members for the development of the project. My interest for this technology makes me admire their effort and I am sure that with their skills they will be able to deploy the first automated commercial units of this kind soon.
During my stay in Delft I was also lucky enough to share my flat with very nice and inspiring people. They also indirectly contributed to this final result.
Finally I wish to thank my family. They supported me under any point of view in all moments of my studies. I hope one day to be able to give to my son the same help and

possibilities I had from them.

Delft, The Netherlands
19-12-2014

Faggiani Pietro

Contents

List of Figures

List of Tables

Nomenclature

Latin Symbols

A	surface kite area	[m^2]
C_d	aerodynamic drag coefficient of the kite	
C_l	aerodynamic lift coefficient of the kite	
D	aerodynamic drag of the kite	[N]
d	tether diameter	[mm]
D_d	drum diameter	[m]
d_u	distance between two units	[m]
E	energy	[MWh]
f	reeling factor	
F_a	aerodynamic force	[N]
F_g	gravitational force	[N]
F_t	tether force	[N]
g	gravitational constant	[m/s^2]
h	height	[m]
ir	interest rate	
k	kinematic ratio	
L	aerodynamic lift of the kite	[N]
M	mass	[kg]
n	number of kites	
P	power	[kW]
P_{avg}	average cycle power	[kW]
$p(v)$	probability density function	
r_{max}	maximum tether length	[m]
r_{min}	minimum tether length	[m]
S	projected kite area	[m^2]
t	year	[y]

t_{out}	traction phase duration	[s]
t_{in}	retraction phase duration	[s]
t_{tra}	transition phase duration	[s]
$t*$	characteristic system time	[s]
v_a	apparent wind velocity	[m/s]
v_k	kite velocity	[m/s]
v_{rat}	rated wind speed	[m/s]
v_t	tether reeling velocity	[m/s]
v_w	wind speed	[m/s]

Greek Symbols

β	elevation angle	[rad]
ζ	power harvesting factor	
η	efficiency	[%]
θ	polar angle	[rad]
λ	tangential velocity factor	
ν	height angle	[rad]
ρ	density	[kg/m^3]
σ	stress	[MPa]
τ	torque	[Nm]
ϕ	azimuth angle	[rad]
χ	course angle	[rad]
ω	rotational speed	[rad/s]
Ω	elevation minus height angle	[rad]

Abbreviations

AEP	annual energy production
AWE	airborne wind energy
CF	capacity factor
HAWT	horizontal axis wind turbine
KCU	kite control unit
KPS	kite power system
LCOE	levelized cost of energy
LEI	leading edge inflatable
OECD	organization for economic co-operation and development
O&M	operation and maintenance
PV	photo-voltaic
RF	ratio phases

Chapter 1

Introduction

At Stockholm conference in 1987 the Bruntland commission (Brundtland [7]) defined sustainable development as
"*[...]when a society meets the needs of the present without compromising the ability of future generations to meet their own needs*".
The current way in which we meet our needs cannot be considered sustainable. The increased concern about sustainability issues has triggered important mobilizations of human and financial resources in R&D departments and private companies to achieve a more sustainable society.
Electricity consumption is expected to increase and the share in the production from renewable sources is expected to grow. Summarizing the outcome of the World Energy Outlook [23], it appears that despite the improvements in efficiency both on the production and consumption sides of the electrical energy chain the primary energy consumption will keep on increasing. This is mainly due to the increase of electricity demands from developing countries.
By looking at the image of the earth at night (Fig. 1.1) and by thinking how the global population is spread around the globe it is clear how uneven the use of electricity is. The brightest spots do not necessarily correspond to the most densely populated ones. According to the BP report [5], this situation will change and developing counties will soon increase their energy consumption approaching the same level of pro-capita consumption of the industrialized countries. Furthermore energy consumption will increase by 41% by 2035, mainly because non OECD countries like China and India will drastically increase their energy consumption reaching an energy consumption per person similar to the western countries.
BP [5] shows also that fossil fuels together accounts for 86% of the global energy production. Electricity generation is expected to rise by 2.2%. Environmental concern along with the worries about security of energy supply in many OECD countries are forcing a shift in the way we fulfill our energy needs.

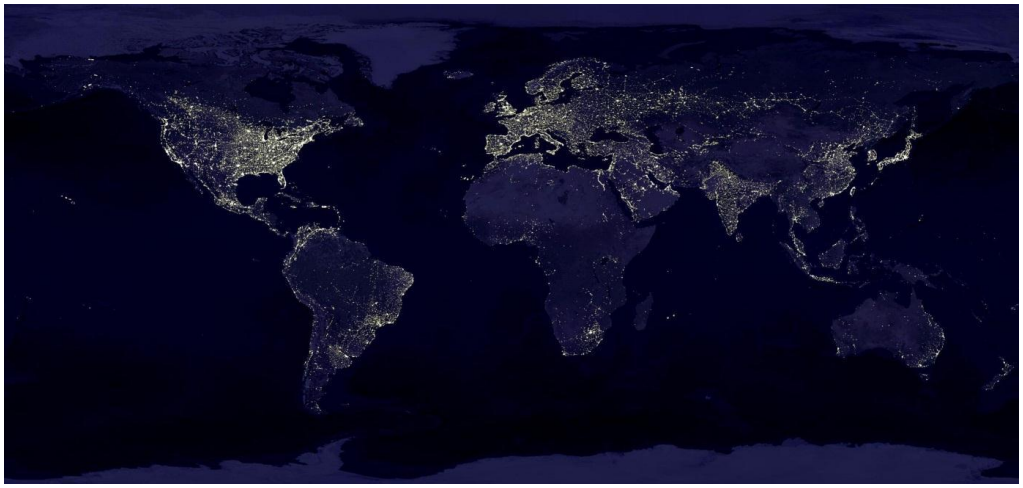

Figure 1.1: Earth at night [29]

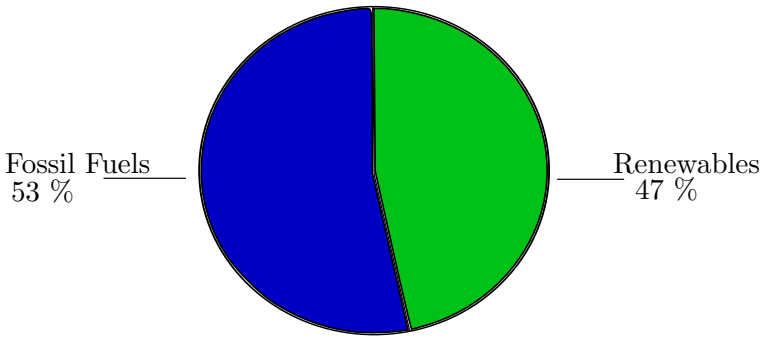

Figure 1.2: New power capacity installed worldwide 2008-2009 [10]

Looking at the new power capacity added worldwide from 2008 to 2009 shows that almost half is renewable (Fig. 1.2). Projections of major energy agencies [5], [43] foresee an increase in the use of renewables in the electricity production from the 18% of today to 23% by 2040 in the conservative side (Fig. 1.3).
Among renewable sources, wind energy seems to be a promising one. For its safety, cleanliness, accessibility and recent technological developments, wind energy is envisioned to contribute to the global energy scenario(Fig. 1.4) . The interest in this technology has seen the size of the turbines increase tremendously over the past few years. However this approach is facing a bottleneck mainly because the mass of the turbine increases faster than the rated power. In fact the power that the turbine can process is proportional to the square of the rotor radius (R), while the total mass of the turbine according to Manwell et al. [28] is proportional to R^3. It follows that going to larger and larger wind turbines does not result in a steady decrease of the cost of the energy produced. Over a certain size the economy of scale is simply counterbalanced by the increase of the cost due to increase of the mass. Additionally there are all kinds of logistical problems of deploying and assembling such huge machines.

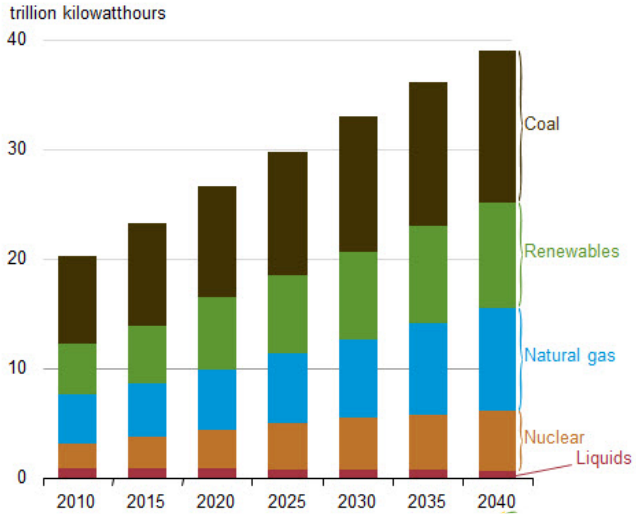

Figure 1.3: Forecast worldwide electricity production by fuel [43]

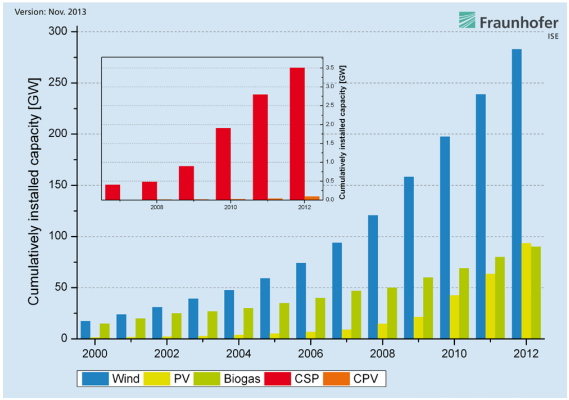

Figure 1.4: World cumulative installed capacity per source [24]

Lately many research institutes, universities and private companies have focused their attention on airborne wind energy (AWE). The world map of those researchers is shown in Fig. 1.5

An AWE system involves the use of an airborne device, tethered to the ground, able to harvest wind power at variable altitudes. The device is kept airborne either by the wind itself or by buoyancy effects, being filled with a lighter-than-air gas. This technology with its low mass per kW installed and the higher operating altitudes compared to conventional wind turbines promises low cost of energy and great possibilities of being scaled up.
The Kite Power Group at the Delft University of Technology is focusing in particular on kite power systems (KPS). The concept foresees a leading edge inflatable tube kite tethered to the ground. The kite is steered in figures of eight manoeuvres to maximize its traction on the tether. The tether in turn drives a generator on the ground being rolled out from a drum under the traction of the kite. When a predefined altitude is reached, the kite is de-powered and the tether rolled back on the drum using only a fraction of the energy produced in the previous phase. When the tether length goes back to the one of

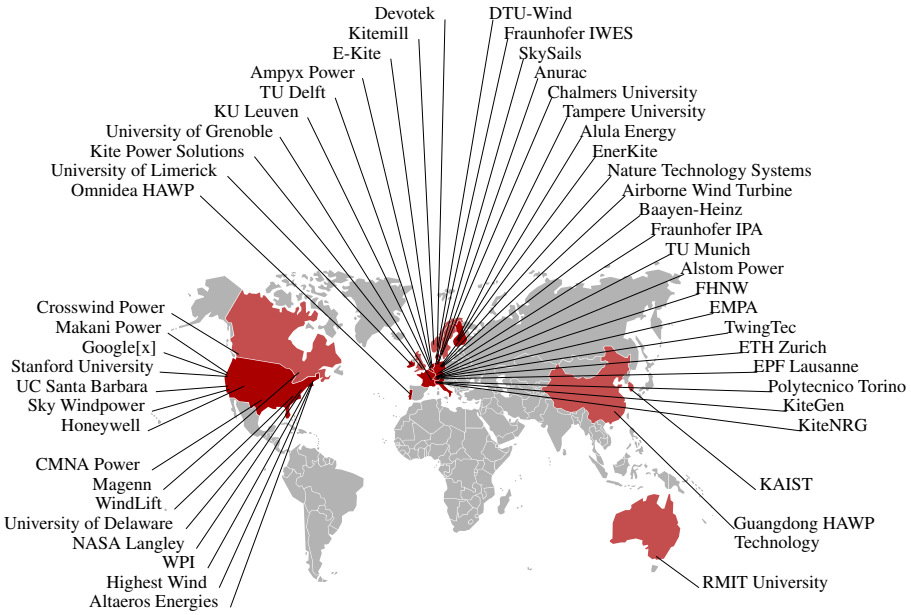

Figure 1.5: Companies and research institutes currently active in AWE [1]

the beginning a new phase of power production can begin. Energy is thus produced in pumping cycles.

This system is the object of study of the present work. With the idea of finding the real financial and physical potential of the pumping kite technology and keeping in mind the idea of deploying this technology in farms, like traditional wind energy , the work is begun. First the relevant previous works are analyzed in the literature study. Those works are the state of the art in the field of AWE and are the starting point to derive an appropriate and useful research question. At the end of the literature study, this research question is presented together with the chosen research methodology.

The aim is to make the best use of the knowledge already gained on this topic by previous works and answer questions that are still unsolved.

After the literature study the work is performed starting from the validation of the model used, followed by the complete design and optimization and study of the wind farm. Finally a sensitivity analysis of the farm on the initial design choices is carried out. Relevant performance and economic indicators are compared with other existing energy technologies to have a clearer idea of the potential of the pumping kite system and its main advantages.

Chapter 2

Literature Study

In this chapter the relevant background information for the development of the work is presented. In the first section an overview of the different AWE concept is given along with the reasons that push the research in this field and the major challenges that it has to face. Then the relevant previous works on TU Delft kite power system which is taken in consideration in the rest of the work are evaluated and briefly presented. The system components and operation are explained. In this section also the mathematical models to predict its power output are presented. The model chosen for the design optimization is presented more in detail in the following chapter. The optimization routine adopted for the operational parameters is explained. Finally the reference works concerning wind farms, their costs, spacing and layout are presented.
Those works are supposed to be the starting point for the design of the single unit, first step to get the cost of energy of the farm. In the conclusions of the chapter is explained the added value of the present work, the way the knowledge on the state of the art is put in a research methodology to obtained the final result of the thesis and why this result is scientifically relevant.

2.1 Airborne Wind Energy Concepts

Airborne Wind Energy (AWE) is mainly driven by the desire to harvest in a cheaper way the wind power where it is stronger and more steady. It has been extensively proven that at higher altitudes the wind is stronger due to a lower effect of the shear stress for the presence of the terrain [18].

It can be deducted from Fig 2.1 that the higher the altitude where the wind power is har-

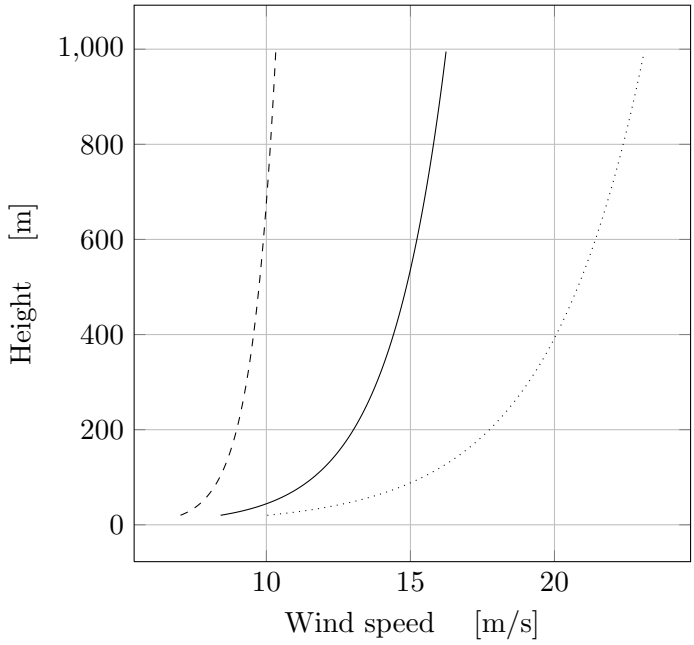

Figure 2.1: Logarithmic profile of the wind speed for a reference wind speed of 6 m/s for different terrains: Sea (dashed), Grass (solid), Suburban environment (dotted)

vested the higher the energy available due to stronger winds. The picture also shows that the type of terrain heavily affects the profile of the wind. The height that the turbine can reach is limited. Building turbine towers to reach high altitudes is not only economically detrimental, but also physically impossible. Airborne devices tethered to the ground can be used instead.

Various AWE concepts can be distinguished (Ahrens et al. [1]) according to their characteristics. In principle those devices can be classified distinguishing:

- Dynamic winch vs. static winch
- Flexible vs. rigid wing
- Control actuators on the ground vs. airborne
- Lift driven vs. drag driven

As explained in the introduction, there are many companies currently involved in developing own AWE concepts. The German company Skysails [39] has developed an automatic system for ship traction with a RAM kite (Fig. 2.2(a)) which is currenlty on the market. For electricity production different companies are investigating the rigid wing option. AMPIX [3] (Fig. 2.2(b)) and Makani [27] (2.2(d)) concepts both foresee a kite plane which is controlled, in its cross wind flight, by rudder and elevator. The difference is in the way to generate electricity. The Makani concept mounts small and fast wind turbines

(a) Skysails concept [39]

(b) Ampix concept [3]

(c) Twing Tec concept [42]

(d) Makani concept [27]

(e) Magenn air rotor concept [38]

Figure 2.2: Different AWE concepts [35]

Figure 2.3: take off of the LEI kite V3 of the prototype developed at TU Delft [46]

on board so to obtain a continuous production at fixed altitude. The AMPIX concept on the other hand keeps the generator on the ground, increasing the aerodynamic performance of the airborne component, bringing the necessity to unwind the tether from a drum on the ground to create the motion necessary to generate electricity. In this concept the electricity is produced in pumping cycles.
Also the Swiss company Twing is developing a concept with a rigid wing (Fig. 2.2(c)) but the flight is guided also with the aid of two tether to control the roll of the kite plane. Also in this case the electricity production happens on the ground.
A completely different approach to produce electricity is taken with the Magenn [38] air rotor (2.2(e)) . A big light weight cylinder is filled with helium which keeps it airborne with the axis perpendicular to the wind. The aluminium tubes mounted around the cylinder restrict the airflow creating the necessary moment to set the entire airborne device in motion. Rotating about its axis, it generates electricity with two airborne generators mounted at both ends of the cylinder.
Many other concept are being developed around the world, but for the sake of compactness are not presented here.

2.2 Pumping Kite Power

The concept taken in consideration this work is the pumping kite power. This concept is being studied and Developed at TU Delft [46]. It is based based on a leading edge inflatable(LEI) kite steered by kite control unit (KCU) suspended beneath it (Fig. 2.3). The generator on the ground spins for the traction force of the kite, transferred by the tether. The main system components are sketched in Fig. 2.4.

Energy is produced in pumping cycles. Each cycle consist of three phases : **traction phase**, **retraction phase** and **transition phase** (Fig: 2.5). Energy is produced in the

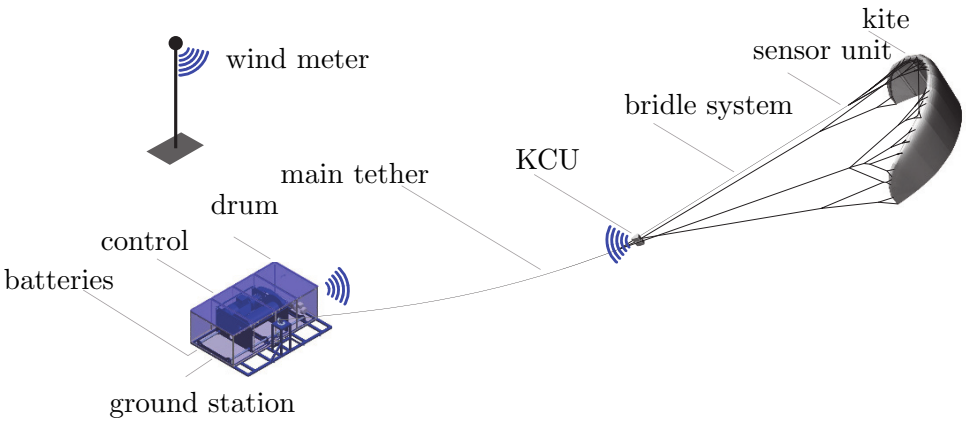

Figure 2.4: system components of the concept developed at TU Delft [46]

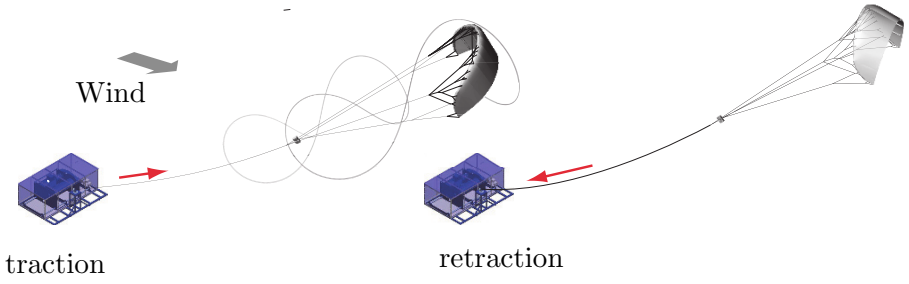

Figure 2.5: Schematic view of the phases of the pumping cycle [46]

traction phase where the kite flies figures of eight maneuver and the traction on the tether is maximized while it is reeled out. Some energy is required in the retraction phase to bring back the kite at its initial position and start. In this phase the traction of the kite is minimized. Thanks to the difference in energy production of the traction phase and the energy required in the retraction phase, net energy is produced and fed to the grid. [46].
The detail of the phases and the control strategy is explained in the following chapter.

2.3 Computational Prediction of Energy Output

Miles Loyd is considered a pioneer in kite research [25]. He was the first to quantitatively analyse the power generation potential of a tether wing with a ground based generation of energy. He distinguished two fundamental flight modes: non-manoeuvring flight, where the kite flies as high as possible with no steering inputs, and perfect cross wind flight, where the the tether is parallel to the wind direction. Real flight occurs in between those two extremes. Loyd derived the aerodynamic forces acting on a kite, assuming a massless kite and a straight tether.
From this first mathematical approach many models have been developed either increas-

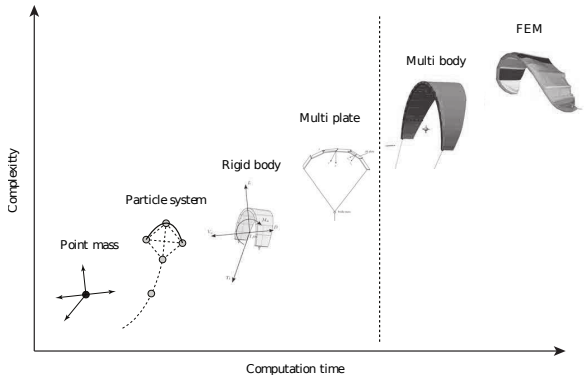

Figure 2.6: Schematic representation of different degrees of accuracy as function of computational time [45]

ing level of complexity and accuracy or focusing more on the assumptions that can be made to keep the computational model computationally fast. Whenever a physical phenomenon has to be modelled, depending on the degree of accuracy that one wants to obtain, different approaches can be taken. It happens that the more detailed the model is the more accurate the results, but the longer the computational time.
This holds also for the case of the pumping kite system the system (Fig 2.6).
Focusing on the models for the pumping kites system Argatov et al. [4] refined crosswind motion law, derived in the case of equilibrium motion of the kite. The paper also presents the theory of a gently sloping tether. A simple approximate formula for the mean mechanical power generated by the deploying kite is obtained.
Erhard and Strauch [13] present a simple model for the dynamics and aerodynamics of a tethered kite systems and validate it by experimental flight data. After introduction of system setup and model assumptions, they derive and discuss the equations of motion for the kinematics. Then the turn rate law for the kite in response to a steering deflection is also introduced. This is particularly important for the understanding of the maneuverability of the kite which is useful to understand at the end the spacing between the units in the wind farm.

Another interesting approach in following the flight path of the kite and a multi-body modeling is taken in the work of Gros and Diehl [20]. Using natural coordinates and algebraic constraints as a representation of the system evolution the author show how to build such models for AWE systems in the Lagrangian framework and how to efficiently incorporate a non-singular representation of the pose of the wing. However the model that is used for the optimization of the operational parameters and the prediction of the annual energy production in this work, is based on the work of van der Vlugt et al. [48]. The trajectory of the kite is followed in a spherical coordinate system, with a ground fixed reference frame. It is assumed that at every flight state there is a force equilibrium. Therefore it is called a Quasi-Steady Model. The kite is treated as a point mass and the tether is assumed to be straight all the time. Effects of inertia are neglected.
It is a simplified model, its simplicity makes it computationally fast, once implemented in an appropriate programming language. This characteristic of the model makes it partic-

ularly suitable for a preliminary design purpose. The main operational parameters have to be optimized (the optimization routine is explained in sec. 2.5), therefore many different system configurations have to be compared to obtain the optimal operation and the highest power output from a given system. The computational speed is a crucial factor to make the optimization feasible.
The exemplification of the computational approach might lead to inaccuracies. Validations trough comparison with experimental data have already led to interesting results [48] [19]. However the real wind that the kite feels is not known exactly and this might lead to inaccuracies.
A Dynamic model, also developed at TU Delft [17], can be chosen for validation. The Dynamic model of Fechner et al. [17] aims to simulate in real time the flight of the kite, having the aerodynamic parameters of the kite and characteristic of the tether set, obtaining a the end a prediction of the power production at the ground station. For the approach of the method, the results are expected to be more accurate than the one obtained with the quasi-steady model. Therefore this model is used as reference for the validation of the quasi-steady solution.
The Dynamic model computes, during the figures of eight maneuvers of the traction phase and during the straight trajectory of the retraction phase, the forces based on the aerodynamic characteristics of the kite and the tether. A four mass points kite is used to obtain an estimation of the side forces and inertia of the system. The tether is segmented to avoid the assumption of the straight tether. A detailed description of the model along with the equations used are in the paper of Fechner et al. [17].
The detail of the Quasi-Steady model, the python implementation and the validation done are presented in chap. 3

2.4 Ground Station Layout

The rotational motion of the drum, induced by the traction of the tether, has to be converted at the ground station into electricity. The choice of the components of the ground-station is not trivial. The optimal retraction and traction phase have very different requirements of force and speed. The retraction phase should be done with high velocity and low traction force, while it is the opposite for the traction phase. Additionally those optimized operating conditions change with the wind speed and within the same cycle depending on where the kite is flying.
It appears that the choice of the conversion system can make a big difference in the efficiency of the conversion process, in the annual energy production (AEP) and by consequence on LCOE.
Already the work of Fechner and Schmehl [16] has shown how the combined efficiency of all the different components of the system are related and which are their impact on the final total efficiency of the energy harvesting process.
In the work of Pijl et al. [32] five different solutions of drive trains for wind turbines are compared. The best solution from the point of view of the cost over energy yield is a geared doubly fed generator. However in the conclusions of the paper it is stated that this ranking is only possible because of the high costs of the power electronics and the

permanent magnets, which are both expected to decrease, and because the reliability of the system has not been taken into account to chose the best solution. Probably with those considerations included the best solution would be a direct drive permanent magnet synchronous machine.
The main advantages of such solution are :

- low iron losses due to low active material
- high energy yield
- high reliability for the absence of the gearbox
- low maintenance cost

In the work of Schölkopf [37] many different configurations for the drive train of a pumping kite power unit are analyzed qualitatively trough a multicriteria analysis. Going from the simple single electrical machine, directly driven, connected to a battery pack (also presented in [47]) to a more complex configuration with freewheels clutches, gearboxes, synchronous generator for the traction phase and a motor for the retraction phase. A set of relevant decision criteria is chosen. Every solution gets a qualitative score on the different criteria and by applying a weight to the criteria is possible to decide which solution is the best. The criteria taken into account are

- Efficiency
- Cost
- Volume and Weight
- Reliability

Unfortunately in the report of Schölkopf [37] the authors do not achieve a singular solution, but the whole analysis leads to the conclusion that the best solution can be either an appropriate synchronous machine directly driven or two different machines with clutches and gearbox. The high score of the first solution is due to the simplicity, which leads to high reliability low volume and weight and low cost. The second solution ensures higher efficiency. However a clear answer is not given, and in the conclusions it is clear the need of a modelling tool for the electrical machines to quantitatively estimate the pros and cons of the two solutions.

2.5 Optimization of the Operational Parameters

Already from the first kite theory presented by Loyd [25], it follows that the tether of a massless kite which flies perfectly crosswind, neglecting the tether mass and drag, should

operational parameters
traction tether force
retraction tether force
minimum tether length
maximum tether length
elevation angle

Table 2.1: Operational parameters that have to be optimized

be reeled out at $\frac{1}{3}$ of the wind speed to obtain the maximum power production.
For a more complex mathematical model (as the one which will be used in this work and which will be explained in the following chapter) the optimum for the reel out factor and other important operational parameters is less easy to find.
From this simple consideration it can be understood that the energy output is really sensitive to the setting of the operational parameters. Moreover it reveals that the optimal setting of those parameters is a function of the wind speed.
Many works ([19], [21], [36]) have already highlighted the importance of the operational parameters in the power production of the single unit.
The work of Grete [19] is used as reference to chose which are the most important operational parameters which need to be optimized.

The parameters that the routine optimizes in the pumping cycle are listed in Tab. 2.1.

It is in total a set of 5 parameters that affect each other and has to be optimized for every wind speed of the operating range of the system.
The choice of the tether force determines the reeling speed. The influence of those parameters on the power production is the highest, and the systems resulted very sensitive to any change from the optimal value.
The optimization of the minimum and maximum tether length comes mainly from the fact that the wind speed is assumed to increase with altitude. This positive effect of higher wind speeds is counterbalanced by the necessity of having a longer tether in the air, which implies high drag force and weight of the airborne components.For this reason an optimal value of the operating altitude where the power production over the cycle is the highest is investigated.
The last operational parameter that is optimized in the model is the elevation angle. The sensitivity of the system to this parameter seems to be rather low. In a range of $\pm$ 5° the power production does not change appreciably. However when the value is far away from the optimum, the power decreases rapidly.

As optimization routine a **genetic algorithm** is used. It belongs to the so called Monte Carlo approaches. Those are algorithms that rely on repeated random sampling to obtain numerical results. In this case the variables, which are chosen randomly in a given range, are the operational parameters which are meant to be optimized.

It begins by choosing randomly a some sets (or families) of operational parameters (the

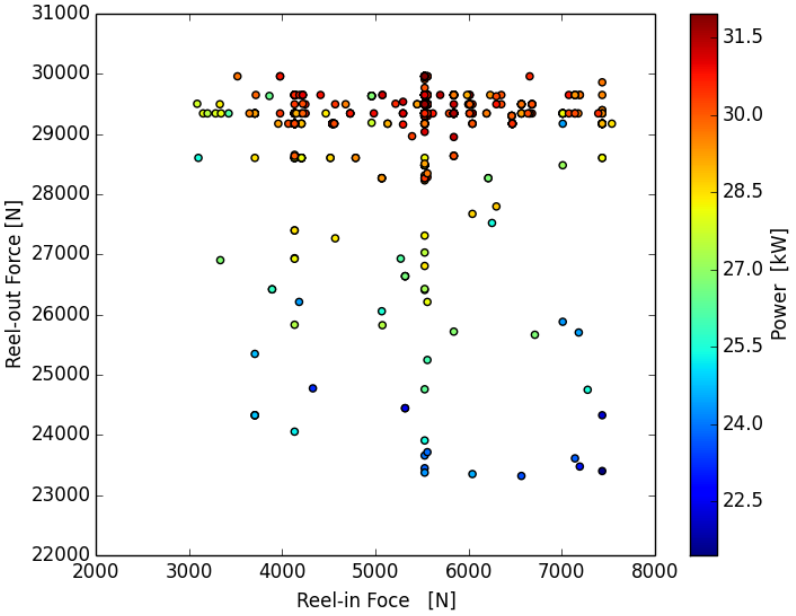

Figure 2.7: Scatter of the search made for the optimum of the tether force during reel-in and reel-out phases for the 150 m^2 kite at 7 m/s of wind speed

population). Among those, only the families of parameters that perform best (which lead to high power production) are kept to proceed with the next generation of the population. The next generations of parameters consider (or inherit) the values of the previous generation which were performing the best. From its similarity with the Darwinian natural optimization of a specie comes the name of the algorithm.
Either when the pre-defined time for the optimization is over or all the next possible generations of parameters are performing worse than the previous or a specified target is reached the simulation is stopped and the best set of parameters is reported. The maximum simulation time is tuned in such way so that the optimum, when it is possible, is found before.
This routine is run for all the wind speeds at which we want to operate the system. The values of the parameters are chosen randomly in a range that is predefined by the user. An effort is made to chose the appropriate ranges where the operational parameters are chosen. The larger the range in fact and the higher is the computational time necessary to find the optimum. The ranges are chosen based on the optimized result obtained for the previous wind speed. For the first wind speed an educated guess of the appropriate range is made.
An off the shelf function of the package openopt has been used. [11].
As example In Fig 2.7 the combination of reel-in and reel-out tether force tried for the optimization of a 150 m^2 at 7m/s. It is clear how the research is refined in the region corresponding to the highest value.

2.6 Pumping Kites Wind Farms

The last important topic that is investigated in the thesis is the study of a wind farm of pumping kite systems. Being a rather new field of development there is no specific literature explicitly referring to it.
For this section the literature on wind turbines farms is used as starting point. The works of Zaaijer [50] and Lundberg [26] is used as reference to identify the most relevant cost items and their functions. Additional evaluations are made when considering the kites farm cost functions, to take into account the system characteristics (e.g. the cost of transport and installation should be considerably lower than the one of the turbines). For the design of the electrical in field connection between the units, the work of Pierik et al. [31] is analysed. In this paper all the different possibilities of connections between wind turbines in a farm are presented. The layouts presented differ in complexity, reliability and cost, and depend on the type of turbines that are installed in the farm. Considering the characteristic of the pumping kite system, the best electrical connection layout is chosen and presented.
Finally concerning the spacing between the units, the approach found in the work of Heilmann [21] is taken in consideration. Coupling it with the considerations on the kite manoeuvrability from Fagiano et al. [14] and Schmehl et al. [36] and the outcome of the optimization routine, the volume that each unit needs for its correct operation is found. From it the minimum distance between adjacent units is derived.

2.7 Conclusions, Research Question and Methodology

The state of the art on AWE has been presented.This, together with the relevant knowledge on optimization routine and computational model to predict the power output of a pumping kite system is the starting point bring the knowledge one step further.
During the literature study it has been found that anyone has assessed the economic potential of a pumping kite wind farm. The objective of the present work is then chosen as to **obtain the levelized cost of energy (LCOE) of a pumping kites wind farm** based on the concept developed at TU Delft, to judge the physical and financial potential of the technology and allow comparisons with other renewable energy technologies.
According to the latest OECD report the LCOE index is
"*the equivalence of the present value of the sum of discounted revenues and the present value of the sum of discounted costs. The LCOE is, in fact, equal to the present value of the sum of discounted costs divided by total production adjusted for its economic time value* "(IEA [22]).Putting these words into a mathematical formula for computing the LCOE yields the following expression

$$LCOE = \frac{\sum_t (Inv_t + O\&M_t + Fuel_t + Carbon_t + Decom_t)(1+ir)^{-t})}{\sum_t (AEP_t (1+ir)^{-t}} \ . \tag{2.1}$$

Two main assumptions are made for the computation of the LCOE:

- The interest rate (ir) used to discount both the costs and the electricity produced does not change during the life time of the system. It is assumed to be 5 %
- The production of electricity remains the same during the life time of the project. No aging factors are included

The assumptions are the same taken by the international energy agency in the report of the projected costs of generating electricity [22].
By looking at the equation 2.1 that has to be solved, two main sub-questions need to be answered.

- How much electrical energy can actually be produced with a unit?
- What are the characteristics of the power produced by a farm composed of several units?
- What is the layout of the farm ?
- What are the costs of the components and services that should be taken into account during the lifetime of the farm ?

The first step to answer those questions is the design of the single unit.
An first estimate is done for the first choice of size of the kite. This is the beginning of the design procedure. From the kite size, knowing its wing loading, the maximum allowable tether force is obtained. From it the tether and the drum can already be designed.
A preliminary optimization of the operational parameters with no constraints of maximum power and speed is done. The computation is based on the quasi steady model [48] briefly presented in Sect. 2.3, after the validation with the dynamic model [17] also mentioned in the same section. The choice of electrical machines along with the best ground station layout is done considering the results of this first preliminary optimization.
Then the operation of the system is optimized again, considering now all the physical constraints of the machines chosen to achieve the maximum energy production. At this point the first block of the work is completed and the farm configuration can be studied (Fig. 2.8). The spacing between the units, the different control strategy depending on the wind direction, the optimal phase shift and other aspects of having multiple units working simultaneously are investigated to get to the cost cost of energy. Finally, after setting up a cost model with the most relevant cost items of the farm, the LCOE is obtained. The result obtained is however dependent on the initial estimate. The initial assumptions made for the unit design is checked trough a sensitivity analysis to understand whether the cost of energy can be decreased even further.

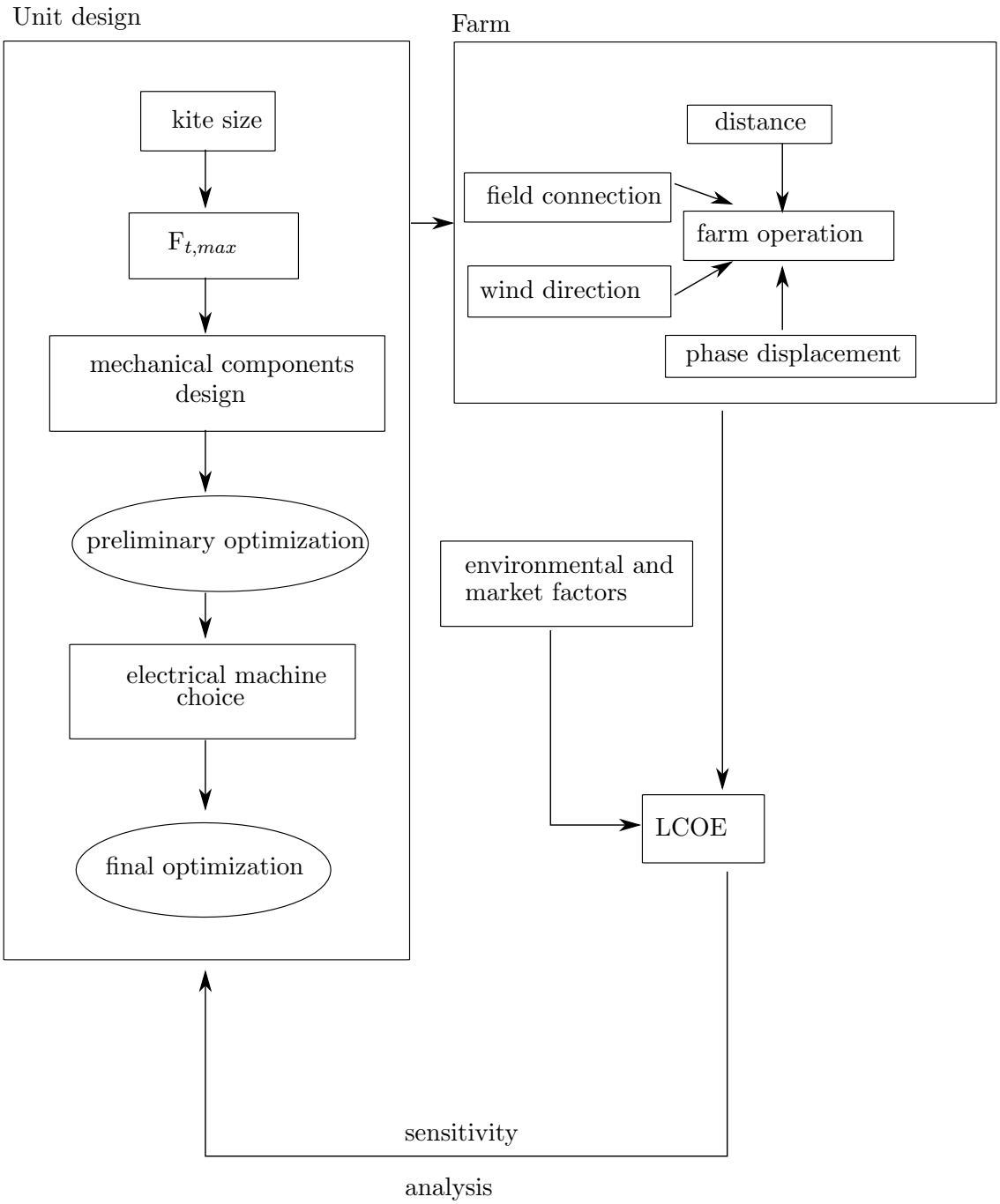

Figure 2.8: Outline of the work

Chapter 3

Operation, Flight Theory and Modeling

First the operation and the control strategy of a pumping kite system are presented in this chapter. Then a more detailed description of the equation used to model it and the algorithm implementation are described. Since the model that is used for this thesis has to be used to run an optimization routine of the operating parameters, it has to be computationally light and fast. In fact many different system settings have to be tested for every operating wind speed. The use of a real-time model would increase tremendously the computational time making the whole optimization routine unfeasible. On the other hand the model has to be realistic and reliable to obtain eventually a plausible values of the LCOE
For this reason the quasi-steady model has been used to obtain a fast and reasonably accurate simulation tool. The model and its implementation in a suitable programming language are presented. The results are verified with the use of another computational tool, based on a dynamic model. The verification led to a small modification of the model to avoid unrealistic behavior when the maximum set tether force is reached. This is explained in the final section of the chapter.

3.1 Operation and Control Strategy of the Pumping Kite System

Every phase of the cycle (Fig. 3.1) has its own control strategy for the KCU and for the ground-station operations, to achieve the maximum power production, minimize the

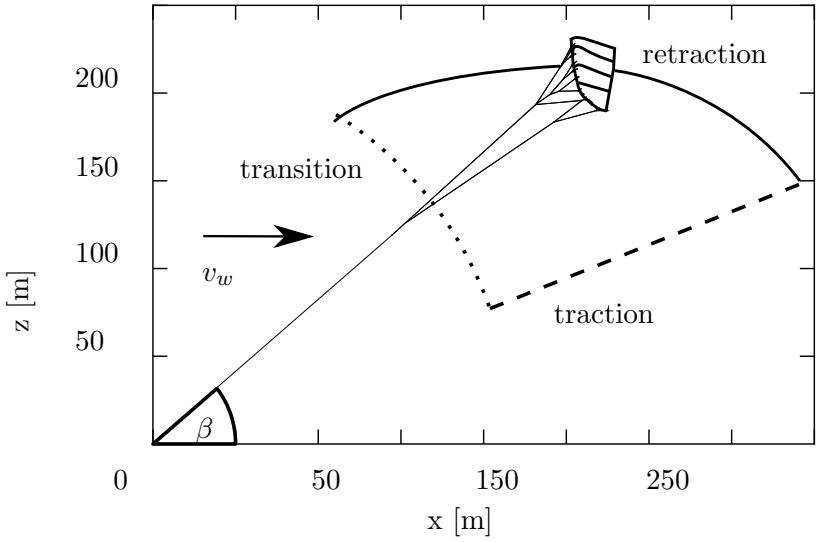

Figure 3.1: Schematic view of the phases of the pumping cycle [19]

power consumption and take into account the system constraints. In the following sections each phase is analysed and the control strategy explained.

3.1.1 Traction Phase

During this phase the kite flies crosswind following a figure of eight trajectory. It is fully powered to maximize the traction on the tether at an optimized elevation angle. Thanks to the aerodynamic properties of the kite, it flies faster than the wind, obtaining a remarkably high aerodynamic force. During this phase the tether, under the traction of the kite is reeled-out from a drum at the ground station. The rotation of the drum is then converted into electricity with a generator. When the tether reaches a predefined maximum length, the retraction phase begins.
The control strategy at the ground station during this phase is based on the force on the tether. The tension on the tether is kept as close as possible to the optimal value by regulating the reeling velocity of the drum. The value of the optimized tether force is found with an optimization routine which will be explained later.

The optimal tether force however increases with increasing wind speed. The maximum wing loading and the design of the tether define the maximum upper limit of the force that the system can withstand.
When that force is reached the power is increased further by increasing the reeling velocity. The final constraint is the generator nominal capacity. When this value is reached the power should not be increased any further. Above this wind load the kite should be depowered or flown in non-optimal regions of the wind window if we still want to operate the system.
The traction phase is complete where the tether reaches the maximum length.

3.1.2 Retraction Phase

During this phase the kite is fully de-powered by the KCU by regulating the angle of attack. It flies straight towards the zenith of the ground station. In the meanwhile the tether is reeled-in to reach the minimum predefined length. Electrical energy is used by an electric motor to complete this phase. Since the kite is fully de-powered and flies this specific trajectory, the amount of energy necessary to complete the retraction is only a fraction of the energy produced in the traction phase.
Similar to the previous phase, the control strategy revolves around controlling the tether force. Also in this phase the system constraint is the maximum power of the electrical machine. Finally also in this phase the optimized retraction force and retraction power increases with the wind speed when we want to maximize the net energy over the cycle. When the maximum power of the electrical machine is reached the retraction velocity cannot be increase any further and the retraction will happen at a lower speed than the optimal one.
The retraction phase is complete when the tether length is at the minimum value.

3.1.3 Transition Phase

At the end of the retraction phase the kite is above the ground station. During transition phase the kite flies a trajectory to reach the right elevation angle for the traction phase. Almost no energy is produced in this phase.
Once completed the transition phase, the kite is at the initial position of a new traction phase and the cycle starts over.
During the transition phase the tether should be neither reeled in or out. However to keep the force within the physical limits for which the ground station is designed, the tether is reeled in or out depending on the force that the kite exerts on it.
The KCU steers the kite downwards until the elevation angle is the one set for the traction phase. Due to the effect of not reeling out and the combined effect of the aerodynamic force and the gravitational force, the kite experiences a strong acceleration which increases the tether force. The duration of this phase is only a fraction of the entire cycle and its contribution to the average power over the cycle is most of the time negligible.

3.1.4 Resultant Power Curve

Thanks to the difference in energy production of the traction phase and the energy required in the retraction phase, net energy is produced and fed to the grid. [46].
The average power over the cycle can be computed as the average of the powers of each phase weighed with the duration of each phase:

$$P_{avg} = \frac{P_{tr}t_{tr} + P_{ret}t_{ret} + P_{trans}t_{trans}}{t_{tr} + t_{ret} + t_{trans}} \tag{3.1}$$

The convention used is that generated power has a positive sign. The transition term has low influence in the computation for its short duration. The traction power increases with the wind speed, but at the same time also does the retraction power (which has a negative sign because it is consumed). The average power increases as long as the traction power increases. When the limit of the generator is reached and it cannot be increased any further, the increase in the retraction power (or retraction time if the maximum retraction power is reached as well) makes the average power decrease.
The resultant power curve peaks and then it decreases differently to the power curve of a turbine.

Knowing the average power the power harvesting factor ζ is defined as

$$\zeta = \frac{P_{avg}}{\frac{1}{2}\rho v_{w,avg}^2 S} \tag{3.2}$$

where the wind speed that is used, to take into account the change over the altitude is

$$v_{w,avg} = \frac{1}{2} r_{max} \cos\beta, \tag{3.3}$$

with r_{max} the maximum tether length in the cycle and β the elevation angle (90° - θ referring to Fig. 3.2).
ζ is not an efficiency. It can assume values larger than 1 for the way it is computed. Every phase of the cycle has its own control strategy to optimize the power production, minimize the power consumption and take into account the system constraints.

3.2 Mathematical Model

The trajectory of the kite is followed in a spherical coordinate system (Fig.3.2) and is assumed that at every state there is a force equilibrium. Therefore it is called Quasi-Steady Model (van der Vlugt et al. [48]).
The kite is treated as a point mass and the tether is assumed to be straight all the time.

To begin with, the apparent wind speed which the kite feels is decomposed in the different contributions of wind velocity (v_w), tangential kite velocity ($v_{k,\tau}$) and radial kite velocity ($v_{k,r}$) with the notation in Fig. 3.2

$$\mathbf{v}_a = \mathbf{v}_w - \mathbf{v}_k = \begin{bmatrix} \sin\theta\cos\phi \\ \cos\theta\cos\phi \\ -\sin\phi \end{bmatrix} v_w - \begin{bmatrix} 1 \\ 0 \\ 0 \end{bmatrix} v_{k,r} - \begin{bmatrix} 0 \\ \cos\chi \\ \sin\chi \end{bmatrix} v_{k,\tau} \ . \tag{3.4}$$

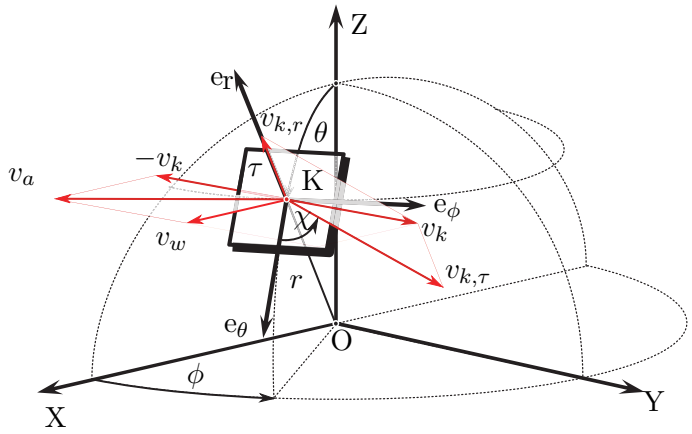

Figure 3.2: Decomposition of the kite velocities [36]

By introducing the reel-out factor

$$f = \frac{v_{k,r}}{v_w} \tag{3.5}$$

and the tangential velocity factor

$$\lambda = \frac{v_{k,\tau}}{v_w} \ , \tag{3.6}$$

the vector of apparent wind velocity can be written as function of the wind velocity in the form

$$\mathbf{v}_a = \begin{bmatrix} \sin\theta\cos\phi - f \\ \cos\theta\cos\phi - \lambda\cos\chi \\ -\sin\phi - \lambda\sin\chi \end{bmatrix} v_w \ . \tag{3.7}$$

The magnitude of the apparent wind velocity can also be written as the quadratic sum of the tangential and radial components:

$$v_a = \sqrt{v_{a,r}^2 + v_{a,\tau}^2} \tag{3.8}$$

From these compositions the expression for the non dimensional magnitude of the apparent wind velocity is found using the same notation of Fig: 3.2

$$\frac{v_a}{v_w} = (\sin\theta\cos\phi - f)\sqrt{1+k^2} \ . \tag{3.9}$$

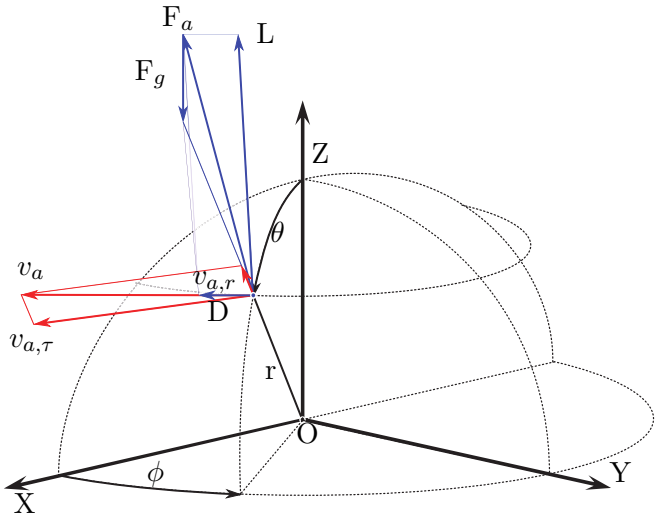

Figure 3.3: Decomposition of the forces and velocities acting on the kite including the effect of gravity [36]

where k, the kinematic ratio is defined as

$$k = \frac{v_{a,\tau}}{v_{a,r}} \tag{3.10}$$

On the other hand, by substituting the radial and tangential components of Eq.3.7 in 3.10 and solving for the factor λ is obtained

$$\lambda = a + \sqrt{a^2 + b^2 - 1 + k^2(b - f)^2} \tag{3.11}$$

with

$$a = \cos\theta \cos\phi \cos\chi - \sin\phi \sin\chi \tag{3.12}$$

$$b = \sin\theta \cos\phi \tag{3.13}$$

From the decomposition shown in Fig 3.3 the traction force acting on the tether is computed taking into account the aerodynamic force and the gravity force.

$$\mathbf{F}_t = -\mathbf{F}_a - \mathbf{F}_g \ . \tag{3.14}$$

For the low mass of the components compared to the order of magnitude of the aerodynamic forces, inertia is neglected.

The aerodynamic force is defined as the sum of the lift and the drag vectors (Fig. 3.3). The latter is in turn the sum of the drag of the kite and the drag of the tether.

$$\mathbf{F}_a = \mathbf{L} + \mathbf{D} \ , \tag{3.15}$$

with

$$L = \frac{1}{2}\rho C_L v_a^2 S \tag{3.16}$$

$$D = D_k + D_t \tag{3.17}$$

$$D_k = \frac{1}{2}\rho C_{d,k} v_a^2 S \tag{3.18}$$

$$D_t = \frac{1}{2}\rho dr C_{d,t} v_a^2 \tag{3.19}$$

$$D_{eff} = D_k + \frac{1}{4} D_t \tag{3.20}$$

We can directly compute the aerodynamic force by introducing the coefficient C_R

$$F_a = \frac{1}{2}\rho S C_R v_a^2 \ , \tag{3.21}$$

with

$$C_R = \sqrt{C_L^2 + C_{D,eff}^2} \ . \tag{3.22}$$

Combining 3.23 with 3.9 we get the expression

$$F_a = \frac{1}{2}\rho v_w^2 S C_R (1 + k^2)(\sin\theta\cos\phi - f)^2 \ . \tag{3.23}$$

Decomposing the tether mass according to the diagram in Fig. 3.4, gravity has the following components

$$\mathbf{F}_g = \begin{bmatrix} -\cos\theta \\ \sin\theta \\ 0 \end{bmatrix} m_k g + \begin{bmatrix} -\cos\theta \\ \frac{1}{2}\sin\theta \\ 0 \end{bmatrix} m_t g \tag{3.24}$$

Since the mass of the tether is decomposed as in Fig 3.4.

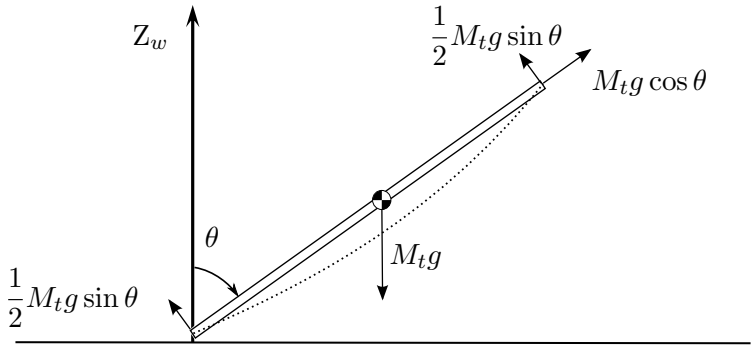

Figure 3.4: Decomposition of the tether mass [48]

The composition of the forces as shown in Fig:3.3 allows us to state that the component in θ direction of the aerodynamic force has just to counterbalance gravity. This is expressed by

$$F_{a,\theta} = -F_{g,\theta} \tag{3.25}$$

and the radial component of the aerodynamic force is found by

$$F_{a,r} = \sqrt{F_a^2 - F_{a,\theta}^2}\ . \tag{3.26}$$

With the mathematical model just presented, all the components of the aerodynamic force, the gravitational force and the apparent wind velocity can be computed. However most of those values are function of the kinematic ratio which is still unknown. This ratio would be, neglecting the mass, equal to the glide ratio L/D, for geometric similarities. However this would lead to inaccuracies in the model. For this purpose, the drag force

$$\mathbf{D} = \frac{\mathbf{F}_a \cdot \mathbf{v}_a}{v_a^2}\mathbf{v}_a \tag{3.27}$$

is rewritten to obtain the expression of the lift-to-drag ratio

$$\frac{L}{D} = \sqrt{\left(\frac{F_a v_a}{\mathbf{F}_a \cdot \mathbf{v}_a}\right)^2 - 1} \tag{3.28}$$

This expression is used to find the kinematic ratio iteratively. Given the quadratic relationship between instantaneous traction power and kinematic ratio, as can be seen in Eq.3.23, the effect of gravity can be significant. For horizontal flight ($\chi = 90°$ and $\chi = 270°$) the kinematic ratio is always lower than the lift-to-drag ratio. It can be

observed that the kinematic ratio increases with increasing mass of the kite for downwards flight and decreases for upwards flight. In a flying-up maneuver this can lead to a gravitational force that exceeds the aerodynamic force. This case reaches no equilibrium state and the algorithm fails to identify a physical solution. Mass consideration also has significant influence on the average power of a pumping cycle. As mentioned previously, the kinematic ratio depends on the kite course angle. Thus, the upward flying regions of a closed-loop trajectory require more time than the downward flying regions. This affects both the traction and the retraction phases [48].

3.3 Python Implementation

The theoretical framework is implement in Python language. The choice of this particular programming environment has been done by the KitePower group for the good balance of ease of implementation and computational speed. In the implementation, to keep the computational time short, not all the flight manoeuvres are simulated but average values of the azimuth angle ϕ and course angle χ are used. The result is a summarized 2D pattern of the flight one example is in Fig. 3.1.

For every time step the kinematic ratio is found iteratively and from it all the resultant forces.
Then the tether length is updated using

$$r(t + \Delta t) = r(t) + v_{k,r}(t)\Delta t \tag{3.29}$$

with $v_{k,r}$ kite radial velocity, equal to the reeling velocity.

The time step Δt is chosen based on the system characteristics using the non-dimensional time step [48]:

$$\Delta T = \frac{\Delta t}{t^*} \tag{3.30}$$

with

$$t^* = \frac{r_{max} - r_{min}}{v_{w,ref}}, \tag{3.31}$$

where $v_{w,ref}$ is the reference wind velocity.

Table 3.1: Classification of roughness [41]

roughness	terrain	characteristics
0.0002	sea	sea, paved areas, snow-covered flat plain, tide flat, smooth desert
0.005	smooth	beaches, pack ice, morass, snow-covered fields grass prairie or farm
0.03	open	grass prairie or farm fields, tundra, airports, heather
0.1	roughly open	cultivated area with low crops and occasional obstacles (single bushes)
0.25	rough	high crops, crops of varied height, scattered obstacles such as trees
0.5	very rough	mixed farm fields and forest clumps, orchards, scattered buildings
1	closed	regular coverage with large size obstacles with open spaces roughly equal to obstacle heights, suburban houses, villages, mature forests
≥ 2	chaotic	centres of large towns and cities, irregular forests with scattered clearings

3.3.1 Wind Profile and Distribution

As seen in the introduction, the wind speed increases with increasing the height due to the roughness of the terrain. In the model the wind speed is assumed following a logarithmic profile(Eq. 3.32).

$$v_w(h) = v_{w\ ref} \frac{\ln \frac{h}{z_0}}{\ln \frac{h_{ref}}{z_0}} \ . \tag{3.32}$$

The reference wind velocity ($v_{w\ ref}$) is the wind speed at the reference height (h_{ref}) which is 6 m in this case. The surface roughness (z_0) depends on terrain. A classification is reported in table 3.1

For further calculation of energy production then the wind speed probability is assumed to follow a Weibull distribution. From years of experience and measurements campaigns

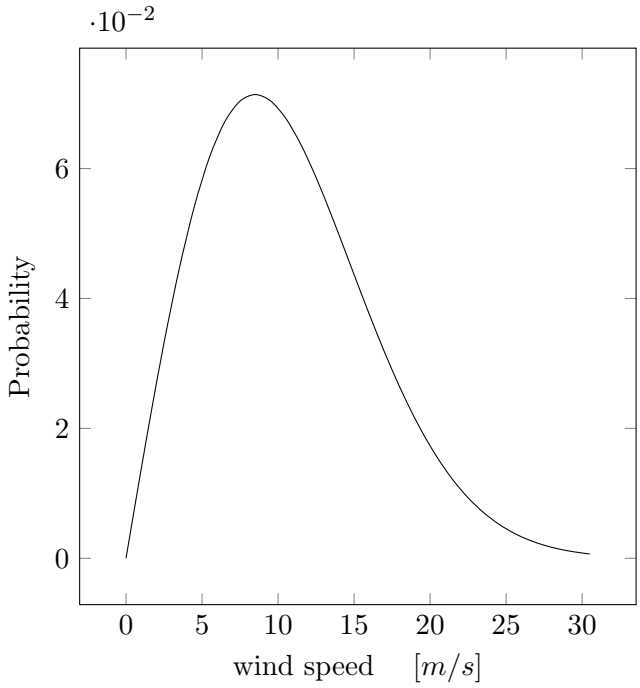

Figure 3.5: Weibull probability density function of the wind speed as presented in Fraunhofer IWES [18] for the city of Emden at 310 m height

in wind energy industry it has been derived that the wind speed can be predicted with this distribution. The probability of having a specific wind speed (V) will be computed as

$$p(v) = \frac{k}{A}\left(\frac{v}{A}\right)^{k-1} e^{-\left(\frac{v}{A}\right)^{k}} \tag{3.33}$$

resulting in a distribution of the kind presented in Fig. 3.5

The k is the so called shape factor and A the scale factor and they are functions of the mean wind speed and the standard deviation of wind speed measurements.
For the choice of the coefficient of the logarithmic wind profile and the Weibull distribution the work of Fraunhofer IWES [18] is used as reference. This work present the result of an extensive campaign of data collecting in different German locations. Rather different profiles and distributions are presented depending on the location. The data taken in Emden (north west of Germany near the border with the Netherlands) are taken as reference. The coefficient of the logarithmic wind profile are tuned to match with the measurements presented in the report. A good approximation for the wind profile is found using the parameters in table 3.2 where also the Weibull parameters are presented.

The wind profile is compared with the actual measurements in Fig 3.6. The wind probability distribution is plotted in Fig 3.5.

Table 3.2: Coefficients of the functions for the logarithmic wind profile and the Weibull distribution

parameter	value
z_0 [m]	0.001
h_{ref} [m]	3
v_w [m/s]	6.6
k	2
A	12

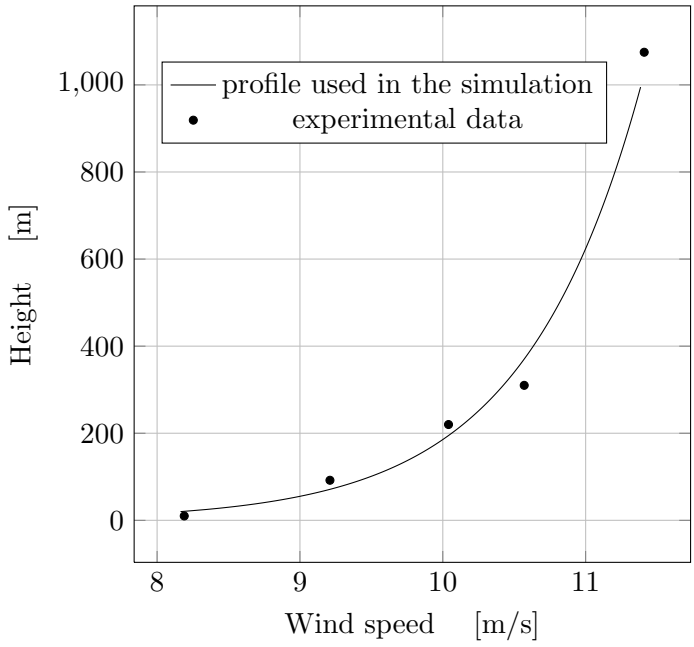

Figure 3.6: Comparison of the wind profile used in the simulation with the experimental data

Table 3.3: Operational parameters for in the cycle.

parameter	value
elevation angle [deg]	26
azimuth anlge [deg]	10
minimum tether lenght [m]	300
max tether lenght [m]	600
reel-out velocity [m/s]	2
reel-in velocity [m/s]	7.9

3.4 Validation of the Model

The simulation tool based on the quasi-steady model is then compared with a more accurate and computational intensive tool to asses the accuracy and reliability of the results. Validation trough comparison with experimental data has already led to interesting results in previous works [48], [19]. However the real wind that the kite feels is not known exactly and this might lead to inaccuracies. Here the dynamic model [17] is chosen for the comparison. This has been used as reference instead of real experimental data because it is more easy to monitor the environmental parameters, avoiding the uncertainties over the actual wind profile. Thanks to the possibility of choosing the wind profile in the more detailed model is possible to simulate the system in the same conditions.
In the dynamic model the aim is to simulate in real time the flight of the kite, having the aerodynamic parameters of the kite and characteristic of the tether set. For the approach of the method the results are expected to be more accurate than the one obtained with the quasi-steady model. Therefore this model is used as reference for the validation of the quasi-steady solution.
During the figures of eight manoeuvres of the traction phase and during the straight trajectory of the retraction phase the forces are computed using the relative equations and a four mass points kite is used to obtain an estimation of the side forces and inertia of the system. The tether is segmented to avoid the assumption of the straight tether. A detailed description of the model along with the equations used are in the relative paper [17].

3.4.1 The Power Cycle

In this section the power cycle that has been simulated with both models is presented. The control strategy, the system components and the operational parameters are set in both models as similar as possible to obtain an identical cycle with both models. The cycle settings for the operational parameters are in table 3.3.

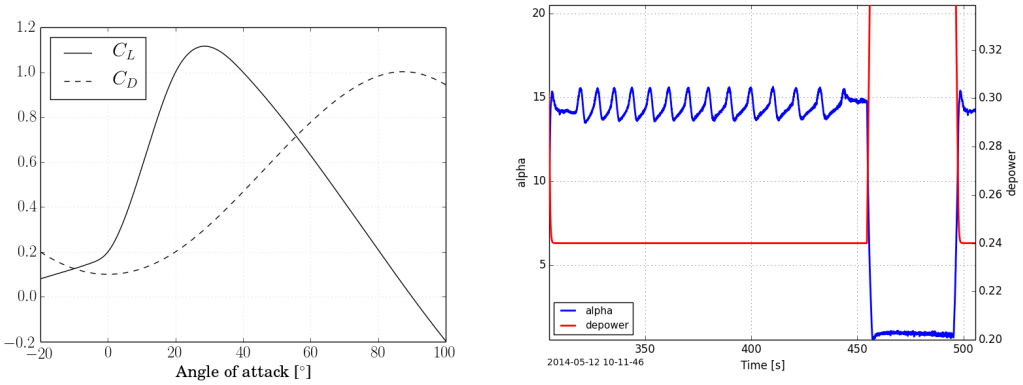

Figure 3.7: Left : C_l and C_d of the kite as function of the angle of attack; Right: angle of attack of the kite during the dynamic simulation of the pumping cycle and the activation of the de-power for the retraction phase [17]

3.4.2 Kite and Tether

The kite used in both simulations has a projected area of 10.18 m^2, a mass of 6.21 kg and the mass of the KCU is 8.4 kg, this add up to a total airborne mass of 14,61 kg.
In the dynamic model the aerodynamic properties of the kite are computed every time step from the angle of attack of the kite and using the relative values of the graph 3.7. The angle of attack can be plotted against the time (3.7(right)) .

With those two information is possible to compute the averages values of C_l and C_d of the kite during the traction phase and retraction phase that have to be set in the other model. From the analysis of the two graphs it results that the angle of attack varies from 13.7° and 15.5° during the traction phase. The C_l and C_d during that phase can be set respectively in a range 0.74 to 0.83 and 0.148 to 0.16. Averages values are taken so the C_l and C_d during the traction phase will be set equal to 0.14 and 0.78. Those values are also used for the transition phase. The same kind of analysis is performed for the retraction phase and the values of C_l and C_d are set equal to 0.22 and 0.1 respectively.
The tether is in the model has a diameter of 4 mm and a drag coefficient of 1.1 and a mass density of 724 kg/m^3.

3.4.3 Comparison and Modifications

The operational parameters are adjusted so to have a resultant cycle with both simulations as similar as possible. The focus in in particular on making the reeling speeds during the phases as equal as possible.
The reel-in velocity which results from the dynamic model results constant, which means that the maximum allowable value has been reached before the maximum allowable tether force. Therefore the set value of the tether force during the retraction phase in the quasi-steady model is set at 1700 N. This value is well above the necessary force to reach the maximum speed. This setting is to make sure that the maximum reel-in speed is reached

Table 3.4: Results of the simulations with reference wind speed = 8 m/s.

	dynamic model	Quasi-steady model	% difference
Energy [J]	1040077	592417	54
average power over the cycle [W]	5389	3047	56
average traction power [W]	8200	7090	14
average retraction power [W]	-3500	-13169	116
traction time [s]	130	149	13
retraction time [s]	40	37	7
transition time [s]	4	7	54
duty cycle %	75	77	3
average traction force [N]	3650	3650	0
average retraction force [N]	450	1700	116
average reel-out velocity [m/s]	2.25	1.8	22
average reel-in velocity [m/s]	-7.9	-7.9	0

before the set tether force. The transition time (estimated in the dynamic model) is rather small compared to the duration of the other phases. Therefore the influence of this phase in the total average energy production and the average power in the cycle should be small as well.
The results of energy production and average power over the cycle differ significantly. The values of energy, average power and average power per phase are extrapolated from the graphs and the results are presented in table 3.4.
From the analysis of the results it appears that the difference in average energy production and power over the cycle mainly depends on the difference in the tether force in the retraction phase. it seems that the setting of the high retraction force, to ensure that the maximum tether velocity is reached, does not lead to the same cycle of the dynamic model. The tether force in fact reaches anyway the set value without taking into account that the maximum tether velocity has been already reached. However if the tether force during the reel-in is set lower, but still high enough to reach the maximum speed the cycle velocities do not change but the power does. This seems to be an unrealistic behavior.
When the maximum tether velocity is reached the force should be computed again so to find the traction power with that specific limited velocity. The algorithm is improved to recompute the aerodynamic force once more after the check on the speed. The difference in the trend of the results of the quasi-steady model before and after the change are presented in Fig:3.8 and Fig: 3.9

The cycle for the comparison with the dynamic model is run once again after the change in the algorithm and the results are compared in Tab.3.5

3.5 Conclusion

After this improvement the results match better. The differences are reduced, in particular the difference in the average retraction power goes from 116 % to 33 %.

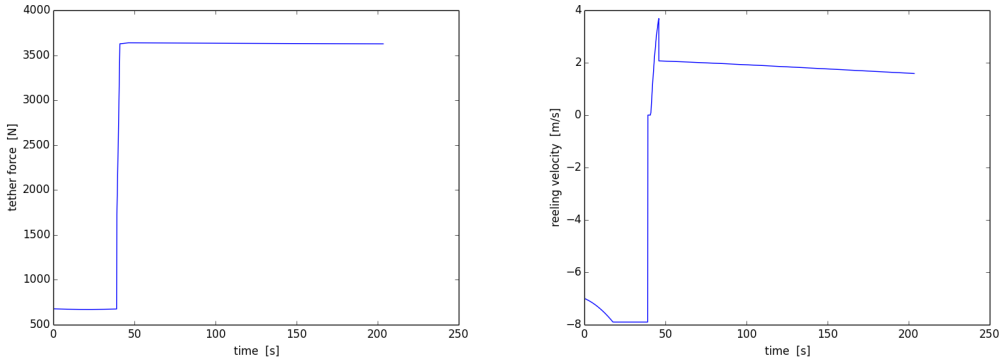

Figure 3.8: Results of the simulation before the change in the algorithm. Left : tether force, for the reel-in velocity has been set to 700 N for a better visualization of the problem; Right: reeling velocity, is clear that it increases until the the maximum of 7.9 is reached, then it remains stable but the retraction force remains the same

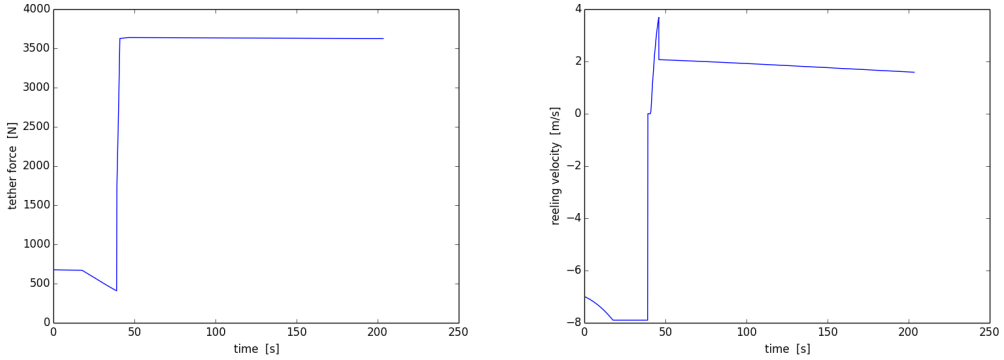

Figure 3.9: Results of the simulation after the change in the algorithm. Left : tether force, Now it is clear that when the maximum reeling velocity is reached the tether force is recomputed and it decreases with the kite flying towards the zenith; Right: reeling velocity

Table 3.5: Results of the simulations with reference wind speed = 8 m/s after the change in the algorithm.

	dynamic model	Quasi-steady model	% difference
Energy [J]	1040077	906531	13
average power over the cycle [W]	5389	4481	18
average traction power [W]	8200	6680	20
average retraction power [W]	-3500	-4927	33
traction time [s]	130	157	18
retraction time [s]	40	37	7
transition time [s]	4	6	20
duty cycle %	75	77	3
average traction force [N]	3650	3650	0
average retraction force [N]	450	627	31
average reel-out velocity [m/s]	2.25	1.8	22
average reel-in velocity [m/s]	-7.9	-7.9	0

With this comparison and change in the algorithm the model is assumed to be accurate enough to simulate the mechanical energy output of a given system in given conditions. The choice of the unit components is Chapt. 7 explained in the relative section . With this simulation tool and some additional considerations about the energy conversion from mechanical to electrical one can obtain the electricity generation. Then, knowing the environmental conditions and optimising the operational parameters for every wind speed, it is possible to compute the annual energy production.

Chapter 4

Optimization Routine

In this chapter the preliminary optimization results are presented. The operating wind range starts from 2 m/s. Then the optimization keeps going until 25 m/s unless the average power over the cycle goes to 0 before reaching that wind speed. The cut in velocity has been found as the lowest wind speed at which the kite is able to fly and perform a cycle even though the average power over the cycle is very low. With the increase of the wind speed the power reaches a maximum and then it decreases for the increase of the energy required for the retraction phase.
The wind speed here is intended the reference wind speed at the height of 6 m. The model computes the logarithmic wind profile and updates it depending on the altitude at which the kite is flying. The average wind speed that the kite feels is generally higher that the reference wind speed. This wind speed is reported by the model as the average wind speed and is the wind speed at the mid point of the traction phase.
The correlation between the optimal values and the wind speed is analysed as well.

4.1 Preliminary Optimization Results

The optimization is performed on a system with a 100 m^2 kite. In this section the results of the preliminary optimization are presented and analyzed.
After choosing the kite size (what the choice is based on will be explained in the section relative to the system design) the first optimization of the parameters is done. This preliminary optimization does not take into account any other constrain than the maximum tether force (21 kN) which comes from the physical limit of wing loading of the kite. From the results it can be seen the maximum power output of the system if there were no power and speed limits.

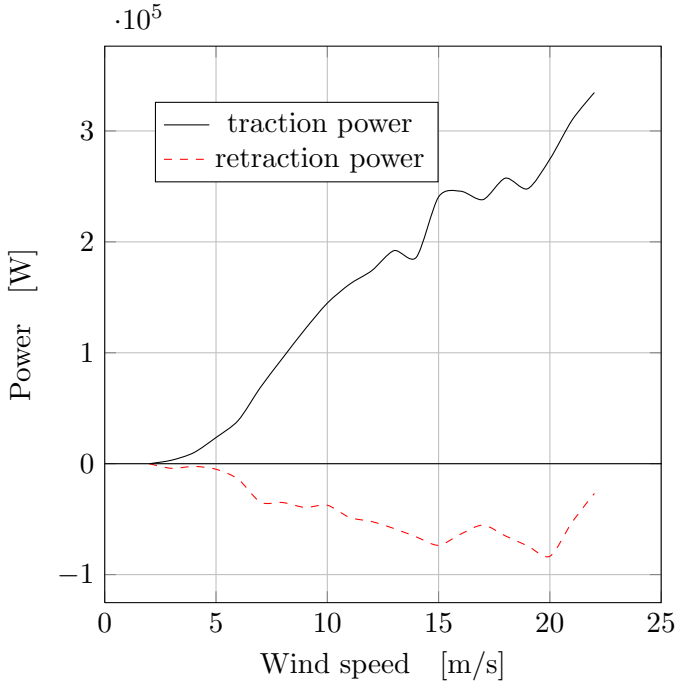

Figure 4.1: Average power during traction and retraction phase at different wind speeds

This optimization will be used to choose an appropriate combination of electrical machines and make consideration concerning the operational speed in order to understand if there is the need of a gearbox.

Because of the discrete approach of the genetic algorithm one cannot be sure that the actual maximum power is obtained for every wind speed. The solution is considered representative of the trend of the optimal value. For this reason the plots in this section are not smooth lines but the trends present some oscillations. Anyway it is possible to derive some consideration over the general trend that the optimal operational parameters should assume at every wind speed can be made.

The Fig. 4.1 reveals that the the instantaneous power increases indefinitely (as expected) in the traction phase with the increase of the wind speed, not having any limit. The retraction power increases as well but much slower and starts to decrease for wind speeds above 20 m/s.

The optimal force increases steeply with the increase of the wind speed. In this case the limitation on the maximum tether force stops the increase already for a wind speed of 7 m/s (Fig.4.2). Above that wind speed the power is increased only by increasing the reeling speed since the force cannot be increased any further. The optimal retraction force increases as well but slower. Eventually it also reached the maximum allowable value but only for high wind speeds (above 20 m/s). The increase of the optimal reeling force is to reduce the retraction time so to have a better average power over the cycle.

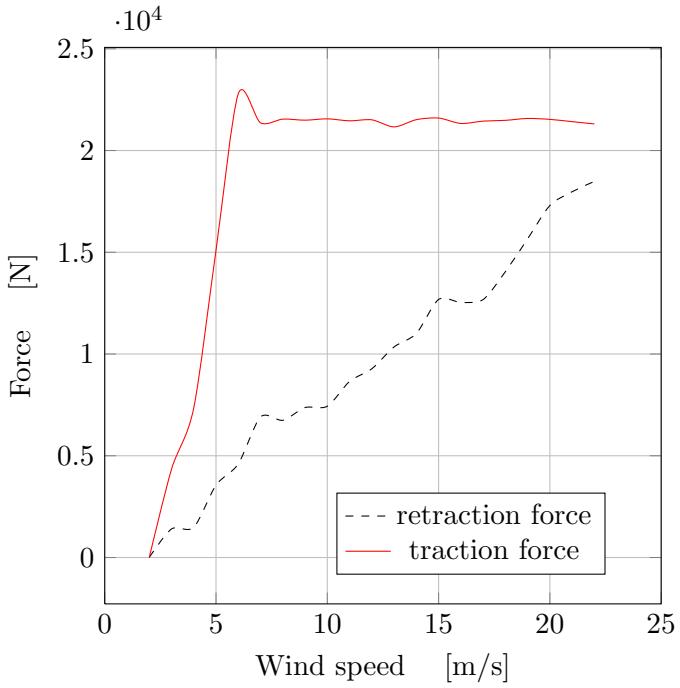

Figure 4.2: Optimal forces on the tether during the traction and the retraction phases

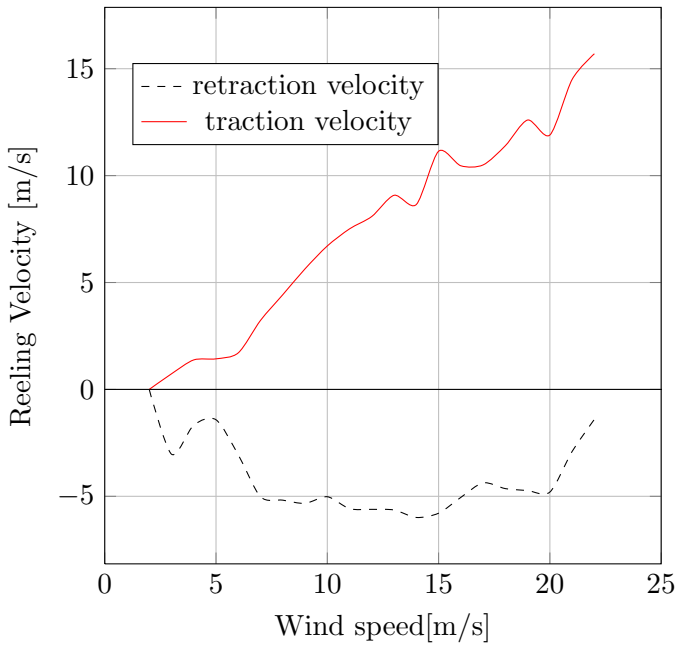

Figure 4.3: Optimal resultant average reeling velocity of the tether during the traction and retraction phases

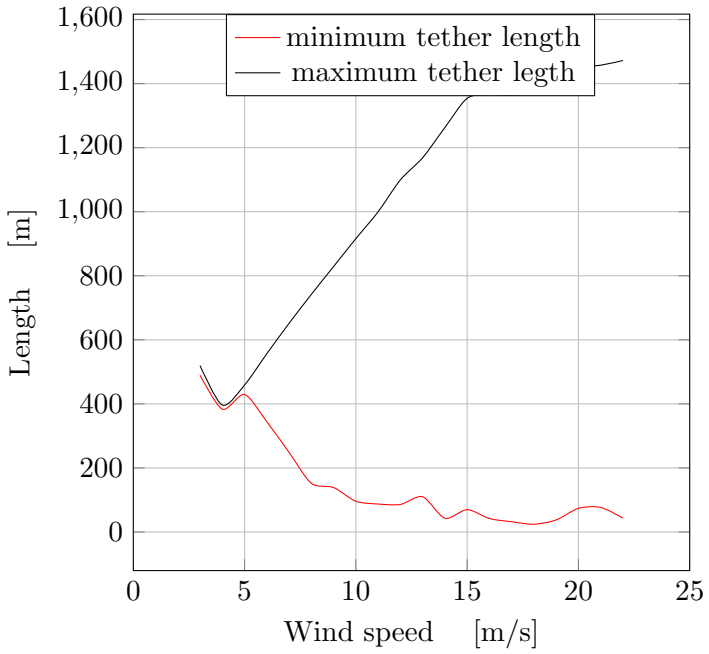

Figure 4.4: Optimal minimum and maximum tether length at different wind speeds

The increase of the reeling velocity (Fig.4.3) would not be possible indefinitely in the real system for physical constraints of overheating of the bearings and electrical machine rotational speed. Above the maximum force and rotational speed (which will be the maximum power point) the kite needs to be de-powered if we want to keep operating the system. Despite the increase of the tether force during the retraction phase, to reduce the retraction time, the time required to reel-in the kite to the initial position keeps increasing compared to the duration of the traction phase (Fig. 4.7). As result the average power of the cycle decreases.

The altitude range at which the kite operates increases with the increase of the wind speed. The optimal maximum tether length increases with the wind speed while the minimum decreases (Fig. 4.4). At the same time the optimal elevation angle (Fig 4.6) increases with the increase of the wind speed. This is to decrease the retraction time. As a result the average height of the cycle increases as well (Fig. 4.5). The set upper limit of 1500 m of tether length does not seem to be a limiting factor. It is approached only at the end of the wind range where the average power is already dropped to low values.

Finally a preliminary shape of the power curve can be presented by using the resultant average power aver the cycle (Fig4.8). It can be already noticed that the only limitation that this preliminary optimization has already affects the shape of the curve. Even if no limitations on the power are imposed the power curve reaches a maximum and then it decreases (differently than the power curve of traditional wind turbines) because of the increase of the energy required during the retraction phase.

However this power curve is still unrealistic. The real system power limitations would

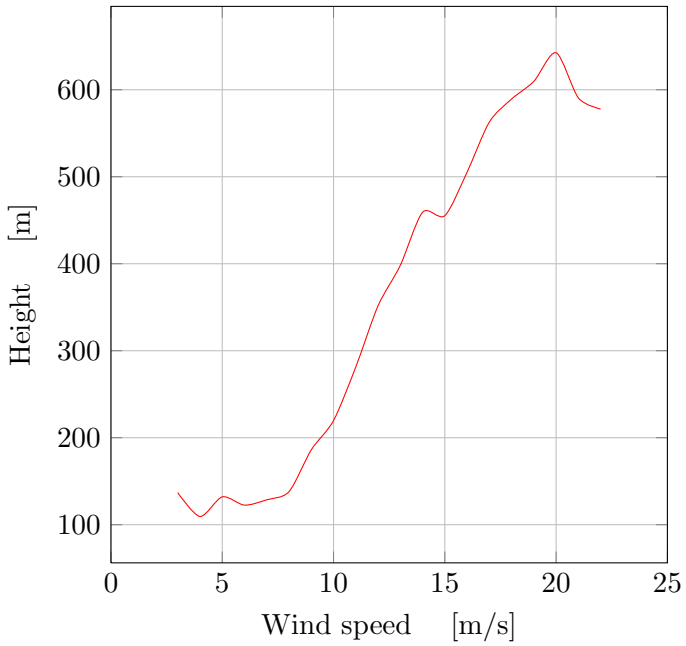

Figure 4.5: Kite average optimal height during the operation at different wind speeds

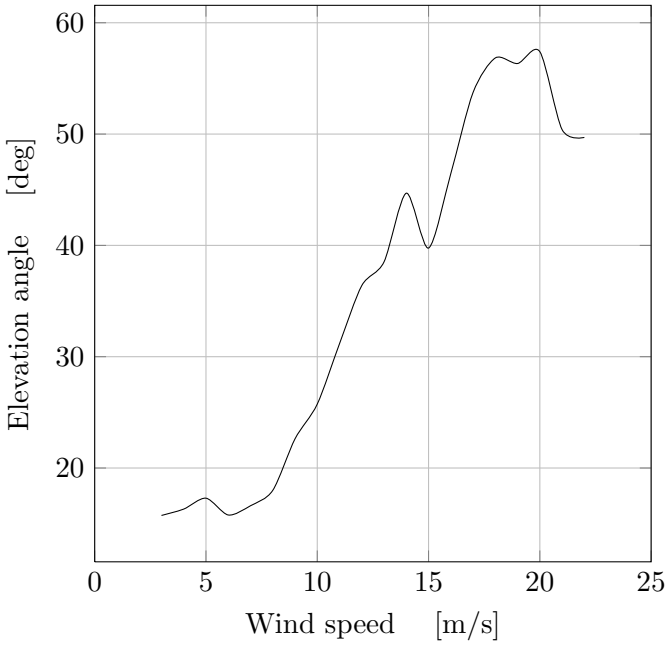

Figure 4.6: Optimal elevation angle during the traction phase

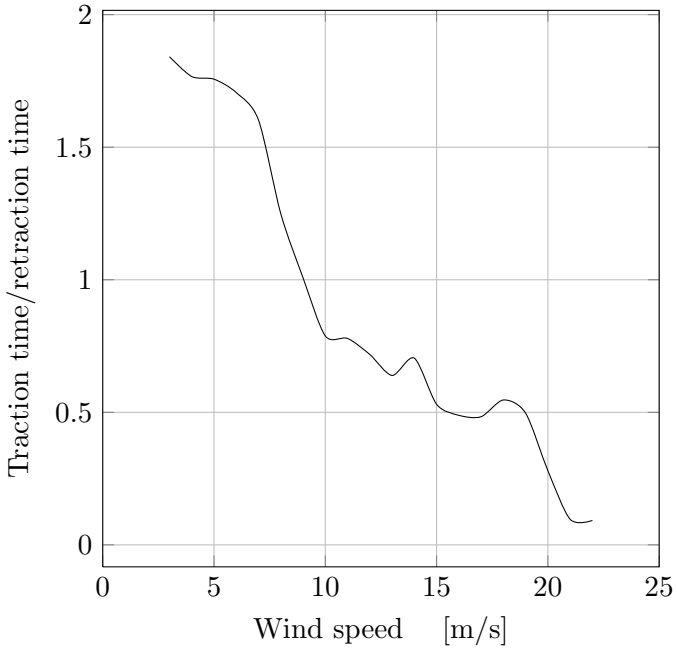

Figure 4.7: Ratio between the duration of the retraction phase and the traction phase

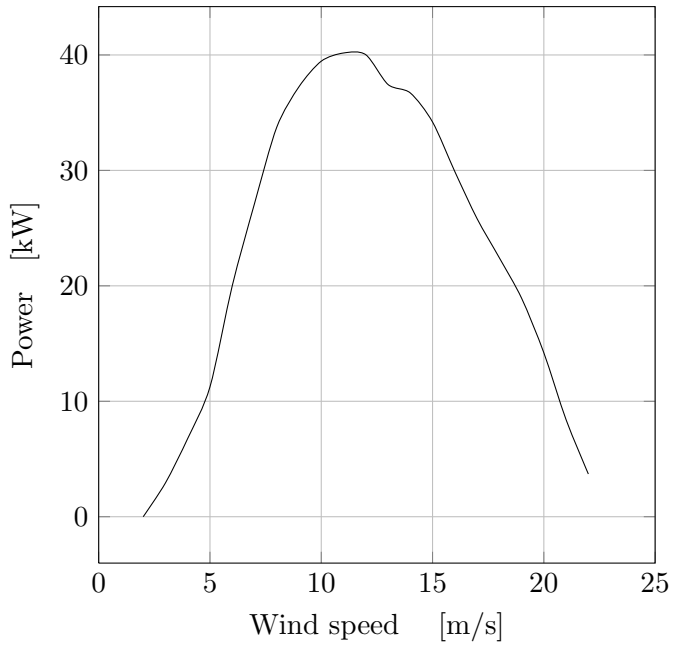

Figure 4.8: Resultant preliminary power curve

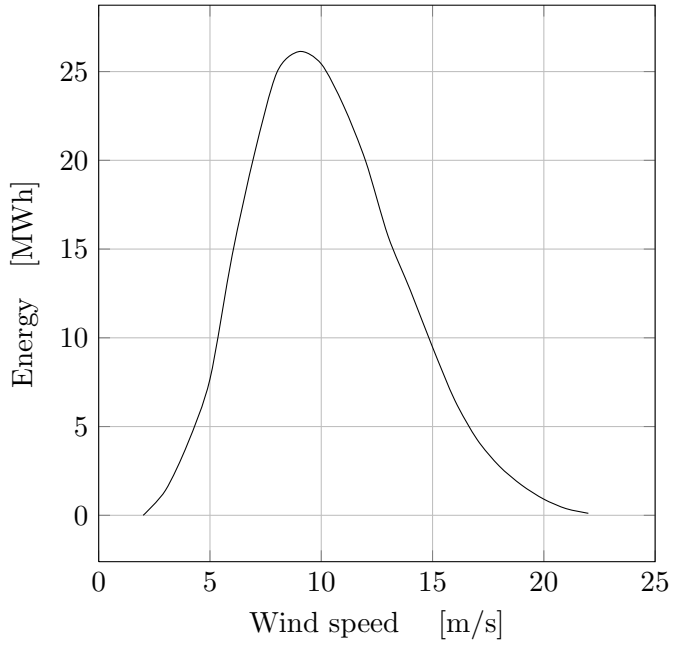

Figure 4.9: Energy production as function of the wind speed

affect the final shape of the power curve, which would probably reach again a maximum to decrease faster depending on the restriction imposed.
Coupling this power curve with the Weibull wind distribution leads to a first gross estimation of the energy output. Estimating for how many hours a given wind speed blows during the year and knowing how much power is being produced by the system at that given wind speed, the energy output at every wind speed can be computed. Then the summation over all the operating wind range of the system leads to the annual energy output.
Intuitively, since both the power and the probability high wind speeds tend to decrease, so does the energy yield. The resultant shape of the contributions to the annual energy output at the different wind speeds result as in Fig.4.9. The integral of the curve sketched will give the annual energy production.

Chapter 5

Electrical Machines Model

The mechanical energy obtained with the model presented has to be converted into electricity through electrical machines. This further step has been modelled as well to obtain a realistic estimation of the annual energy production. In this chapter the model to obtain the conversion efficiency of the electrical conversion is presented.

5.1 Electrical Efficiency

The efficiency of the electrical machines is modeled as function of rotational speed ω and torque τ of the machine. In fact the operating point of the machine changes within a single cycle and within the operating wind range depending on the reference wind speed. The efficiency is by definition the ratio of the power output over the input

$$\eta = \frac{P_{out}}{P_{in}} \ . \tag{5.1}$$

Since only the mechanical power is known for the traction and retraction phases, the efficiency has to be expressed as function of it. The efficiency of the generator and the motor are respectively

$$\eta_{gen} = \frac{P_{el}}{P_{mech}} = \frac{P_{mech} - L_e - L_m}{P_{mech}} \tag{5.2}$$

$$\eta_{mot} = \frac{P_{mech}}{P_{el}} = \frac{P_{mech}}{P_{mech} + L_e + L_m} \ , \tag{5.3}$$

where the two terms L_m and L_e are the mechanical and electrical losses. The mechanical power is the product

$$P_{mech} = \omega\tau \tag{5.4}$$

The mechanical losses in this model consist in two main contributions: friction losses, which are directly proportional to the rotational speed, and ventilation losses, which are proportional to the square of the rotational speed. Those losses are computed with the equation

$$L_m = \tau_f\omega + C_v\omega^2 \ . \tag{5.5}$$

The electrical losses, on the other hand, go with the square of the current in the machine and the phase resistance following

$$L_e = 3kR_gI^2 \tag{5.6}$$

and the current in turn is proportional to the mechanical torque of the machine

$$I = c_g\tau \ . \tag{5.7}$$

with Eq: 5.6 , Eq: 5.5, and Eq: 5.7 in 5.3 we get the following expression for the electrical efficiency.

$$\eta_{gen} = 1 - 3Rgkc_g^2\tau^2/P_{mech} - \tau_f\omega/P_{mech} - C_v\omega^2/P_{mech} \tag{5.8}$$

$$\eta_{mot} = \frac{P_{mech}}{P_{mech} + \tau_f\omega + C_v\omega^2 + 3Rgkc_g^2\tau^2} \tag{5.9}$$

with the coefficients c_g, k, τ_f and C_v to be determined.
Knowing the efficiency and the current at two different operating points of a machine it

Table 5.1: Parameters to be found in the data sheet of the electrical machine for which the model has to be applied

	unit
η_1	
η_2	
R_g	Ω
τ_1	[Nm]
τ_2	[Nm]
ω_1	[rpm]
ω_2	[rpm]
U_1	[V]
U_2	[V]
I_1	[A]
I_2	[A]

	unit
c_g	[A/Nm]
k	
C_v	[Nm/rpm]
τ_f	[Nm]

Table 5.2: Unknowns of the system of equations

is possible to set up the following system of equations

$$\begin{cases} \eta_1 = 1 - 3Rgkc_g^2\tau_1^2/P_{m1} - \tau_f\omega_1/P_{m1} - C_v\omega_1^2/P_{m1} \\ \eta_2 = 1 - 3Rgkc_g^2\tau_2^2/P_{m2} - \tau_f\omega_2/P_{m2} - C_v\omega_2^2/P_{m2} \\ c_g = \frac{I_1}{\tau_1 - (\tau_f + C_v\omega_1)} \\ c_g = \frac{I_2}{\tau_2 - (\tau_f + C_v\omega_2)} \end{cases} \tag{5.10}$$

which can be solved for the coefficients we are interested in (Tab. 5.2) knowing the efficiency at two known operating points.

5.2 Application of the model

With the possibility now to compute the efficiency of an electrical machine in every mode of operation and at any given operating point further investigations are possible concerning the present work. The model has been used to chose the best layout of the drive train for the ground station and the specifics of the machine that should be installed. The details of the problem to solve, the approach and the results are explained more extensively in the following chapter.

Chapter 6

Layout of the Ground Station

While there is not much to think about the airborne components, there are still many uncertainties on which layout of the ground station is the best, in particular, how to convert mechanical power into electrical in the most efficient and cheap way.
As explained in Chap. 2, in previous works there is not a clear answer of which is the best layout of the ground station. For best layout is intended the one that leads to the lowest cost of energy.
With the aid of the efficiency model presented in the previous chapter the two best layouts found by Schölkopf [37] are compared and finally a clear answer of which layout is the best can be given.

6.1 Design possibilities

The analysis is performed for a system with a 25 m^2 kite for availability of data of suitable electrical machines suitable for this kite size. The results and the same considerations hold also for scaled up systems.
Once again a preliminary optimization is run as for the case of the bigger kite with the same approach taken in Chap. 4. The outcome of the preliminary optimization, the shape of the power curve and optimal forces obtained and the trend of the operational parameters resemble the one presented in Chap. 4 with the only difference of being scaled down. Therefore for the sake of compactness, the outcomes will not be presented in this section.

After the preliminary optimization the required power of electrical machines is known.

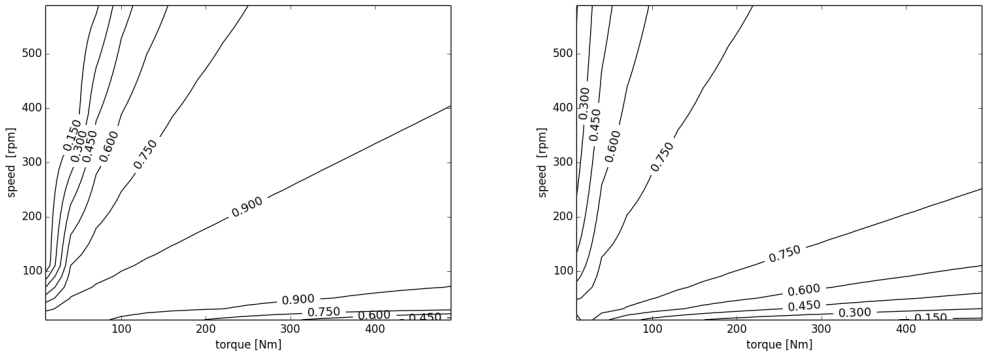

Figure 6.1: Efficiency of the ALXION 500 STK 8M 400 as function of the torque and the speed when operates as a motor (right) and as generator (left).

One singular machine or two separate can be chosen from catalog [2]. Their constrains of maximum power output and maximum velocity are included in the simulation and appropriate gearbox ratios are chosen as well to reach the highest efficiency. To let the system operate also when the maximum reel out power of the generator is reached, a partial de-power model of flight is included in the model. It comes into operation when the power during the traction phase exceeds 1.5 times the nominal power of the electrical machine. The kite is partially de-powered until the power at the generator is within the constraint. For the partial de-power of the kite the values of the lift coefficient and the drag coefficient are decreased progressively by 2% and 1 % from the previous calculation until the power results within the boundary.

6.1.1 Singular Machine

The system is simulated with a ALXION 500 STK 8M- 400 [2] working as motor and generator in the two phases. This electrical machine has a nominal power of 48 kW and the resultant efficiency diagrams from the model are presented in Fig 6.1. It has been chosen after a preliminary optimization not to have power limitations until a wind speed of 16 m/s. Above that speed the kite will have to be depowered not to exceed the nominal power of the generator. The retraction power remains lower than 20 kW also for high wind speeds. The preliminary optimization is run until a wind speed of 20 m/s.

A fixed gearbox ratio of 6:1 is considered, both for the traction phase and the retraction phase. This is the ratio that makes the machine operate closest to its nominal operating point for the most likely wind speeds, according to the Weibull distribution (from 5 to 10 m/s). The electrical efficiency is computed at every time step, then averaged over the traction phase, the retraction phase and in total. The trend of the efficiency during a single cycle at 8 m/s of wind speed is plotted in Fig. 6.2 starting from the retraction phase, followed by the transition phase and the traction phase.

It is clear that the electrical efficiency is rather low for the retraction phase with the

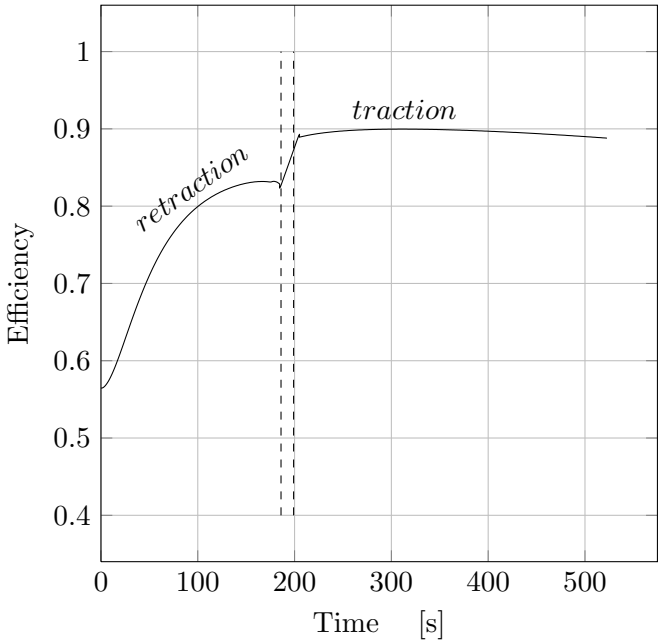

Figure 6.2: Electrical efficiency during a cycle with 8 m/s of reference wind speed between the dashed lines the transition phase, the cycle starts with the retraction phase

configuration chosen. In particular, at the beginning of the phase when the reeling velocity is very low. On average it results 75.4 % for the retraction and 89.5% for the traction phase. However average values do not tell enough about the weight of the efficiency in the final average power over the cycle. To compute this value of average conversion efficiency all the time steps are considered having the same value. But the power changes continuously, specially in the retraction phase and so does the efficiency. In the case of 8 m/s for example the average efficiency would be 84,4 %. But the resultant power over the cycle is only 5.33 kW which is only 66.7 % of the mechanical power that the tether transfers at the ground station. This can be explained with a mismatch of high power and high efficiency during the cycle and the efficiency of the additional motors for the drum and controllers (considered 98 %) and the gearbox efficiency (considered 99%).
The same computations has been performed for many wind speeds where the system will have to operate.

From Fig. 6.3, we can see that the reel- in efficiency during the retraction phase will tend to decrease at the increase of the wind speed. This will result in a decrease of the mean cycle power.

6.1.2 Two Electrical Machines

Now the same simulations are run with two different electrical machines, one for each phase. The generator is kept the same as its gearbox ratio. As motor the choice is for ALXION 300 STK 6M-800 which has higher efficiency at lower values of torque and

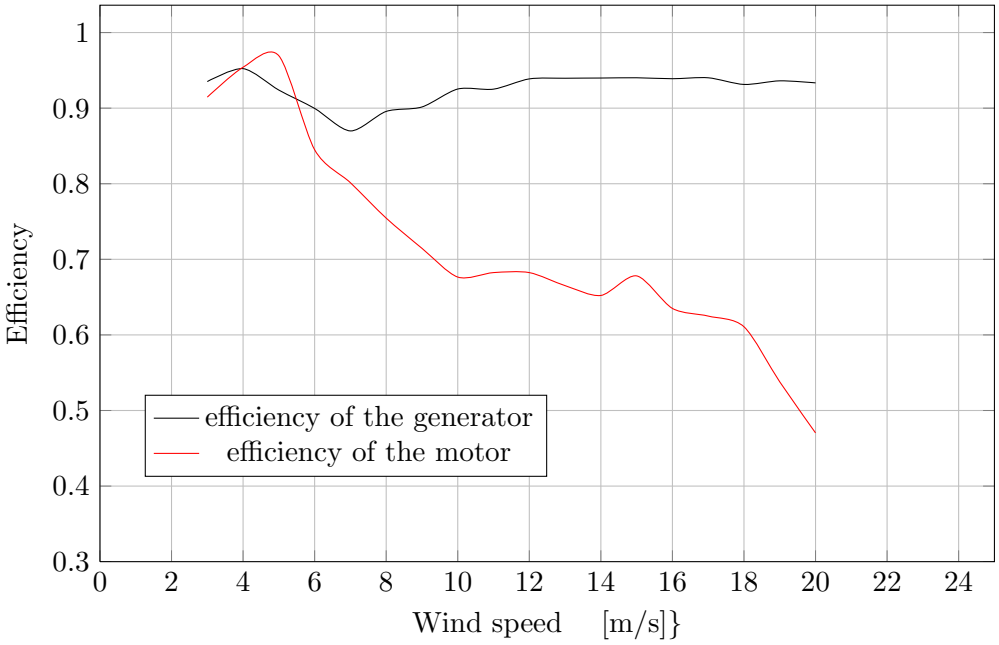

Figure 6.3: Electrical efficiency in the operating wind range

higher speeds compared to the 500 STK. Therefore a higher gearbox ratio of 35:1 is chosen, making the same considerations done for the previous case.
The efficiency diagrams for the machines can be seen in Fig. 6.4

The higher efficiency of the new configuration can be already seen over the single cycle at 8 m/s (Fig. 6.5) The efficiency is now remarkably increased in the retraction phase, reaching an average value of 84 %, while the efficiency of the traction phase remains the same.

By visual comparison of the two graphs in Fig. 6.6 and Fig. 6.3, it is clear that using two electrical machines has a positive impact on the efficiency at different wind speeds. The

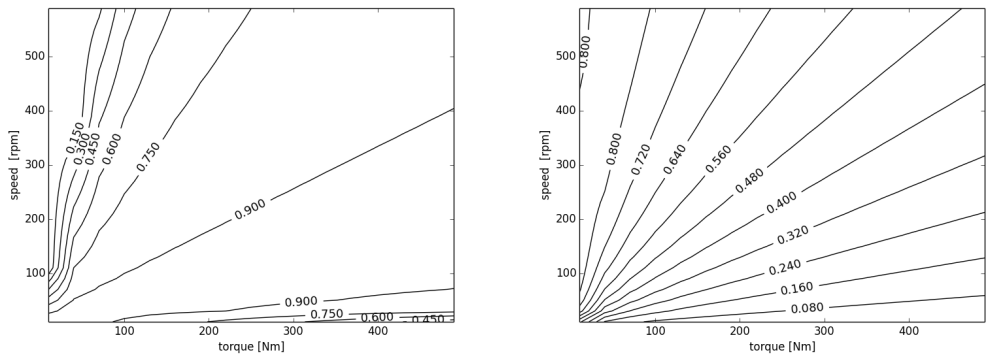

Figure 6.4: Efficiency of the ALXION 500 STK 8M 400 working as generator as function of torque and speed (left) and of the ALXION 300 STK 4M 800 working as motor.

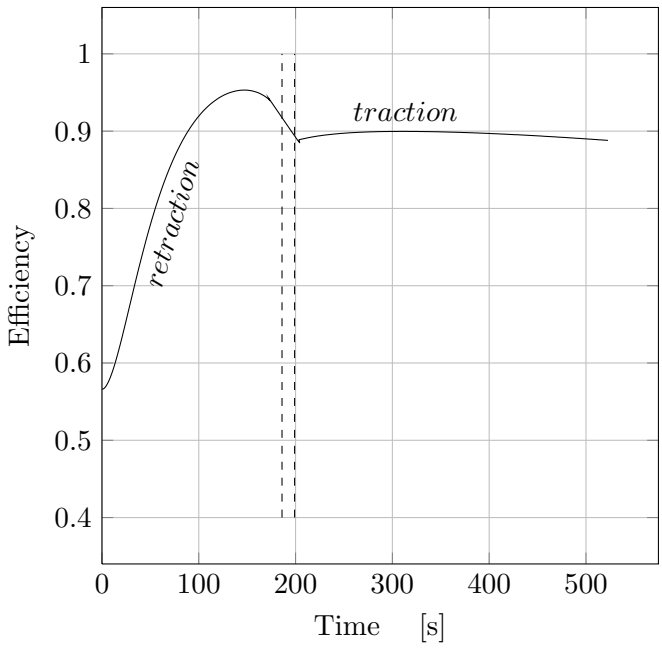

Figure 6.5: Electrical efficiency during a cycle with 8 m/s of reference wind speed with two electrical machines configuration. The simulation begins with the retraction phase and between the dashed lines is the transition phase.

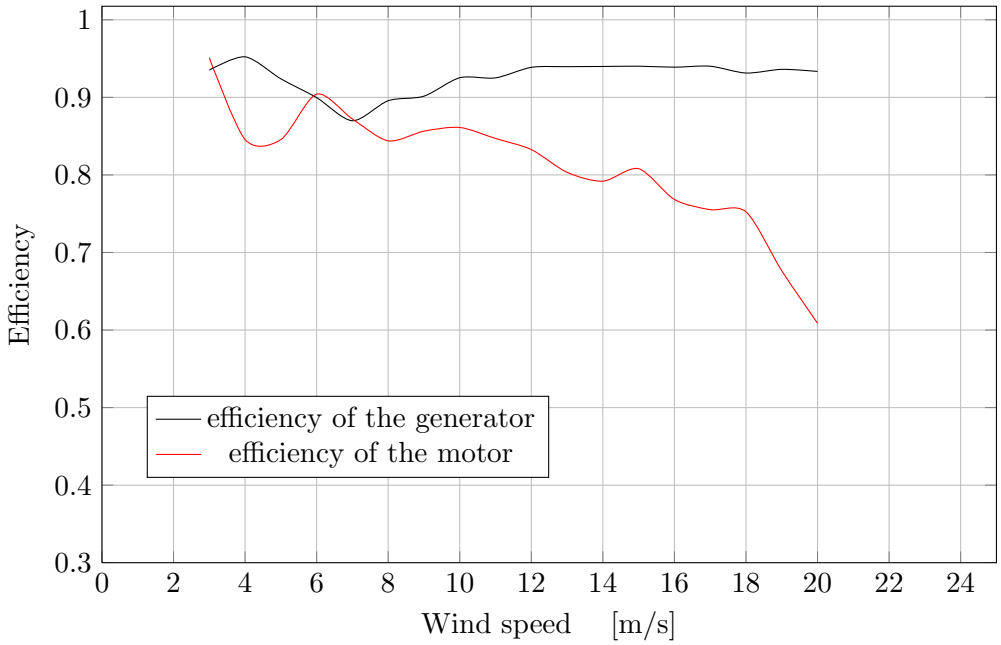

Figure 6.6: Electrical efficiency in the operating wind range considering two electrical machines

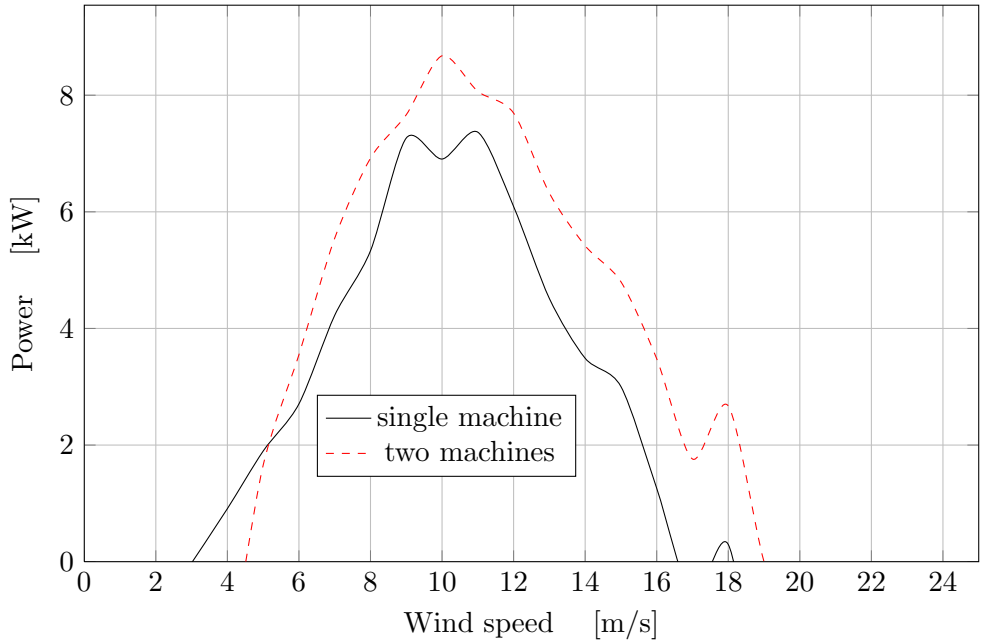

Figure 6.7: Comparison of the power curves with the two different configurations

retraction efficiency decrease is less pronounced and the average remains higher. If this is enough to justify an higher investment and maintenance cost remains to be investigated and discussed in the following section.

6.2 Conclusion of the Analysis

To assess which setting is the best, an indication of the LCOE should be computed for the two cases.
To this purpose the power curve is obtained again from the simulation for the two different configurations.

The increase in efficiency results in a higher mean power of the system with the two machines (Fig.6.7) in particular for higher wind speeds.
From the value of the power at every wind speed and considering the Weibull distribution, the annual energy production can be computed. A simplified cost model is applied (cost functions will be explained in the following sections) including only the costs of the replacements of the kite, KCU and tether and the installation and maintenance cost the electrical machines, and the gearboxes.
Using, at this stage, a simplified cost model ensures a conservative analysis. This because here we want to assess the impact on the total cost of an additional motor and gearbox. If all the system costs are evaluated, the impact on the total cost of the additional components would be even lower than for the simplified case.
It results that the LCOE considering 20 years of lifetime of the system is around 14 % lower in the case of two machines(Tab. 6.1).

Table 6.1: Comparison of LCOE with the two configurations

configuration	LCOE [€/MWh]
single machine	130.78
two machines	111.47

The values in Tab 6.1 should not be considered as a realistic LCOE and should not be used as reference. This result is obtained without taken into account additional costs (like installation costs, cables and maintenance) to keep the model simple. The real LCOE is expected to be higher for the both cases. The outcome of the present analysis not the real LCOE of the system but the assessment of the best layout of the drive train. The answer to the problem posed at the beginning of Sect. 6.1 is that the increase in efficiency by installing two electrical machines overcomes the higher price for installation. And the system is designed taking into account this result.

Chapter 7

Unit Design and Components Choice

This chapter deals with the design and the choice of the components for the unit. To make the estimation of the LCOE as realistic as possible, all the most relevant components have to be taken into account. Unfortunately nowadays there are no units available on the market or producing electricity continuously which one can refer to, therefore many assumptions have to be made.
Component sizes are chosen considering previous works on the same topic (Heilmann [21] and Grete [19]), results of computations and on personal considerations. Obviously the result of the previous chapter on the optimal layout of the ground station is adopted.

7.1 Components Specifics

The components of which the size can be freely chosen are:

- kite area
- rated power of the electrical machines

From the kite area the size of most of the components that enables the production of electricity follows by consequence. Those sizes are derived taking into account material properties and loads that the components have to withstand, trying to reach a reasonable practical lifetime of the components.
The maximum tether force follows from the maximum wing loading assumed. Knowing

the tether strength modulus and fatigue resistance characteristics [33] it is possible to derive the tether diameter and from that the drum diameter. It has been proved in the work of Rigo Bosman, Valerie Reid, Martin Vlasblom [33] that, if the ratio of the drum diameter over the tether diameter is too small, it heavily affects the tether life time. From the rated power of the generator and its characteristics we can get the maximum power that can be achieved during the traction phase.
Choice of the rated power of the electrical machines is not trivial. Previous works (Grete [19]) have shown that the resultant LCOE is heavily affected by the combination of kite area and generator size. The final result however depends on many environmental parameters, scaling and cost functions and assumptions. That is why only the kite size is chosen and not the combination with the generator.
The choice of the electrical machines is done by looking at the power curve and the instantaneous mechanical power during the traction and retraction phases obtained with the preliminary optimization (Ch: 4).

7.1.1 Kite

The kite is the main component of the unit. It can be considered as the engine and fuel of the system and from the choice of its size and its characteristic follows the dimensions of most of the components of the unit. The mass of the kite depends on the amount of fabric that it is being used.
Only few very big ram air wings have been produced and mainly for military applications of deploying goods in remote and inaccessible areas (Dunker [12]). Very few kites have been produced so far for ship traction (one example can be found in Staack [40]).
It has been decided to start with a kite size of 100 m^2 kite. However this choice is debatable. An optimization on the kite size would be required once the whole model is set to compute the LCOE of a wind farm. The ratio total/projected area is assumed to remain the same as well as the aerodynamic properties and the de-power characteristics.
The mass of the kite scales with the amount of fabric used and so proportionally to the total surface area of the kite and the thickness of it. The thickness scales proportionally to the wing loading (WL). By knowing the specifics of the demonstrator at the kite research group at TU Delft (prototype V3) it is possible then to derive the mass of the scaled up kite.

A strong limiting factor is the maximum WL: a measure of the force that the kite can pull per unit area.
The latest version of the kite of the TUDelft demonstrator (the V3 which has an area of 25 m^2) has been capable of a maximum pulling force of around 12260 N during the tests, which leads to a WL of 490 N/m^2. A smaller value has been found in literature [12] where the maximum WL for very large kites is reported equal to 450 N/m^2. This value is used as reference. Finally according to Skysails [39], their 300 m^3 RAM air kite is able to reach a pulling force up to 320 kN. This means WL over 1000 N/m^2. However tt is assumed that to reach reasonable lifetime of the kite it should not operate always close to the maximum WL. That is why a safety factor of 1.5 is set for the computation of the

Table 7.1: Kite specifics

surface area [m^2]	100
projected area [m^2]	72
mass [kg]	48
wing loading [N/m^2]	450
maximum traction force [N]	21600
C_l traction	0.8
C_d traction	0.2
C_l retraction	0.34
C_d retraction	0.15
Lifetime [h]	5000
Safety Factor	1.5

maximum operating traction force. Using thicker material for the canopy can increase the WL at the expense of the weight that would increase. The thickness of the fabric of the canopy is computed as directly proportional to the kite WL using the TU Delft demonstrator as reference.
The estimation of the lifetime of the kite is not trivial. Being one of the most expensive components of the system and having a relatively short life time, the kite costs give the major contribution to the LCOE. It can also be seen as the fuel of the system since it has to be replaced quite often. Therefore the estimation of the lifetime can make a big difference in the final result of LCOE.
The major factor responsible for fabric degradation is UV radiation. In his work Dunker [12] defines all the contributions to the degradation of a ram-air kite. Joint degradation, abrasion, fatigue, moisture, UV radiation are considered. He finds degradation factors to scale the design factor with, for a chosen lifetime.
The design is assumed to be done to reach a lifetime of the kite of 5000 working hours.
All the results obtained and the kite specifics are summarized in Tab: 7.1

7.1.2 KCU

The KCU (kite control unit) is the component that hangs beneath the kite, controls its flight path and adjust its traction force, acting on the angle of attack depending on the phase that the kite is flying and the wind conditions.
At the current state of the art, the heaviest part of the KCU is the frame and the protection structure, but in a future possible industrialization phase, the heaviest part are expected to be the drive train (motors and gearboxes) and the battery pack.
In the kite-power field for AWE applications, the KCU can be powered by a small and fast airborne wind turbine which is attached to it. There is not much industrial experience with this component and the mass scaling function has to be derived by reasoning. The heavy components of the KCU are the batteries and the electric motors that have to steer the kite and de-power it when necessary. The sizes of those components is expected to be a function of the kite area, but a direct proportionality would lead to an overestimation of the weight. The mass of the KCU is then assumed to scale with the square route of

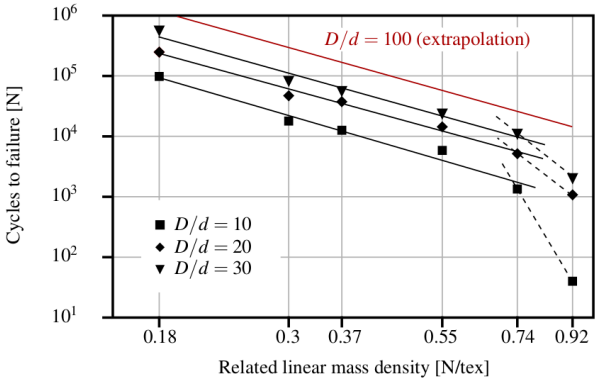

Figure 7.1: Bending cycles to failure for the tether as function of the stress and ratio of tether diameter and bending diameter [33]

the kite area.
For the 100 m^2 kite then the mass of the KCU results

$$M_{KCU} = 16kg \tag{7.1}$$

leading to a total airborne mass of 64 kg.

The same considerations made for the kite holds also for the KCU. This component also has to be replaced during the lifetime of the unit, but not as often as the kite. The lifetime of 10 years assumed in Grete [19] seems too optimistic. In this model the lifetime of the KCU is assumed equal to 5 years. The KCU is supposed to be powered by a small and fast airborne wind turbine placed on top of the KCU itself.

7.1.3 Tether

What is critical in the tether design is the fatigue load rather than the rupture load, due to the continuous bends that the the tether has to undergo. From the maximum traction derived from the kite area and the maximum wing loading, it is possible to compute the diameter knowing the allowable stress that results in a tether lifetime of around 10^5 bending cycles when the right ratio of the drum diameter over tether diameter is chosen. By visual interpolation of the curves in Fig: 7.1 the tether allowable stress is assumed 370 Mpa, when the ratio D/d is set to 50

Assuming the conservative value for the pumping cycle duration of 130 s results in a tether safe life time of 75 days, which can be boosted by a factor of 3 with an improved tether construction according to Rigo Bosman, Valerie Reid, Martin Vlasblom [33], reaching 225 days of operation.

σ [MPa]	370
d [mm]	12
m [kg]	122
l [m]	1500
ρ [kg/m^3]	724
safety factor	1.5

Table 7.2: characteristics of the tether

With such data, a tether with a cross section of 1.2 cm is required considering an additional 1.5 safety factor. The tether weight can be computed from the volume density of the material and the maximum tether length

$$M_{tether} = \rho \frac{\pi d^2}{4} l \ . \tag{7.2}$$

The maximum tether length has been chosen so to remain below the 3000 ft altitude which is the altitude allowed in restricted fight areas [6]. The relevant parameters are summarized in Tab. 7.2

7.1.4 Ground Station

As derived in Chap. 6.2 the ground-station layout will have a drum, freewheel clutch, permanent magnet generator, converter gearbox and motor on the same shaft. In the following section each of these components is analyzed, designed or chosen.

Drum

The drum is the cylinder where the tether is wound. It has to be as light as possible, not to have a big rotational inertia, but at the same time it has to be able to withstand the pressure exerted by the tether.
The diameter is chosen from the diameter of the tether. The ratio $D/d = 50$ is chosen so to prevent a rapid deterioration of the tether due to bending fatigue. Therefore the external diameter of the drum has to be 0.6 m.
The mass of the drum is computed from its volume assuming aluminum as construction material ($\rho = 2{,}70 \quad \mathrm{g/cm^3}$) with equation

$$M = \frac{\pi (D_{out}^2 - D_{in}^2) L \rho}{4} \tag{7.3}$$

For simplicity the thickness of the wall of the cylinder is taken

$$t = 0.05 \ D \tag{7.4}$$

and the length is chosen so that the tether is wound on it on 10 layers resulting in a drum length of

$$L = \frac{ld}{\pi(D + (5d))10} = 0.87\ m \tag{7.5}$$

It results in a drum mass of 126 kg

Tether Handling and Bearings and Yaw system

The tether has to be guided somehow to avoid entanglement, being consecutively rolled and unwound around the drum. To do so the drum has to be moved up and down with a speed which is a function of its rotational speed. Additional motors, pulleys and bearings for the drum are required.
Moreover the rotational axis of the drum shall be always perpendicular to the wind direction. To do so it has to be able to adjust its position. Everything has to be mounted on a bearing, like the nacelle of a wind turbine.
The friction losses are taken into account in the bearing efficiency. Assuming good lubrication the efficiency is 99%

Electrical Machines

As already explained, the choice of the specifics of the electrical machines has to be derived from the preliminary optimization (Ch: 4). The choice of the rated power of the generator installed is the upper limit of the power production during the reel-out phase. A close look at the results of the preliminary optimization and optimal tether force is needed to pick the right choice.
In the traditional wind energy industry a rated wind speed is chosen. For a chosen wind speed the power at the shaft reaches the rated power of the generator. Further increase in the wind speed does not lead to an increase of the power output, not to overload the generator. Above the rated wind speed the blades have to be adjusted (pitched) so the power transferred to the shaft is less than the available power in the wind.
The choice of the rated wind speed usually is based on the location. A trade off between increase the investment costs (for a larger generator) and increase the energy production is found.
The same approach is taken in this work, but additional considerations have to be made. The impact of additional costs for electrical machines (as already noticed in Sec:6.2) is rather low compared to the total cost of the system. Therefore it is reasonable to chose a relatively high wind speed (compared to the typical rated wind speeds of the turbines) as rated wind speed. The optimal value will depend also on the wind distribution. By looking at the energy yield plot (Fig. 4.9) it is clear that it is useless to look at speeds above 24 m/s because the energy production is already null. It should also be considered that the preliminary optimization does not take into account any constraint but the maximum

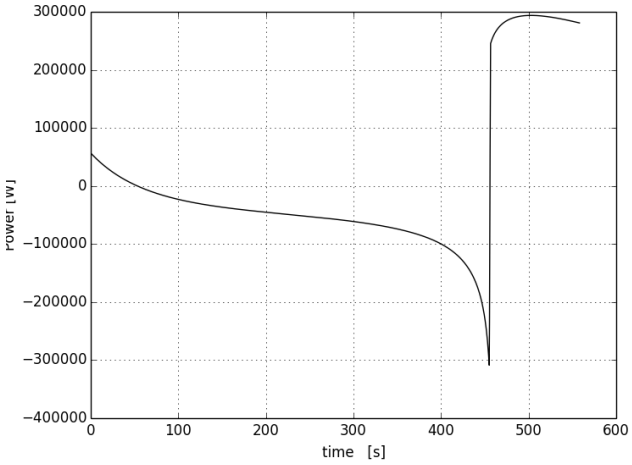

Figure 7.2: Instantaneous mechanical power at the ground station of the preliminary optimization at 21 m/s

tether force. Likely the power curve (and consequently the energy yield curve) decreases more rapidly above certain wind speeds.
For those reasons the rated wind speed is chosen equal to 21 m/s. Above the chosen speed the kite has to be de-powered and the power production would not be optimal, but not null yet. According to the preliminary optimization only 5% of the total energy is produced with wind speeds above 21 m/s.
From this choice follows that the generator and motor are chosen based on the traction and retraction average and instantaneous powers found in the preliminary optimization at 21 m/s.

While the power produced is rather constant in time during the whole duration of the traction phase, the power of the retraction phase is not. The retraction power increases steadily until peaking at the end right before the beginning of the transition phase (Fig. 7.2) in particular when the wind speed is high. During the retraction phase the kite flies progressively towards the zenith where its traction force reduces. Keeping a constant retraction force allows the reeling velocity to increase steadily during the all phase.

Two assumptions are made on the power that the machine can handle. Since the power is produced in cycles the machines have enough time to cool down during the phase when it is not operating. The average power during the phase can exceed the nominal power of the machine by a factor 1.25 and instantaneously by a factor 1.5 [19].
At the chosen rated wind speed according to the preliminary optimization the average traction power is 308 kW. Since during the traction phase the instantaneous power do not deviate much from its average value, the rated power of the generator is chosen equal to $\frac{308}{1.25} \simeq 250$ kW.
Sizing the motor according to the average value of the retraction phase is too restrictive due to the large deviation of the maximum retraction power from the average value. To ensure the correct operation up to the rated wind speed it will be then sized according to

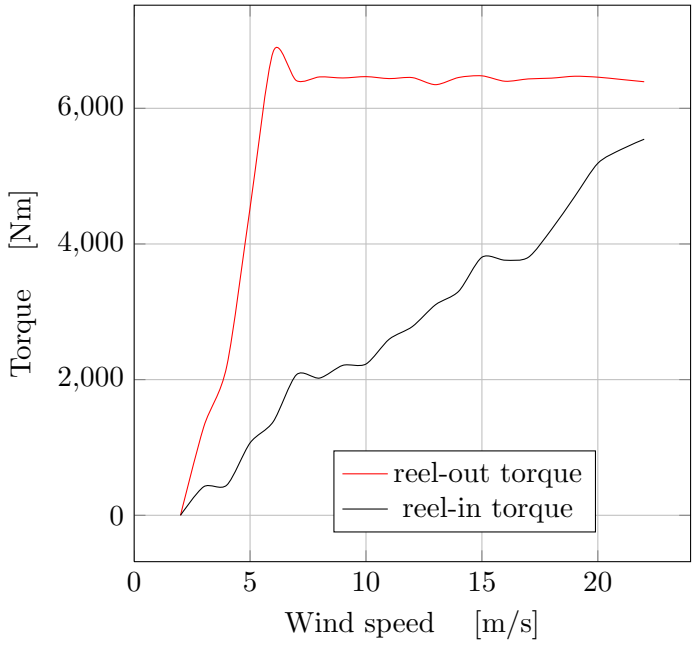

Figure 7.3: Optimal torque at the drum during the reel-out and reel-in phases

the maximum instantaneous power. From the simulation result, the maximum mechanical power reached during the retraction phase is around 200 kW, which leads to a motor with a nominal power of 134 kW, when considering the 1.5 factor.
As seen in the preliminary optimization the optimal reeling speed depends on the wind speed. Knowing the drum diameter (Sec: 7.1.4), force and speed obtained with the preliminary optimization can be converted in torque and speed (Fig 7.3 and Fig 7.4).

The relation between the synchronous rotational speed and the frequency of the electricity is

$$rpm = \frac{f\ 120}{P}\ . \tag{7.6}$$

Where f is the frequency and P the number of poles.

Generator

Concerning the generator, literature on the topic of kite power [37] and on wind energy in general [32] has been taken in consideration. The choice is a direct drive machine machine.
The disadvantages of this type of generator are [32]

- high total mass
- larger diameter

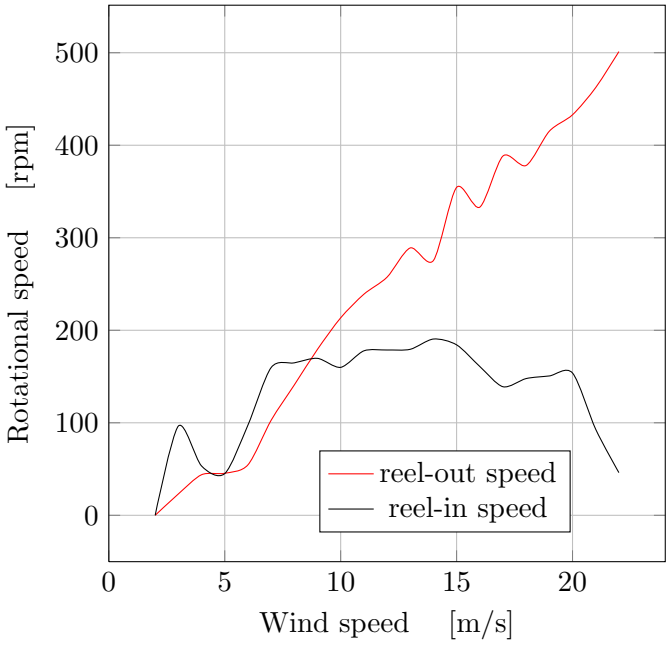

Figure 7.4: Optimal rotational speed

- cost
- necessity of converter to reach the grid frequency

.

Those disadvantages are considered not very restrictive since there is not really a mass or volume restriction at the ground station. The higher cost would be anyway a fraction of the cost of the replacement of the kite and the other airborne components. The necessity of power conversion cannot be avoided using other configurations. Fig. 7.4 considering the Eq. 7.6 reveals that the generator works in a speed range from 20 rpm to 460 rpm. The speed at which most of the energy production occurs (considering the Weibull distribution) is around 200 rpm (at 9 m/s of wind speed). By having a machine with 30 poles at that speed the electricity produced will be already at 50 Hz. With such a machine the maximum frequency of the electricity is 115 Hz (at 21 m/s of wind speed) and the minimum is 5 Hz (at 3 m/s) which has to be converted in 50 Hz by the power electronics before being fed in the grid.
From the analysis done in Sec: 6.2, an appropriate electrical generator can have an electrical efficiency of around 90 % on average over the whole operating wind range and this value is used for the final optimization.

Motor

Referring once again to the work of Schölkopf [37], the typology of the machine is chosen so as to avoid the need of the gearbox. The same typology of permanent magnet synchronous machine is chosen. From Fig. 7.4 the operating points required at different

wind conditions are known. The optimal average value of the retraction velocity remains between 150 and 200 rpm. Sizing the machine for a nominal speed of 175 rpm results in a machine with 34 poles .
Even for this component the result of Sec: 6.2 is used as reference and the electrical efficiency is assumed equal to 80 %.

Freewheels Clutches

With the configuration proposed there are two counter rotating machines, one per phase. This requires that when one is rotating the other is not, otherwise the energy fed to the machine which is rotating is processed also by the other machine with consequent increase in losses. The decoupling can be made with freewheels clutches. It is mechanical, does not require any kind of active control and it does not increase the risk of failure.
From catalog [30] the appropriate component has a weight of 38 kg and negligible losses.

7.1.5 Transformer

A transformer is necessary to step up the voltage right after the production of electricity. The voltage is stepped up to decrease the joule losses in the cables. Those are proportional to the square of the current. The choice of the in-field voltage is a trade off between current and voltage. Increase the voltage implies thicker (and therefore more expensive) insulation, on the other hand higher currents densities implies high joule losses. The appropriate voltage level is discusses in the following chapter where the costs are analyzed.

Power Electronics

As already stated in the previous section, having a variable speed synchronous machine implies that the frequency at which the energy is produced is changing, depending on the rotational speed of the drum which in turn depends on the wind speed. However the electricity that goes to the grid has to be at 50 Hz.
By using the formula of the frequency of the energy from a generator

$$f = \frac{\omega P}{120} \tag{7.7}$$

where ω is the rotational speed in rpm and P is the number of poles of the generator, and knowing the range of rotational speeds where the system will have to operate determines the frequency of the electricity in a range from 5 Hz to 115 Hz for the generator.

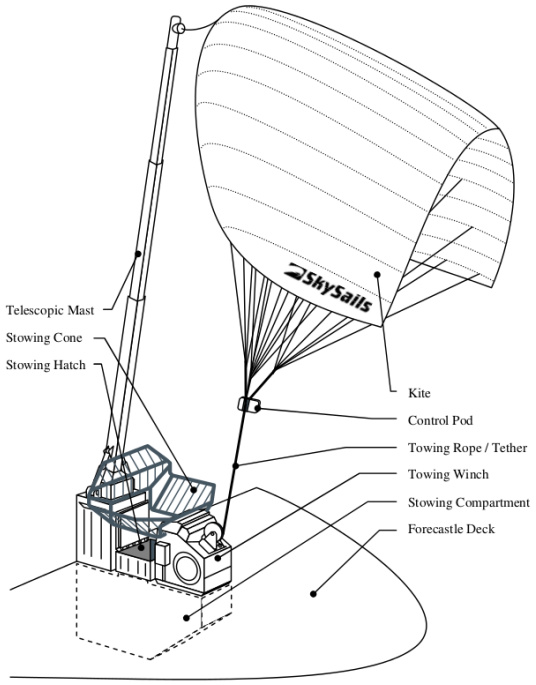

Figure 7.5: Skysails ground station for ship traction Falko Fritz [15]

Launching and Landing System

The only automatic launching and landing system for flexible ram-air kite nowadays implemented in industrial applications is the patent of Skysails (Staack [40]). This system consist in a telescopic mast as depicted in Fig: 7.5

A thin string connects the middle of the leading edge of the kite to the top of the mast. This string also has to elongate as the kite flies further away from the mast. A set of sensors detects when the kite is inflated and is ready to take off. Then the main tether is unrolled slowly until the kite reaches the desired altitude.
When the kite has to be recovered, the process is repeated in reverse: the kite is guided by the small string to the top of the mast while the main traction tether is retrieved. Once is in the final position, right at the top of the mast, the steering lines are shortened and the kite deflates and can be recovered.
The design criterion for the mast should be the maximum force from the kite that it has to withstand. This would be the aerodynamic force of the kite when it is recovered in high wind.
A detailed design of it is beyond the scope of this work.

Cover Frame and Recovery Room

Everything should be covered with a light, resistant and accessible frame to protect the component from the outdoor environment. There is also the need to recover the kite during the periods of non operation when the wind speed is too high or too low. Therefore The volume inside the cover has to be sufficient to contain all the components and the deflated kite then.
Considering 0.5 m^3 needed every 25 m^2 of kite area results in a recovery volume of 2 m^3 on top of which the space for the drum and the generator has to be added.
An appropriate sizing of a sort of dome which includes everything would be an half ellipsoid with a elliptic base of 4 m by 2 m and 1.5 m high in the middle. This result in a surface area of 37 m^2. Considering a cover in plexiglas 3 cm thick with a density of 1.19 g/cm^3 result in a mass of the cover of approximately of 1300 kg

Chapter 8

Farm Design

In this chapter the unit that has been designed in Chapter 7 is placed in array. Additional aspects have to be investigated, and the advantages of having clusters of units producing at the same time is studied.

8.1 Spacing Between Units

The first aspect to be investigated when considering the farm configuration is the distance between the units. From the spacing many aspects of the farm are derived like the length of the infield connection and land requirements.
In traditional wind farms the spacing between the turbines is mainly chosen to reduce the mutual interaction of the turbines due to wake effects. This approach however does not lead to conclusions in case of kite farm. No studies have ever been performed on wake effects from kites. The wake is neglected in this work. This assumption is justified by the size of the kite area, which is smaller than the turbine area relatively to the swept area. Moreover experience with sport kites suggest that the wake of a kite is negligible. Finally the possibilities to fly at different heights or maneuvering the kite in a way to avoid that the downwind one is in the wake of the up wind one, justify the assumption made. A more extensive and quantitative analysis of the wake of the kite is reported in App. A.
The spacing between the units is determined by the correct operation of the systems, avoiding entanglements of the airborne components.

In Fig. 8.1 two system are sketched from a top view and the wind is assumed according to the arrow. The blue area is the area swept by the tether and the two areas should not interfere to ensure the correct operation of the units. In this case the minimum distance

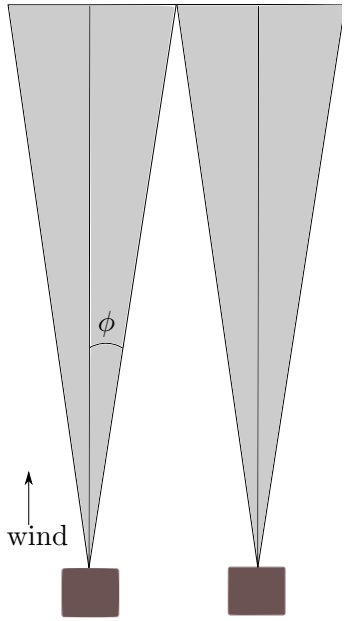

Figure 8.1: Top view of two units lying perpendicular with respect to the wind direction

between the units to avoid interference is

$$d_u = 2L\sin(\phi). \tag{8.1}$$

Another aspect that should be taken into account is the distance of two synchronized units which are aligned with the wind velocity. The approach of Heilmann [21] is followed to analyze the minimum safe distance between two units aligned with the wind direction (Fig. 8.2).

In this case the minimum distance (d_u) between the upwind unit (1) and the downwind one (2) can be computed considering the red triangle in Fig. 8.2 and reported in Fig 8.3. The sum of $L_{1,1}$ and $L_{1,2}$ is equal to the tether length (L), which in the worst case scenario is the maximum tether length.
Those two segments can made function of the segment G as

$$L_{1,1} = \frac{G}{\tan(\Omega)} \tag{8.2}$$

$$L_{1,2} = \frac{G}{\tan(\eta)}. \tag{8.3}$$

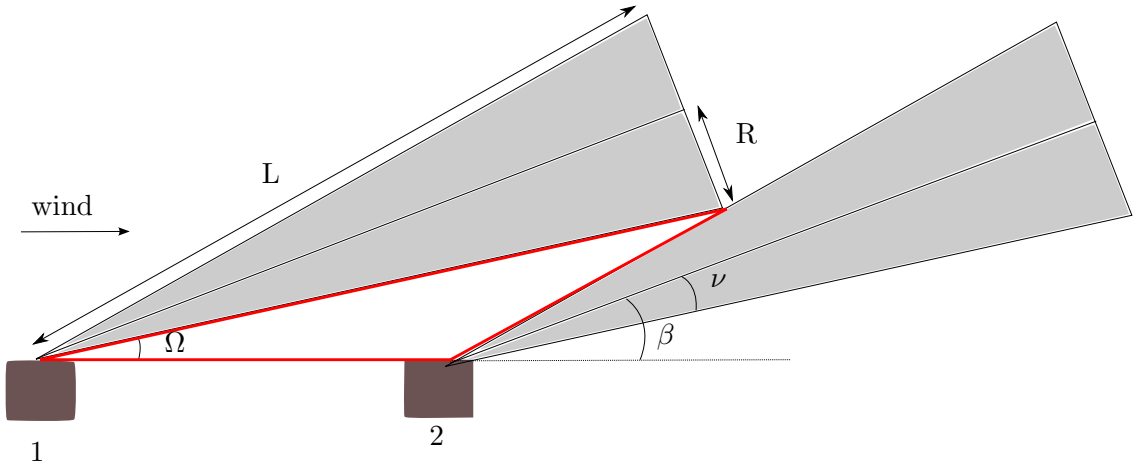

Figure 8.2: Side view of two units aligned with the wind direction

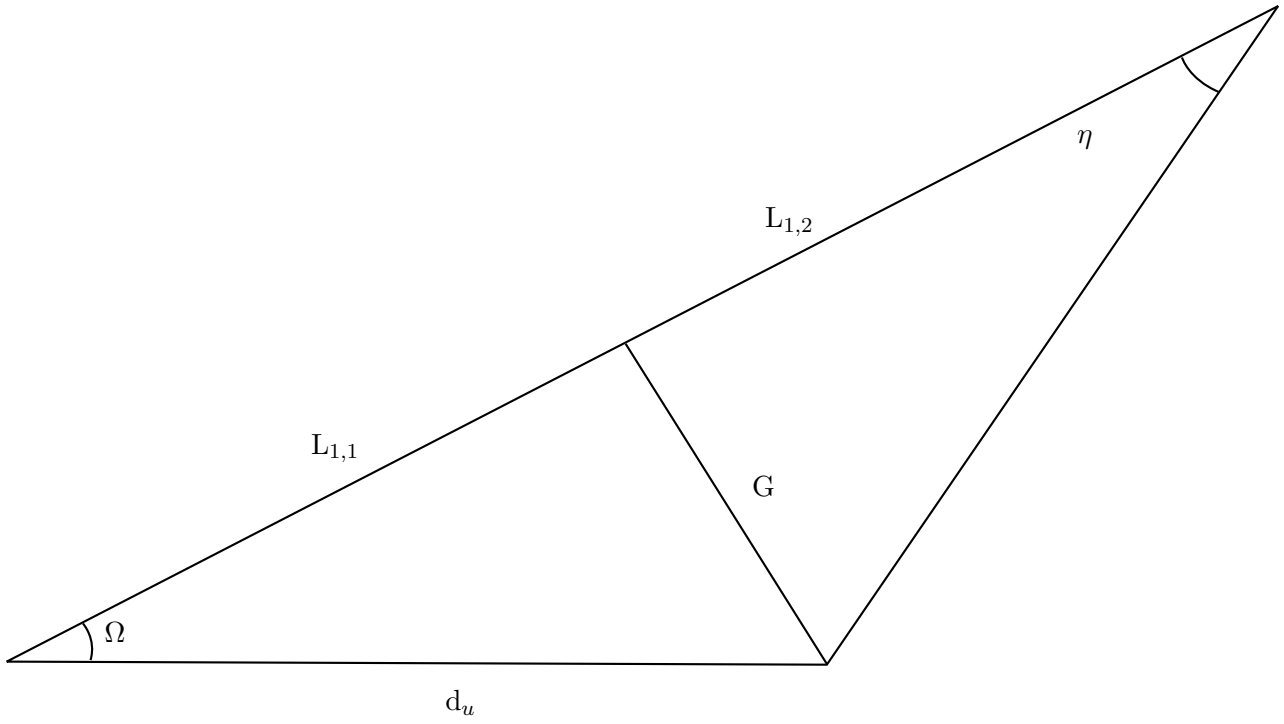

Figure 8.3: Analysis of the distance between the units

Therefore

$$G = \frac{L}{\frac{1}{\tan(\Omega)} + \frac{1}{\tan(\eta)}}. \tag{8.4}$$

The minimum distance (d) to avoid entanglements is

$$d_u = \frac{G}{\sin(\Omega)}. \tag{8.5}$$

by coupling Eq. 8.4 and Eq. 8.5 and considering the following relations of the angles

$$\Omega = \beta - \nu_1 \tag{8.6}$$
$$\eta = \beta + \nu_2 - \Omega = \nu_1 + \nu_2 \tag{8.7}$$

the expression for the minimum distance between two perfectly synchronized units aligned with the wind direction result.

$$d_u = \frac{L}{\sin(\beta - \nu_1)(\frac{1}{\tan(\beta - \nu_1)} + \frac{1}{\tan(\nu_1 + \nu_2)})} \tag{8.8}$$

The most restricting of the two distances results the one in down-wind direction. Iter-units control is required, the position of every kite should be known so to operate the farm safely.
The distance between the two units is studied considering the possible phase shift between the units and the maneuverability of the kite.
The phase shift of the units aligned with the wind should anyway kept small. If the downwind kite is delayed with respect to the upwind one, it would start the retraction phase when the other one is still in the traction phase. It would start to fly upwards in the direction of the other kite and the two tethers might entangle. On the other hand if the upwind one is delayed the risk of entanglement is at the beginning of the traction phase. The upwind kite would start to fly with a low elevation angle while the downwind one is still retracting and likely has overflown its ground station. Even in this case the risk is too high and shall be avoided.
The solution of flying with very different azimuth angles would decrease tremendously the traction power which is maximized for an azimuth angle of 0. For those reason the Eq. 8.8 is be used for equal spacing between the units considering the units are synchronized. For safety reason only a small phase shift is assumed. It results that the distance increases if the downwind kite (2) is delayed respect to the upwind one (1) (Fig 8.2).
The distance a is function of the values of the two angles β and ν. The minimum value that it can assume deserves some additional thoughts.

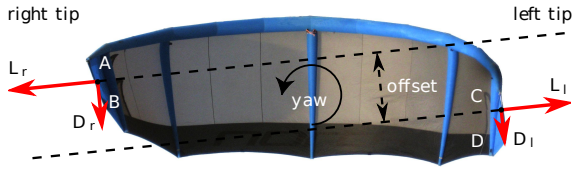

Figure 8.4: Vector representation of the side forces on a kite with a steering input on the right tip [34]

The elevation angle (β) is an operational parameter. Even thought it is not the most relevant and the sensitivity of the model to variation of it has been proven to be rather low [19] it should not be set to ensure the minimum distance but the highest system efficiency. The minimum value of alpha is around 15° for very low wind speed with the system analyzed.
The value of the angle ν is simply a measure of the height (R) of the figure of eight trajectory that the kite flies.

It can be written as

$$\nu = \arcsin(R/L) \tag{8.9}$$

So it is function of the trajectory that the kite can fly and the tether length. Large values are not desirable because it implies that the kite spend more time in the turning maneuver which take place far from the perfect downwind position and therefore with a lower resultant traction force.

To understand how fast the kite can steer first an overview of the basic dynamics of the kite in the steering maneuver is necessary. By pulling one of the steering lines the kite, due to its flexible structure, deforms and the angle of attack of one tip increases while the tip itself moves a bit forward in the direction of the flight. The non aligned and different aerodynamic side forces create a turning moment which makes the kite yaw (Fig. 8.4).

It has been suggested [14] that a good approximation of the aerodynamic side force that makes the kite steer when the steering input is small, is linearly dependent on the steering input (δ, which can be considered as the difference in length of the steering lines) and can be computed as

$$F_{a,s} = C_{st} v_a^2 \delta, \tag{8.10}$$

with v_a the apparent wind velocity.

The speed at which the kite can turn ($\dot{\chi}$) has been modeled in previous works [14] assuming that the roll angle is small, as function of the aerodynamic parameters (C_l and C_d ant their ratio G), position (elevation angle α azimuth angle Φ kite course angle χ) and mass

of the kite (m), and the steering input that the control unit is able to apply (δ) and the constant K which depends on the shape of the kite.

A simpler more intuitive derivation of it is to compute the equilibrium of the forces in the plane tangent to the top surface of the kite and perpendicular to the tether. Which results including the mass (m)

$$F_{a,s} + m\mathbf{g} \cdot \mathbf{e}_y^k = mR\dot{\chi}^2 \tag{8.11}$$

Were the unit vector $\mathbf{e}_y^k$ is the one defined by

$$\mathbf{e}_y^k = \frac{\mathbf{e}_r \times \mathbf{v}_{k,t}}{v_{k,t}} \tag{8.12}$$

Assuming that $v_{k,\tau} >> v_w$ and therefore $v_a \simeq v_{k,\tau}$ considering the kinematic relation

$$v_{k,\tau} = R\dot{\chi} \tag{8.13}$$

where R is the instant curvature radius, the Eq: 8.11 can be written as

$$C_{st} v_a^2 \delta + m\mathbf{g} \cdot \mathbf{e}_y^k = m v_a \dot{\chi} \tag{8.14}$$

which can be solved for the turning speed $\dot{\chi}$ in the form

$$\dot{\chi} = \frac{C_{st} v_a \delta}{m} + \frac{\mathbf{e}_y^k \cdot \mathbf{g}}{v_a} \tag{8.15}$$

The type and design of kite obviously affects its maneuverability: a more flexible kite deforms more than a rigid one making it more sensitive to steering input; a kite with larger tips develops higher side forces, making it turn faster. Those aspects are taken into account in the coefficient C_{st} With the turning rate law the kinematic ratio (Eq. 8.13) can be solved for the curvature radius and the height of the figure of eight maneuver can be estimated.

Plotting the minimum distance as function of the elevation angle and the height of the figure of eight maneuver (Fig.8.5) results that the distance is very sensitive to the height of the figure of eight which in turn depend on kite maneuverability and control units characteristics. For additional reasoning on the distance considering a small phase displacements between the units see App. B

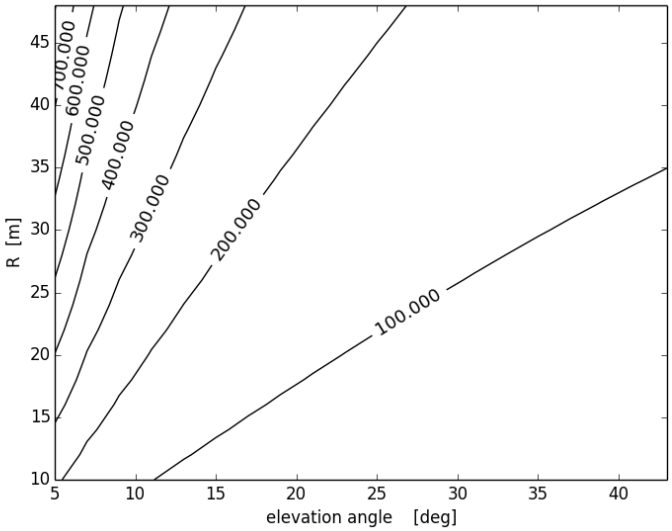

Figure 8.5: Minimum distance between the units as function of the elevation angle and the height of the figure of eight considering the maximum tether length (1500 m)

8.2 Electrical Connection

Even for this aspect the analysis starts from the traditional wind energy industry. The difference is that the production of energy is not continuous. The farm acts like a grid with loads (when a unit requires energy) and production nods depending on the moment. The kites in the retracting phase take the necessary energy for the retraction phase from their connection. The higher production during the traction phase and the phase displacement among them ensures that there is always a positive net energy flowing out of this in-field connection which can be fed to the grid, and there is no need of batteries, which would be a necessity for the case of a single system.
Many different in-field electrical configuration are listed in literature. In the work of Pierik et al. [31] an extensive analysis is performed over the different possible configurations, to choose the type of connection that leads to the lowest production cost. The cheapest solution results constant speed system and individual variable speed with back to back converters.
The first solution would not be feasible for kite system. Every units needs to work independently to the others to allow phase shift. Therefore the best electrical configuration remains the one with individual variable speed.

Every unit needs the appropriate power electronics unit to convert the electricity to the right frequency. Then a transformer steps up the voltage to 22 kV avoid high in field losses.

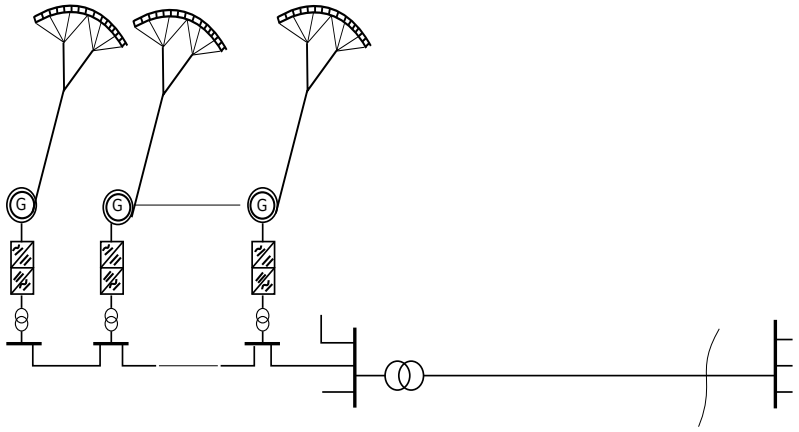

Figure 8.6: Electrical layout of the farm

8.3 Energy Production

Some thoughts are put into understand the power production of different units. A model is set up for this purpose. The instantaneous maximum power of the single unit obtained (results of the final simulation are presented in the following chapter) with the quasi steady simulation is cycled for a defined number of cycles (Fig. 8.7).

It is now possible to build a farm, adding more kites and summing up all the contributions of the single units.

From the previous section of this chapter it is already clear that the units aligned with the wind shall be approximately synchronized, while the units that are lying mutually in the cross wind direction shall work with a phase shift. The kites aligned with the wind direction are addressed as columns and the ones perpendicular to the wind direction are called rows. Imagining a squared array of units, there are two extreme possibilities. The wind can blow perpendicular to the side of the farm (as in Fig. 8.8) or perpendicular to the diagonal of the squared array of units (as in Fig 8.9).

The computation of the sum of the contributions differs for those two situations. In fact in the orthogonal wind case (Fig. 8.8) the columns are all with the same number of units, while this is not case when wind blows in the diagonal direction (Fig. 8.9). The time phase shift between the columns is chosen depending on the wind situation. For the case of orthogonal wind case the phase shift is set equal to the cycle duration divided by the number of columns in the array. For the case of the diagonal wind the phase shift is the double of cycle duration divided by the number of columns. This ensures that the outer columns (far from the diagonal aligned with the wind direction) are synchronized and in opposite phase of the inner columns, which in turn have a higher number of units. Those phase shifts have proven to lead to the lowest normalized percentage standard deviation for both wind cases (see App. D).
Additionally the feature of a small phase shift between units on the same column is im-

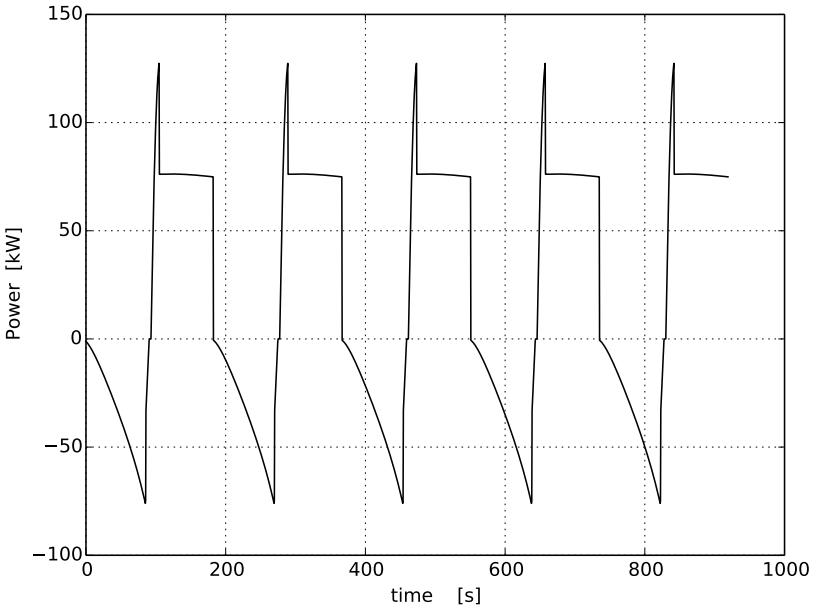

Figure 8.7: Instantaneous electrical power of a single kite as function of time at 8 m/s of wind speed

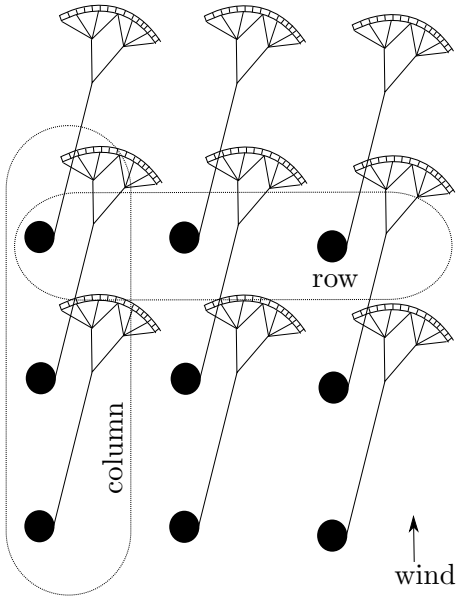

Figure 8.8: Schematic view of the farm

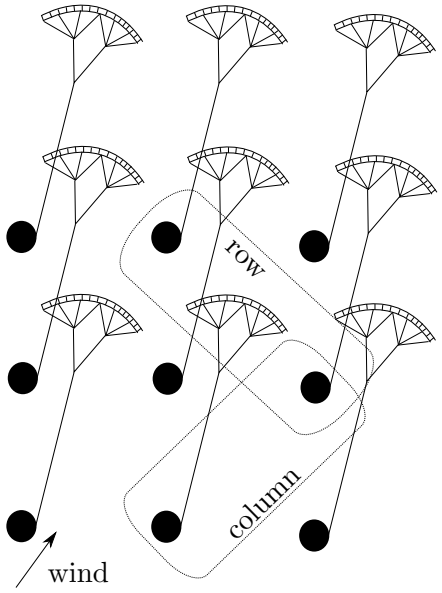

Figure 8.9: Nomenclature when the wind is perpendicular to the diagonal of the farm

plemented. The distance is set according to the maneuverability of the kite and to the maximum phase shift of the units in the same column. The phase shift of the units on the same column can be chosen as a percentage of the total cycle duration.

The power production changes depending on the number of kites (Fig. 8.10), the wind direction with respect to the array (By comparison of Fig. 8.11 and Fig. 8.10) and the wind speed (Fig. 8.12).

It appears that the oscillations of the instantaneous power increase in frequency when the number of kites is increased at the same wind speed (Fig. 8.11 and Fig. 8.10). It can be noticed that the the power remains always positive increasing the number of units. This is a good advantage with respect to the stand alone unit, because it removes the need of energy storage to operate the system when the kite is in the retraction phase. From a first visual comparison it seems also that the orthogonal wind speed leads to a more constant power, while the diagonal wind situation leads to periodic and larger oscillations.
Meanwhile with the increase of the wind speed, the power necessary for the traction phase and the retraction phase of a unit increase as well. Having different sign (negative for the retraction and positive for the traction), the power oscillates more. This effect is shown in the Fig. 8.12 and Fig. 8.13 for a fixed array of kites respectively with orthogonal wind and diagonal wind. The different length of the simulation time is because the same number of cycles is simulated, but the duration of one cycle varies with the wind speed. The duration of each cycle decreases from 4 to 7 m/s because the optimized reeling velocity increases with the wind speed. Then the duration increases again from 7 to 12 m/s because the maximum reel-in velocity is being reached. From this comparison the periodic oscillation of power in diagonal wind conditions is made more clear.

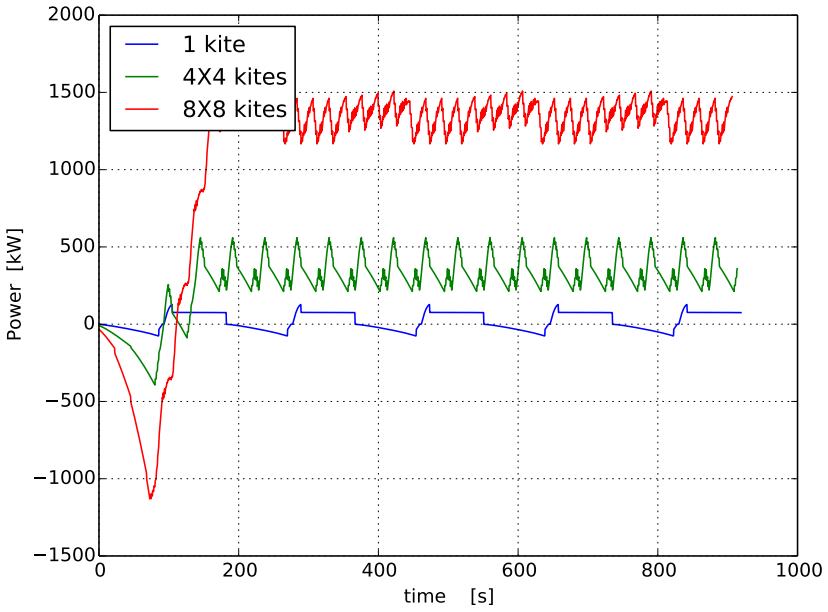

Figure 8.10: Instantaneous power production with different array sizes with 8m/s of wind orthogonal to the array

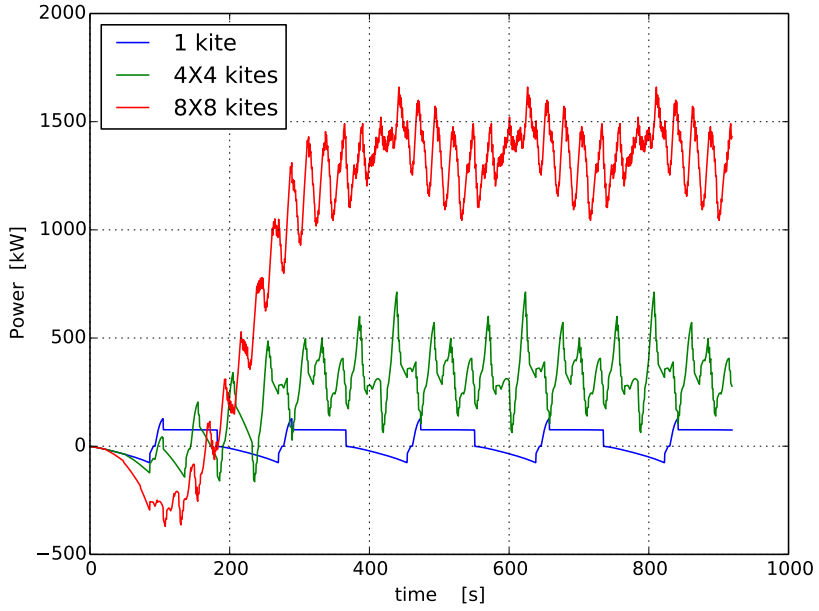

Figure 8.11: Instantaneous power production with different array sizes with 8m/s of wind diagonal to the array

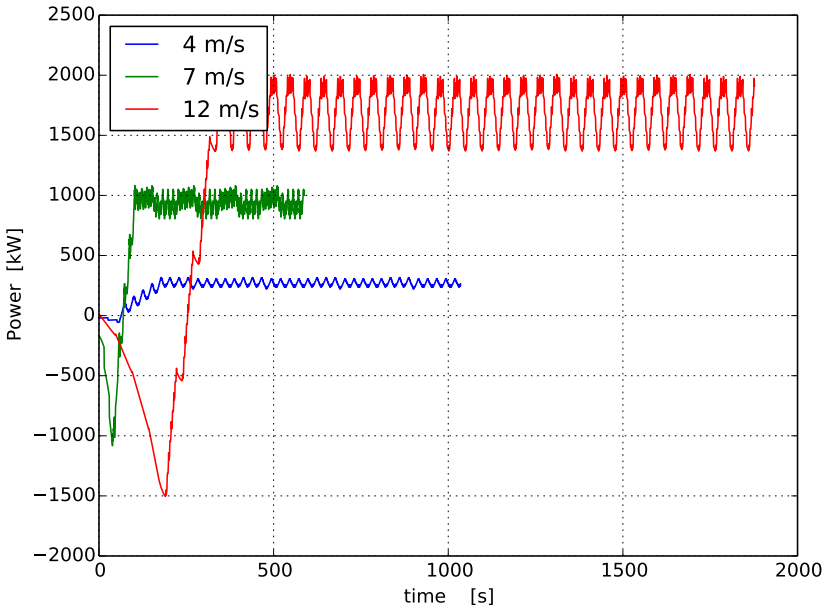

Figure 8.12: Instantaneous power production with different wind speeds for an array of 8X8 kites. The figure refers to the case of orthogonal wind

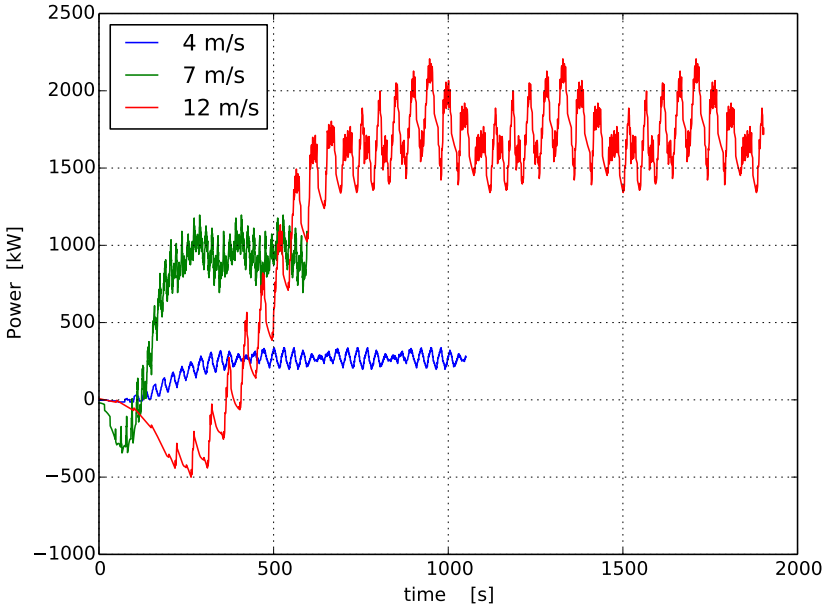

Figure 8.13: Instantaneous power production with different wind speeds for an array of 8X8 kites. The figure refers to the case of diagonal wind

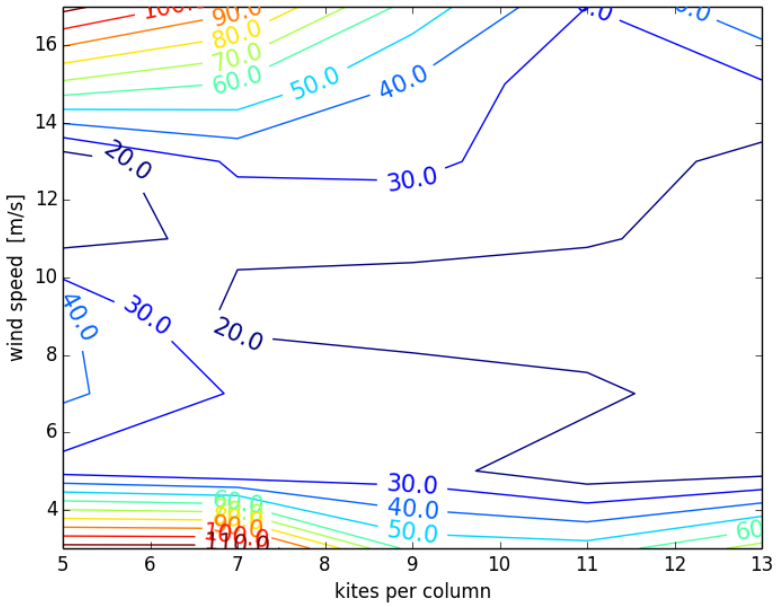

Figure 8.14: Normalized standard deviation of the instantaneous power for different number of kites in the array and different wind speeds orthogonal to the side of the farm

The power trend is analyzed using the normalized percentage standard deviation. The normalized standard deviation is the ratio between the standard deviation and the average value of the sequence (App. D). Looking at the graphs presented, it can be understood that the normalized standard deviation is be both affected by the wind speed and the number of kites per column of the farm. The value is plotted in Fig. 8.14 and Fig 8.15 in a contour as function of these two variables for the orthogonal and diagonal wind cases. It can be noticed that the value of the normalized standard deviation decreases increasing the wind velocity as long as the average power increases. Above 12 m/s the average power decreases (as already seen in 4) due to the increase of the energy required to reel-in the kite. As a consequence the normalized standard deviation increases, being inversely proportional to the average value of the power.
Increasing the number of kites has the positive effect of decreasing the standard deviation. The power oscillation remains of the same amplitude, its frequency increases with the number of columns, while the average power increase with the number of units. The two contours show that the situation with diagonal wind is generally better than the orthogonal case. The reason for this is because with the same array the diagonal wind case results in more columns which can be phase shifted and the power output can be leveled out better.

In all the graphs presented the phase shift between the units in the same column is assumed null. The graphs change when this is not the case and there is a phase shift between the units in the column. The effect differs if there is orthogonal wind or diagonal wind for more details and effects of the phase shift in the columns read App. D. In this work the phase shift between units in the same column is assumed null. A perfect control

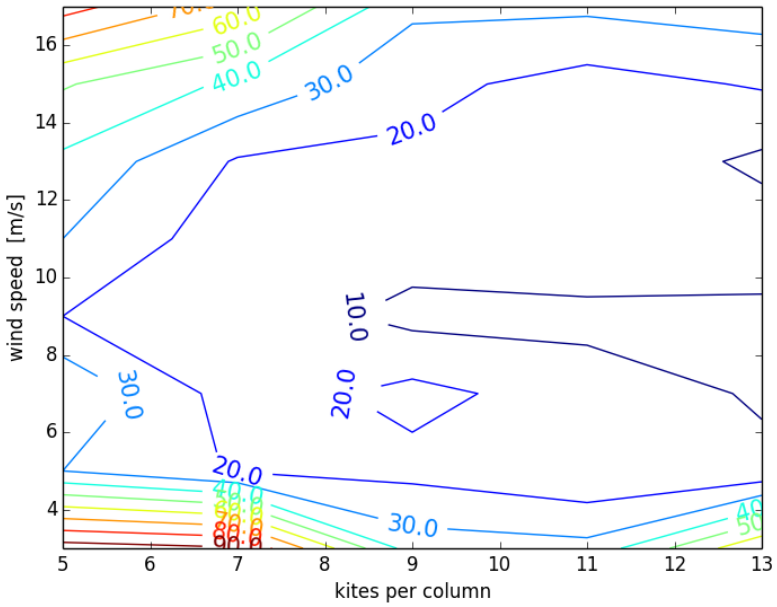

Figure 8.15: Normalized standard deviation of the instantaneous power for different number of kites in the array and different wind speeds diagonal to the side of the farm

on every single unit is known to be impossible and small phase shifts between units in the same column might be always present due to this reason. Moreover this would be affected by the wind velocity and direction in the array. A comprehensive analysis of the behavior of the farm would imply the analysis of two stochastic phenomena (not perfect synchronization and wind turbulence in the array). For the sake of simplicity of the analysis, stochastic phenomena are not taken into account here. Only Some extreme results when the synchronization in the columns is not perfect are presented in App. D. The real behavior of the farm is expected to be within those extremes.

8.4 Control Strategy

The central control of the farm should be able to detect the wind direction relative to the farm layout and adjust the mutual control strategy of the single units so to apply the right strategy according to the wind direction. In conclusion all the possible directions can be divided into 8 sectors of 45° each. The central control unit of the farm has to be set in such a way so to detect in which sector the wind is blowing and adjust the mutual control of the units so to obtain the right and safe operation of the farm.

To avoid continuous changes when the wind direction is on the boundary between two sectors (Fig. 8.16), a hysteresis based control can be implemented. There is no need to change sharply the control strategy when the wind direction crosses the boundary.

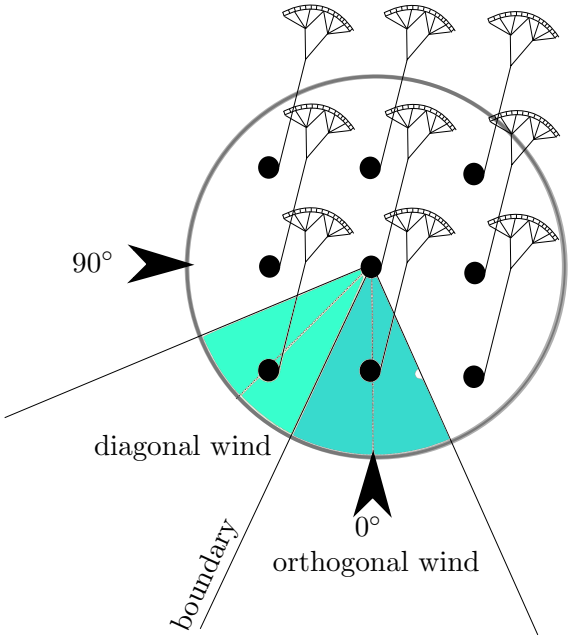

Figure 8.16: Orientation of the farm

Therefore an interval of 10° can be set around the direction of the boundary to implement the hysteresis loop for the control. The principle of the hysteresis control strategy is sketched in Fig. 8.17.

8.5 Final Farm Design

With the considerations made in the previous section an idea of a plausible on shore farm configuration is presented.
The estimation of the minimum distance is done with the Eq. 8.8 . The value of C_{st} is extrapolated for a 100 m^2 kite from data in Fagiano et al. [14] and set equal to 8.8 kg/m^2 . The curvature radius considering a steering input of 0.3 m and the apparent wind speed (25 m/s) is estimated to be around 35 m. (see App. B for the details)
In the worst case scenario the elevation angle is the minimum (15°) and the tether length is at the maximum (1500 m). To consider the case that the control is not perfect, the downwind unit is assumed to be delayed respect the upwind one of 10 % of the duration of the cycle. This ensures us to be on the conservative side of the distance leave the possibility to have small disturbances in the control.

In this case the distance between two units aligned with the wind direction computed with the Eq. 8.8 results 215 m. For a more extensive explanation of the computations made see App. B

The criterion used to choose the number of units per row is to have positive power output

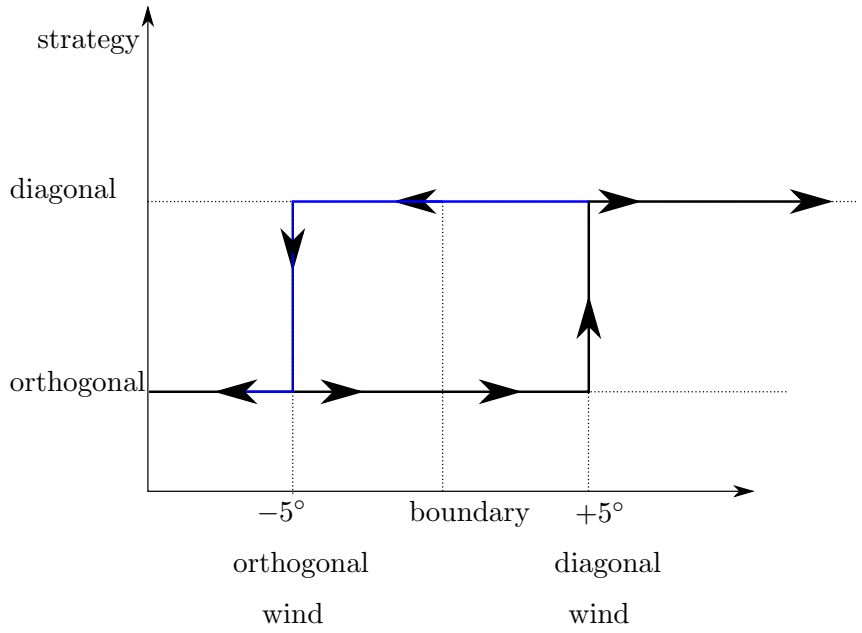

Figure 8.17: Hysteresis based control strategy

in any operational conditions. As seen in Sec: 8.3 the cumulative instantaneous power decreases with the increase of the wind speed. According to the simulation the power of the farm remains always positive in both cases (wind perpendicular to the side of the farm and wind perpendicular to the diagonal of the farm) at the highest operating wind speed (22 m/s) when there is a number of kites on each row ≥ 24 (with all the units in the column perfectly synchronized).

The rated power of the farm is the rated power of the single unit multiplied the number of units of the farm. The rated power of the unit in turn is not the power at the rated speed, which is rather low, nor the rated power of the generator, which would be too high, but is the highest average power over the cycle that the unit can achieve. This power is only a fraction of the maximum mechanical power of the traction phase because of the presence of the retraction phase (duty cycle efficiency) and the efficiency of the mechanical and electrical components.

Chapter 9

Cost Model

In this Chapter a list of all the relevant costs for a farm of kites and their functions is presented. The costs are referred to an on shore farm.
The analysis and the relations used are taken from similar works specifically on the topic of kite power [21] and [19] and on wind turbines farm [50] [26]. The costs are expressed in €(2014) per component or per service. When are referring to periodic services ,the interval to which are referring to is indicated.

9.1 Farm Design Costs

Under Farm Design costs are collected all the costs of the management engineering and design, necessary to come up with the most appropriate and layout of the farm. Also data collecting campaign, feasibility study and site assessment are included.
Since so many aspects of the project are under this voice, the independent variable is not easy to choose. In literature has not been found a common agreement on what influences most the design cost. Simplifying the approach of Zaaijer [50] used as reference, the farm design cost are evaluated as

$$C_{farm\ design} = 0.027 \cdot P_{farm}\ , \tag{9.1}$$

This costs are supposed to include also all the permits and the paper work and it is assumed to be paid at the beginning of the lifetime of the farm.

9.2 Hardware

9.2.1 Ground Station

Foundations

For this aspect of the cost the literature is rather scarce, and no system in operation can be taken as reference. In papers on wind turbines usually those costs are made function of the tower mass [50]. The literature which refers specifically to kites [21], referring to the cost of the foundations, with some reasoning on mass and moment at the ground station, considers those costs negligible. Therefore the cost of the foundations are considered negligible in this work as well.

Electrical Machines

A single cost model for the electrical machines can be implemented and since the generator and the motor chosen seem to have fairly similar characteristics. Every electrical machine in principle could be used in both modes of operation without big structural changes. According to literature [21] the following formula is used

$$C_{electrical\ machine} = P_{nom} \cdot 1208 \cdot \omega_{nom}^{-0.6} \tag{9.2}$$

Where the power is expressed in kW and the rotational speed in rpm

Drum

The cost of the Drum, according to Heilmann [21], is function of the row material which is proportional to the mass and the labor which is made function of the diameter

$$C_{drum} = c_{al} \cdot M + c_{lab} D \tag{9.3}$$

with the coefficient $c_{al} = 1.54\ €/kg$ and $c_{lab} = 5000\ €/m$

Freewheel clutch

This is the component necessary to decouple the machines when are not operating. The cost of the clutch is considered as function of the nominal torque [30] as

$$C_{clutch} = c_{clutch} T \tag{9.4}$$

With $c_{clutch} = 0.6$ €/Nm

Power Electronics

The power electronics cost is usually made function of the power (expressed in [kVA])that the component has to process. From Lundberg [26] the following formula is used

$$C_{power\ electronics} = 108 \cdot P_{rated} \tag{9.5}$$

Transformer

The choice of the transformer follows from the choice of the layout of the farm. In wind energy industry different type of clustering the turbine implies different number of transformer, with different characteristics. The cost of this component is in literature [50] function of the nominal power and the winding ratio (r). The following formula is used

$$C_{transformer} = (3.06 \cdot 10^{-3} \cdot P_{rated} + 610) \cdot e^{0.039r} \tag{9.6}$$

To reach an infield voltage of 22 kV and assuming an output voltage of the generator of 500 V the winding ratio is set equal to 44. No optimization has been done on this voltage level because considered beyond the scope of the present work.

Tether Handling, Bearings and Spindle Motors

Even if those components are really specific for the kite power technology, for a first estimation in previous work the cost has been derived from the cost of similar components of the wind turbines. In the work of Heilmann [21] the costs of those components are function of the maximum tether force are used

$$C_{tether\ handling} = 50 \cdot \sqrt{F_{tethermax}} \tag{9.7}$$

$$C_{bearings} = 40 \cdot \sqrt{F_{tethermax}} \ . \tag{9.8}$$

Cover Frame

Even for this component the cost has been derived from the wind turbine industry, in particular from the cover frame of the nacelle of the turbine, which needs to have similar requirements. The empirical relation with the rated power derived by Heilmann [21] is used as reference

$$C_{cover\ frame} = 10 \cdot P_{rated}^{0.85} + 300 \ . \tag{9.9}$$

Launch and Landing System

For this components the research groups and the industries involved in the topic still seem to require some time to come up with a common solution. In fact every kind of airborne wind energy system requires a peculiar solution.The coefficients of the equation used in the work of Heilmann [21] are adjusted to match with the result of the Design Synthesis exercise of Van Baelen et al. [44]. The cost function results

$$C_{launch\ and\ landing} = 10 M_{kite} \sqrt{Area} \ . \tag{9.10}$$

9.2.2 Airborne Components

Kite

For the cost of the kite the approach of Grete [19] and Heilmann [21] is followed. In their model the cost of the kite is function of the material used and the additional costs for the manufacturing and delivering it, which are proportional to the area. The row material scales with the total surface area of the kite and the thickness of it. In turn the thickness of fabric of the kite is made proportional to the wing loading.

$$C_{kite} = c_{k,m} A t_k + c_{k,o} A. \tag{9.11}$$

The thickness in unknown. The cost is made then function of the wing loading, using the wing loading of the TU Delft demonstrator kite as reference. The cost function becomes

then

$$C_{kite} = c_{k,m} A \frac{WL}{WL_{ref}} + c_{k,o} A. \tag{9.12}$$

The coefficient $c_{k,m}$ and $c_{k,o}$ accounts respectively for the material cost and for all the other costs (manufacturing, deploying R&D etc.)

Taking the kite of the TU Delft kite power group as reference, the coefficient are derived and the total cost of the kite is computed with the coefficients

$$c_{k,m} = 54 \ \text{€}/m^3 \tag{9.13}$$
$$c_{k,o} = 1.5 \ . \tag{9.14}$$

KCU

The cost of the KCU is computed using the same approach taken by Grete [19]. The approach is as follows

$$C_{KCU} = c_{KCU,fix} + c_{KCU,var}\sqrt{A} \ . \tag{9.15}$$

Considering the current state of the art, the possible decrease in price due to scale effect of mass production the fix and variable costs coefficients are set

$$c_{KCU,fix} = 2000 \ \text{€} \ , \tag{9.16}$$
$$c_{KCU,var} = 100 \ \text{€}/m \ . \tag{9.17}$$

Tether

The cost function of the tether is quite straightforward. On the market and literature [33] the price of the fiber function of the cross section and length of the cable.

$$C_{tether} = c_t \frac{\pi d^2}{4} l \ . \tag{9.18}$$

With $c_t = 0.045$ €/mm^2/m.

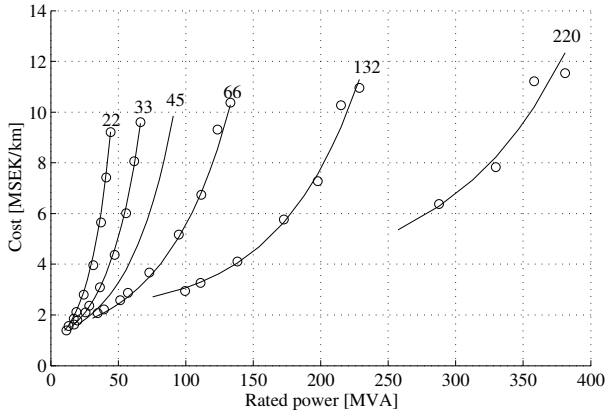

Figure 9.1: Cable cost as function of the power the different lines refer to different voltage levels Lundberg [26]

9.2.3 Electrical in Field Connection

The Cost of the cables depends on the voltage and the current that they are required to transmit, since the voltage increase the mass of the insulation and the current the mass of copper (9.1). Moreover lowering the voltage increase the current (keeping the same power), and the losses due to high currents increase as well. Therefore an optimum for the infield voltage level should be found and the cables should be chosen according to that.

For the 22 kV cables the cost per km is expressed by the following formula

$$C_{cables} = (0.284 \cdot 10^6 + 0.583 \cdot 10^6 \cdot e^{6.15*\sqrt{3}*U*I/10^8}) * 0.1087 \ , \tag{9.19}$$

which results in a costs for the cables of

$$C_{cables} = c_{cabbles} d \ , \tag{9.20}$$

with $c_{cables} = 21675$ €/ km

9.2.4 Controls

The automated flight requires automated controls, a set of sensors on the kite and on the ground station to check and run the correct operations of the system. The additional costs of those components are made function of the rated power [21]

$$C_{control\ and\ monitoring} = 10960 \cdot P_{rated}^{0.2} \ . \tag{9.21}$$

9.3 Assembly Transport and Installation

Those costs refer to the installation of the units, the in field cable installation and civil works necessary to access the site. For some aspects can be similar to wind turbine industry, with the difference that the installation costs of the wind turbines are much higher of the one of the pumping kite system.
Without going too much in detail with the cost functions that would be required to model extensively this part of the costs those are divided in costs for transport and installation (TandI) of the unit (Eq. 9.22) , costs of civil works (Eq. 9.23) and costs for installation of the cables (referred to on shore installation 9.24)

$$C_{TandI\ per\ unit} = 10 \cdot P_{rated} \tag{9.22}$$

$$C_{roads\ and\ civil\ work} = 157 \cdot dist\ , \tag{9.23}$$

where *dist* is the distance of the installations, thus the length of the road that should be build.

The cable installation cost will be a linear function of the length of the cables that have to be installed

$$C_{cables\ installation} = c_{installation\ cables\ per\ row} d_u^{0.5}\ , \tag{9.24}$$

where $c_{installation\ cables} = 87000$ €/km.

The cost of the installation of the farm are computed as the sum of the single installation costs.

9.4 Operation and Maintenance

To keep the model simple those costs are going to be dived into cost of components that need to be replaced, which is nothing more that the cost of the new component, to be added when the lifetime finishes; costs of the operation of maintenance; management; insurance and land lease. With the following relations [21] [50] [19]

$$C_{replacements} = \text{cost of the component which needs to be replaced} \tag{9.25}$$
$$C_{maintanence} = 4500 + (4.5 AEP_{unit}) \quad €/y/unit \tag{9.26}$$
$$C_{insurance} = 0.01 C_{unit} \quad €/y/unit \tag{9.27}$$
$$C_{landlease} = 0.8 \cdot AEP_{farm} \quad €/y\ . \tag{9.28}$$

9.5 Decommissioning

At the end of the lifetime, for a complete estimation of the energy production cost. the cost of decommissioning has to be taken into account. Once again taking the wind turbine industries as reference the costs are divided into management, removal and disposal of the units and removal of the cables [50]

$$C_{unit\ rem\ and\ disp} = 80 M_{unit} \tag{9.29}$$
$$C_{cable\ rem} = 40 \cdot L\ . \tag{9.30}$$

With L the length of the cables to be removed.

9.6 Final Considerations

The costs here presented are implemented in the model to obtain the cost of the energy for the farm of kites. Already some considerations can be done.
Not all the costs of the farm are linearly dependent on the number of units. For some important cost (i.e. functions like the maintenance the land lease) the independent variable is the energy production which grows faster than the number of units. Therefore those costs items increases faster than the ones which are directly related to the number of units (i.e. the investment cost for the installation and the hardware of the single unit). The cost sharing of the different cost items is expected to change depending on the number of units.

Chapter 10

Final Optimization

The model presented so far is ready to be investigated. All the components are chosen and the cost function are set as well as the model for the analysis of the power production of several units together. Now is possible to run the second optimization of the operational parameters taking into consideration also the efficiency and physical limits of the machines and the components chosen. Once the annual energy production is obtained ,the levelized cost of energy of the farm is computed with the costs functions and the assumption presented so far.

10.1 Maximum Power and Velocity Limitations

The model has to be modified from the preliminary optimization to include physical limits of the generator and the motor. The limitations are on the maximum reeling speed and on the maximum power of the machines.
Two different approaches have to be taken depending on the phase that we are looking at.
Having imposed the limit on the force already in the optimization routine, the limitation is only reduced on the maximum tether velocity and automatically the limitation the limitation on the maximum power is satisfied.
The tether velocity is checked at every time step. When the tether velocity results higher than the physical limit of the generator, the kite is partially de-powered. The values of c_l and c_d are decreased respectively of 2 % and 1% until the resultant velocity is within the given boundary. For the velocity limitation during retraction phase the kite is already fully de-powered. When the limit is reached, the retraction force is adjusted not to make the velocity increase further .

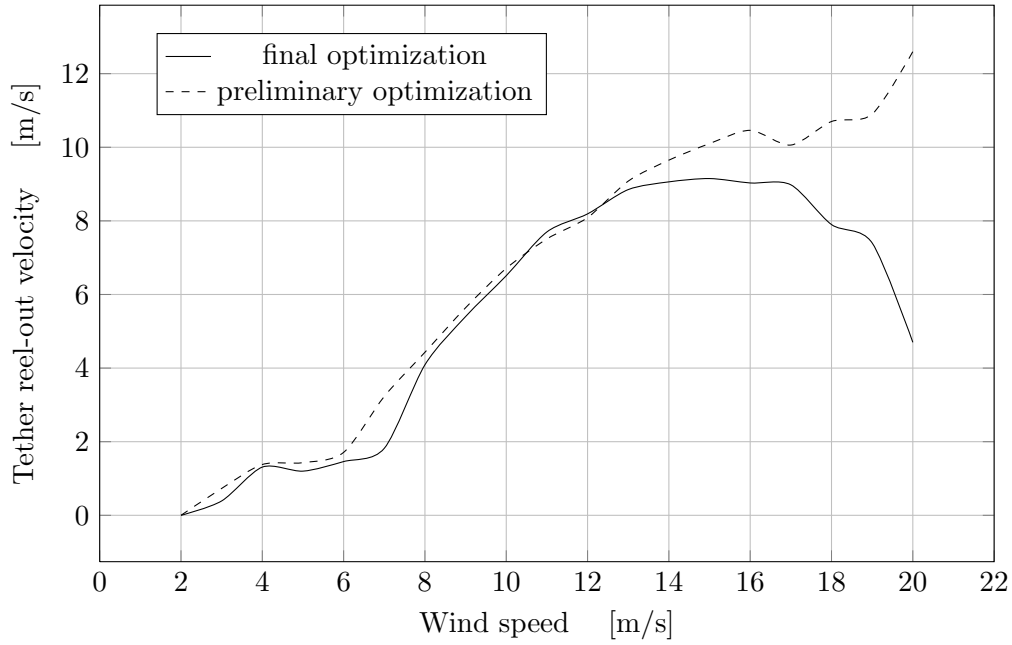

Figure 10.1: Comparison tether reel-out velocity obtained in the final optimization and in the preliminary

After this check on the, velocity the instantaneous power is checked once again to make sure that the maximum power of the machine is not exceeded. If it is, the cycle is considered not valid. Once the phase is completed a second check on the average power ensures that the average is not above the limit of the machine. If it happens, the cycle is considered non valid.
The availability of the farm is assumed to be 90 % for the maintenance jobs. The in field electrical losses are taken into account as 2 % of the power.

10.2 Results of the Final Optimization

As expected, the combined effect of the efficiency of the electrical machines, the losses of the in field cables and the limitation on the maximum reeling velocity makes the power curve decrease respect to the one obtained in the preliminary optimization.
The limitation in the maximum reeling velocity becomes progressively more important with the increase of the wind velocity. In Fig. 10.1 it can be seen that the reel-out velocity starts to deviate from the preliminary optimization already at 14 m/s.
The same trend cannot be seen in the reel-in velocity because its mean value over the cycle do not change considerably. The increase of the retraction time when the retraction velocity reaches the limit makes the average value of the retraction velocity remain the same.
The other operational parameters (optimum elevation angle and optimal tether force during each phase) follow the same trend shown in the preliminary optimization, therefore are be presented here.

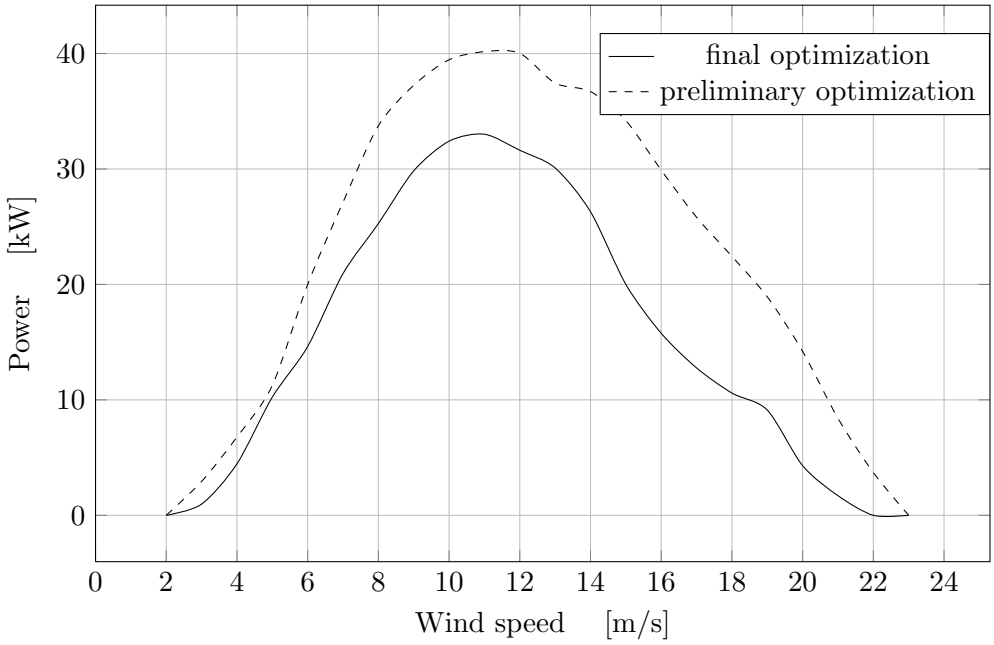

Figure 10.2: Comparison of the power curve obtained with when the limits and efficiency of the machines are included and the preliminary optimization

number of kites	LCOE [€/ MWh]
1	125

Table 10.1: Levelized cost of energy of a single unit

Finally the real power curve is obtained. By comparison with the one obtained previously with the preliminary optimization (Fig. 10.2), one can appreciate that the shape is very similar. The peak is at the same point (11 m/s). However the difference between the two curves increases with the increase of the wind speed.
The rated power of the unit is then assumed to be 33 kW, which is the maximum average cycle power that the unit can reach. Differently from the wind turbine, once the rated power is reached the power curve doesn't flat out but it decreases until going back to null.

The lower power curve has obviously an effect on the annual energy yield. The largest difference between the two curves in Fig 10.3 is at the peak of the graph, due to the lower power of the real system at those wind speeds. For higher wind speeds the difference decreases, since the energy production is decreasing following the Weibull distribution

The resultant LCOE of a single unit is in Tab. 10.1

The value obtained is more pessimistic than the results of similar studies [21] [19]. But the focus of those works was mainly the optimization of the single unit to reach the lowest cost of energy. In this work the optimization was only necessary to obtain the maximum power production from the unit. The LCOE is highly dependent on the initial choices of kite size and rated wind speed. It can be considered more conservative than the results

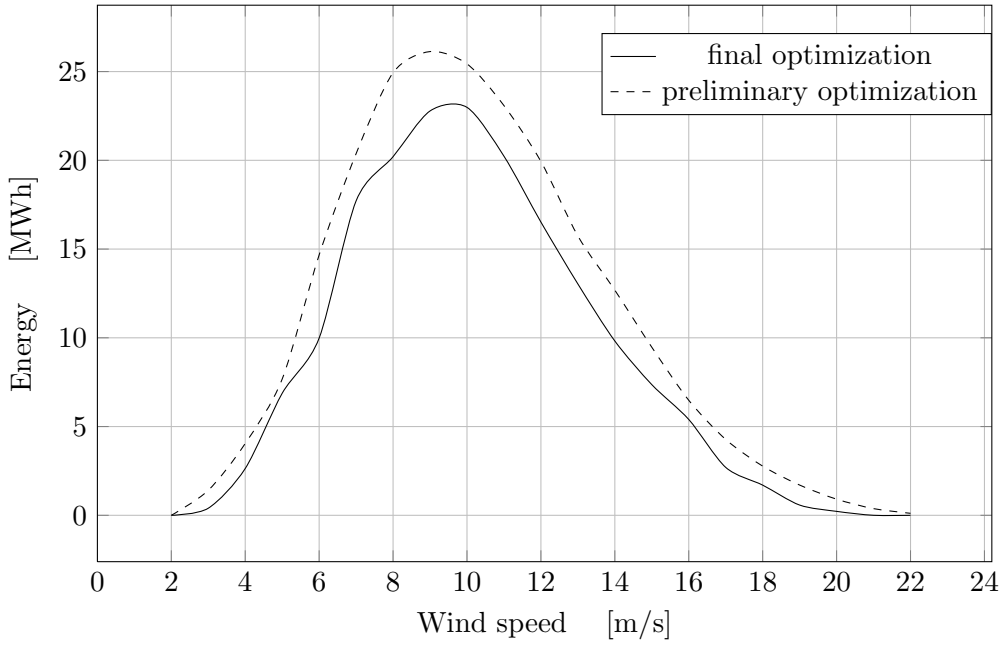

Figure 10.3: Comparison of the energy yield curve obtained with the preliminary optimization and with the final optimization

Kites per row	LCOE [€/ MWh]
24	118

Table 10.2: Levelized cost of energy of a farm

of previous studies and it leaves room for improvements. For the time being let us derive some conclusions in the next section over the farm configuration starting from this value.

10.3 LCOE of the Farm

It is possible now to compute the levelized cost of energy of the farm with the assumption made and presented in the work so far. The levelized cost of energy, for a farm of kites with a square configuration and 24 kites on the side of the square, is presented in Tab. 10.2

The farm configuration brings also an financial benefit. The cost of energy decreases of 5 % from the cost of the single units (Tab. 10.1).

Increasing the number of units, the combined effects of increasing energy production and scale effect on the installation costs and cable costs of the farm, make the cost share of the O&M gain progressively more share in the total costs (Fig. 10.4).Counting only around 54% of the total costs of the single unit, it increases asymptotically towards 57 %.

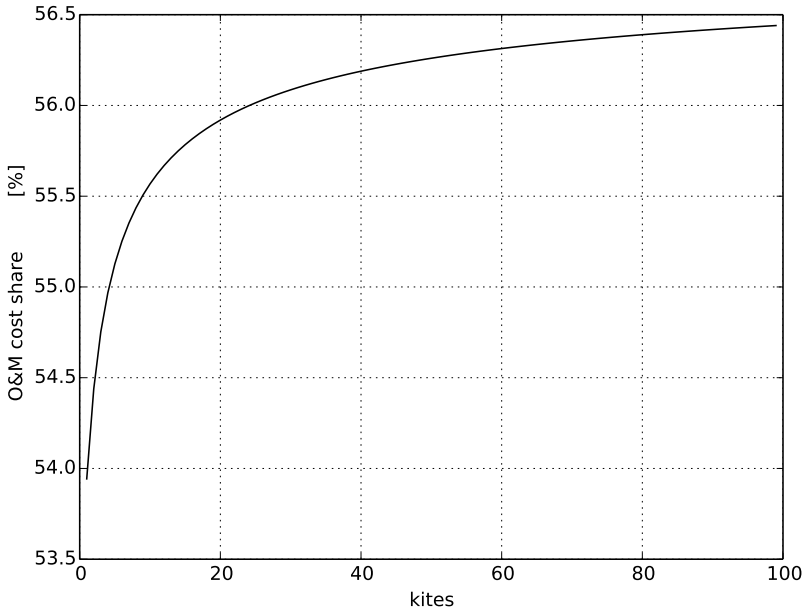

Figure 10.4: Cost share of the O&M costs as a percentage of the total cost during the whole lifetime of the unit.

Such high share of the O&M costs is rather unusual in the renewable energy industry. Being powered by free source of energy, rather than fossil fuels, renewable energies technologies are usually characterized by low O&M costs and high initial costs compared to fuel powered technologies. However in this case, the short lifetimes of the airborne components bring the necessity of replacing them often, with consequent increase of the value of O&M. The consumables airborne parts can be considered as the fuel of the pumping kite unit.

For low number of kites (2-5 kites per row) the farm configuration results rather expensive. The scale effect, that makes the investment cost decrease compared to the O&M, also has an impact on the LCOE of the farm. Following the trend of the cost share of the initial cost, the LCOE decreases asymptotically to a specific value increasing the number of units.

To better understand the result presented in Tab. 10.2 and its trend in Fig. 10.5 it has to be compared with the same index for other power sources.

The LCOE for different renewable and non renewable sources can change depending on the source that we are looking at. In Tab 10.3 are reported the ranges of the LCOE from IEA [22] for different sources for comparison with the result obtained with the present model. In Fig. 10.6 the same index computed by Kost et al. [24].However the cost of energy from the pumping kite system is in line with the other wind technologies.
This can be considered as a very promising result, considering that is a new field and the initial choices have not been optimized yet.

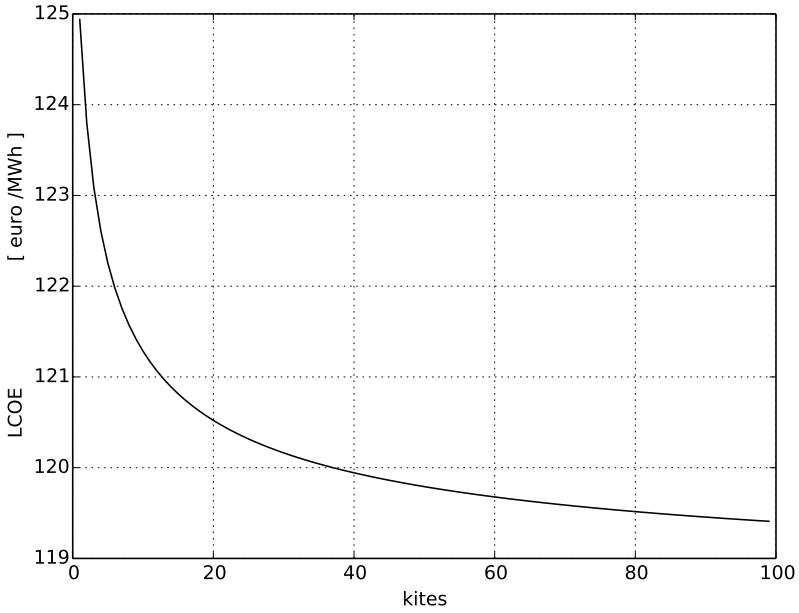

Figure 10.5: LCOE trend as function of the number of units

Technology	LCOE [€/ MWh]
Nuclear	51 ÷ 87
Coal	41 ÷ 51
On-shore Wind	77÷ 113
Off-shore Wind	89 ÷ 144
PV	537 ÷ 908
Solar Thermal	175 ÷ 255

Table 10.3: LCOE by source [22]

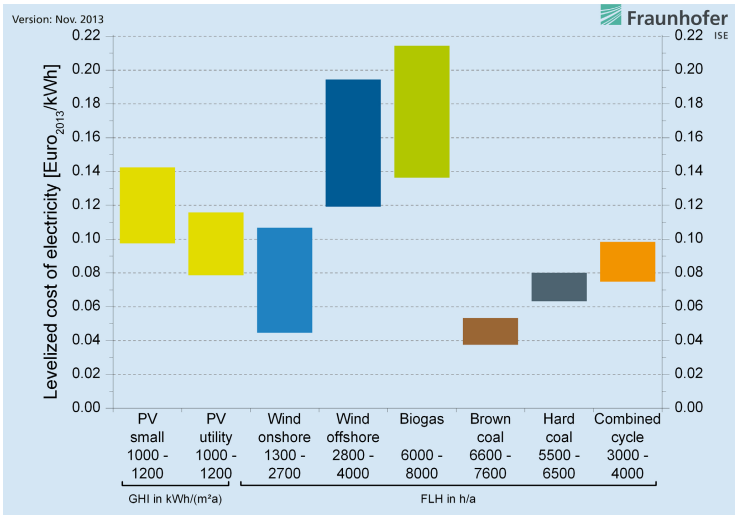

Figure 10.6: LCOE for different sources [24]

Technology	initial investment per kW [€/ kW]
on shore wind	1450 to 2960
off shore wind	2540 to 4380
PV	2300 to 4300
nuclear	1354 to 4000
coal	478 to 1590
pumping kite system	**2830**

Table 10.4: Comparison of the investment cost per kW installed between different technologies IEA [22]

10.4 Considerations about the Results Obtained

With the assumption made, the cost model implemented and the simulation model used, it has been demonstrated that the farm configuration brings some advantages with respect to the stand alone configuration.
Firstly it has been shown how there is a physical advantage of having a continuous production of energy over the whole operating wind range when the number of units is high enough. This cancel the need of expensive battery packs or the need to be fed from the grid to complete the retraction phase.
The second advantage is on the economical side. For how the costs function are implemented, the cost of energy approaches asymptotically a value lower than the one of the single unit.
The results can also be considered on the conservative side, since in previous works more optimistic LCOE values were found for a single unit.
Things become even more promising when obtaining some additional performance and economical indicators for the farm to be compared with other wind turbines farms and other renewable energy harvesting methods.

Firstly the investment cost per kW installed is computed. This indicator is often used to compare different technologies because it gives an indication on the ease of finding investors. The comparison of the different technologies is made in Tab. 10.4

The pumping kite technology is the high side for the initial capital investment per kW when compared to other technologies. When compared to the value rages of the wind turbines industries, the value obtained is similar to the off-shore cost even though it has been computed for on-shore situation. Those values appears anyhow promising, considering the early stage of development of the technology.

More promising are the indicators which are related to the land usage. In particular land requirement of the pumping kite technology is suited to be compared with the land requirement of wind turbines, being two technologies which harvest from the same renewable source of energy. The indicator which is usually computed for this purpose is

Technology	power per unit area [W/m^2]
wind turbines	0.4 to 8
pumping kite system	**87.3**

Table 10.5: Per unit area of the different wind technologies [9] and [8]

Technology	Capacity Factor [%]
on shore wind	20 to 41
off shore wind	34 to 43
PV	9 to 24
nuclear	85 to 90
coal	80 to 85
pumping kite system	**52**

Table 10.6: Capacity factors for different energy technology [22]

the average power per unit area measuring the W/m^2 that is possible to obtain with a given technology. The results are presented in Tab 10.5.

As already explained in Sec. 8.1 the spacing between the turbines is mainly chosen to reduce the wake effects and increase the array efficiency of the farm. It has been shown why the wake effects on kite technology can be neglected and how the spacing between pumping kite units is reduced to the minimum. This approach results in a power per unit area which is one order of magnitude higher than the power per unit area of wind turbines. In his work David JC MacKay [8] uses this indicator to set the maximum physical limit to the spread of wind technology in the UK. By allowing much denser wind farms using the pumping kite technology the physical limit to the spread of wind energy is at least one order of magnitudes higher.

The final performance indicator that has been computed is the capacity factor. This is the ratio between the energy that is actually produced by the unit and the energy that would be produced if the system would have worked all the time at the rated power (Eq 10.1). The value obtained with the model is compared with the values found in literature for other sources in Tab. 10.6 .

$$CF = \frac{AEP}{P_{rated}8760} \tag{10.1}$$

Also with respect to this index the pumping kite technology performs remarkably good. The reason for such high capacity factor is mainly thanks to the shape of the power curve. High levels of power are reached for rather low wind speeds.

Chapter 11

Sensitivity of Design Choices

Already some promising results have been found and presented, but when looking at the single unit and compared with the results of other works. However the numbers presented so far are on the conservative side. In this chapter the initial design choices made for the single unit are investigated checking if a better solution can be achieved with other input parameters.
The design choices that are investigated are the choices of the rated wind speed from which it follows the electrical machines sizes, and the area of the kite. The sensitivity of the model on the kite wing loading is also investigated.

11.1 Rated Speed Sensitivity

In Ch. 7 the rated speed was set equal to 21 m/s. The reason for the choice comes from the qualitative analysis of the system. However a lower or higher rated wind speed might lead to a lower LCOE because of the consequences on the power production and cost of the unit.
The design process is started over from the choice of the electrical machines. The results of the preliminary optimization are used again to pick the new electrical machines, making the same considerations but taking as rated wind speed 19 m/s and 23 m/s. Once again the rated power of the generator is chosen from the average power of the traction phase and the rated power of the motor from the maximum instantaneous power of the retraction phase.
The rated powers of the electrical machines chosen are presented in Tab 11.1. With the value is also presented the percentage difference to the value from the value at 21 m/s as rated wind speed.

v_{rated} [m/s]	$P_{rated\ gen}$ [kW]	$P_{rated\ mot}$ [kW]
21	250	130
19	170 (-32 %)	116 (-10%)
23	280 (+12%)	180 (+38%)

Table 11.1: Rated powers of the electrical machines at the different rated wind speed

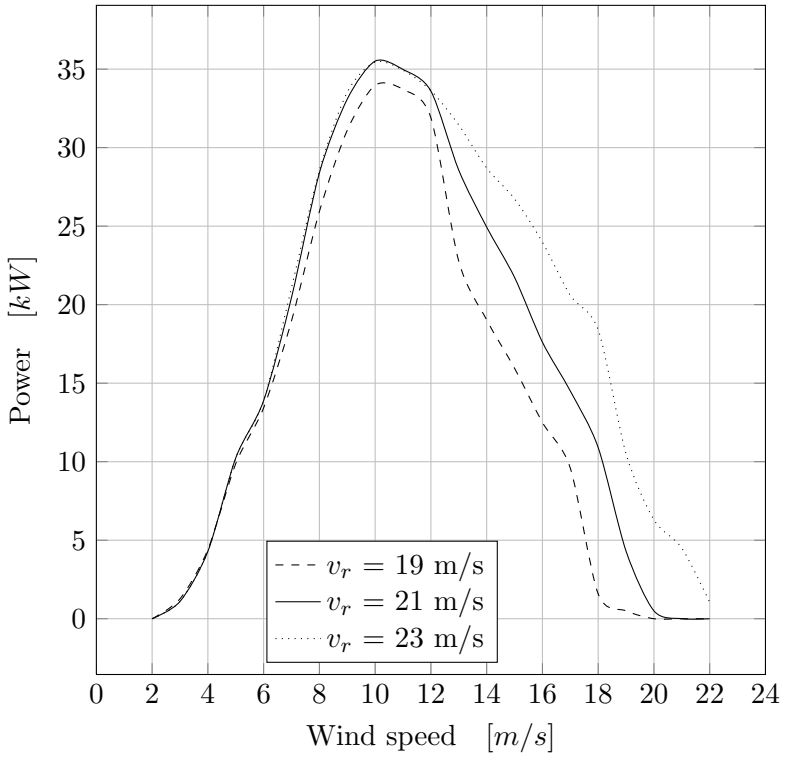

Figure 11.1: Power curves obtained with different choices of rated wind speed

The final optimization of the unit is performed again. With the power curves obtained (Fig. 11.1) for the two new configurations, the output energy is derived and from it the LCOE.

As expected the power curves differ from the one obtained before. The differences are particularly visible at high wind speeds, where the limitations of the electrical machines impose their restrictions.
As consequence the energy production of the unit changes according to the changes in the power curve.

The difference in energy production between 21 and 23 m/s matches with the reasoning made in Sec.7.1.4.

At the same time the initial installation cost varies depending on the rated speed because

rated wind speed [m/s]	Annual energy production of a unit [MWh]
21	155.3
19	134.6 (-13%)
23	162.4 (+5%)

Table 11.2: Annual energy production of a single unit with the different rated wind speeds

rated wind speed [m/s]	initial investment cost [k€/unit]
21	96.3
19	92.6 (-4%)
23	98.9 (+3%)

Table 11.3: Initial investment per unit depending on the rated wind speed chosen

of the different costs of the electrical machines with different rated powers.

Taking into account the change in costs the LCOE is computed again. In Fig 11.2 the different trends are shown. The different results for the single unit and for the farm are compared numerically in Tab. 11.4. For the case of the lower rated wind speed the LCOE results higher. This because the annual energy production decreases more (-13% as shown in Tab 11.2) than the decrease of the cost of the unit (only -4% as shown in Tab 11.3), making the energy from this solution more expensive.
On the other hand the increase of 5% in the energy production with the high rated wind speed pays off the additional 3% of higher initial investment cost and makes the energy cheaper.

The conclusion is that it is more convenient to maximize the energy production by setting the rated wind speed equal to the maximum operating wind speed of the machine. The increase in energy production makes the LCOE decrease despite the increase of the initial investment.

v_{rated} [m/s]	LCOE one unit [€/MWh]	LCOE farm [€/MWh]
21	124	118
19	139 (+12%)	132 (+11.8%)
23	120 (-3.3%)	115 (-2.5%)

Table 11.4: LCOE of the single unit and of the farm at the different rated speeds

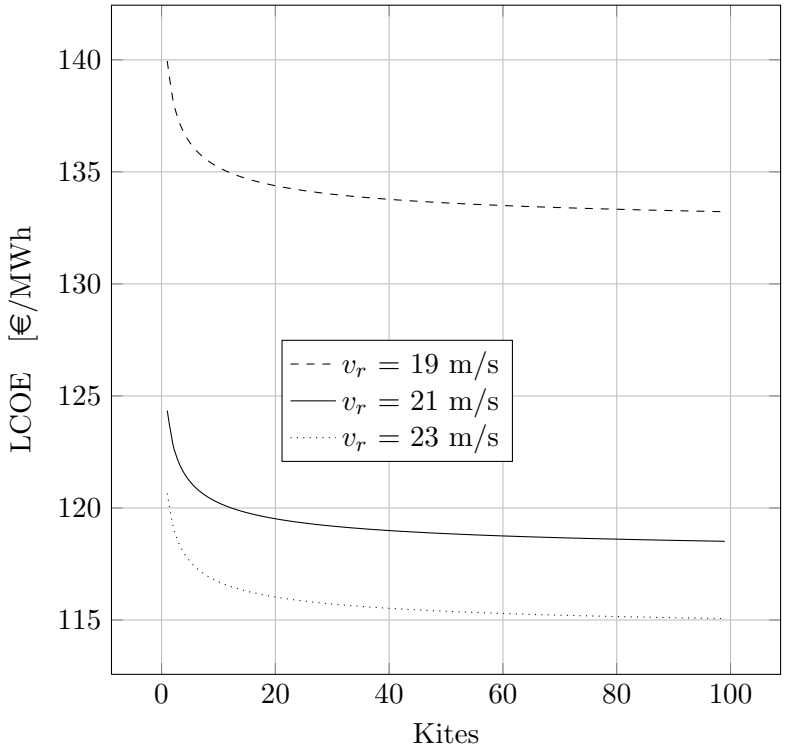

Figure 11.2: LCOE trends as function of the number of kites for the differenc choice of the rated wind speed

11.2 Wing Loading Sensitivity

As explained in Sec. 7.1.1, the kite wing loading has been chosen based on available literature on the topic, but the discrepancy on literature on the exact value, made the choice rather uncertain. The wing loading is considered a crucial parameter of the system and heavily affects many other physical (maximum tether force and power curve) and economical aspects (kite and tether costs) of the farm. The sensitivity to this parameter is investigated for the 100 m^2 kite. The kite wing loading is increased from 300 N/m^2 to 600 N/m^2 with a step of 50 N/m^2. The entire design process is run again from the beginning. The resultant generator and motor rated power, energy production, power curves and LCOE are compared.

In Fig. 11.3 the effect of the wing loading on the power curve curve is clear. The peak of the curve increases and is shifted towards higher wind speeds. The operating wind range becomes progressively larger, being expanded for high wind speeds. The rated power of the electrical machines that have to be installed at the ground station increases and the same happens for the electricity production. (The exact values are reported in App. C). As result of the increase of the energy production, the LCOE of the single unit and of the farm configuration decreases with the increase of the wing loading (Fig. 11.4).

Despite the increase of the cost of the kite due to the thicker fabric used, and the increase

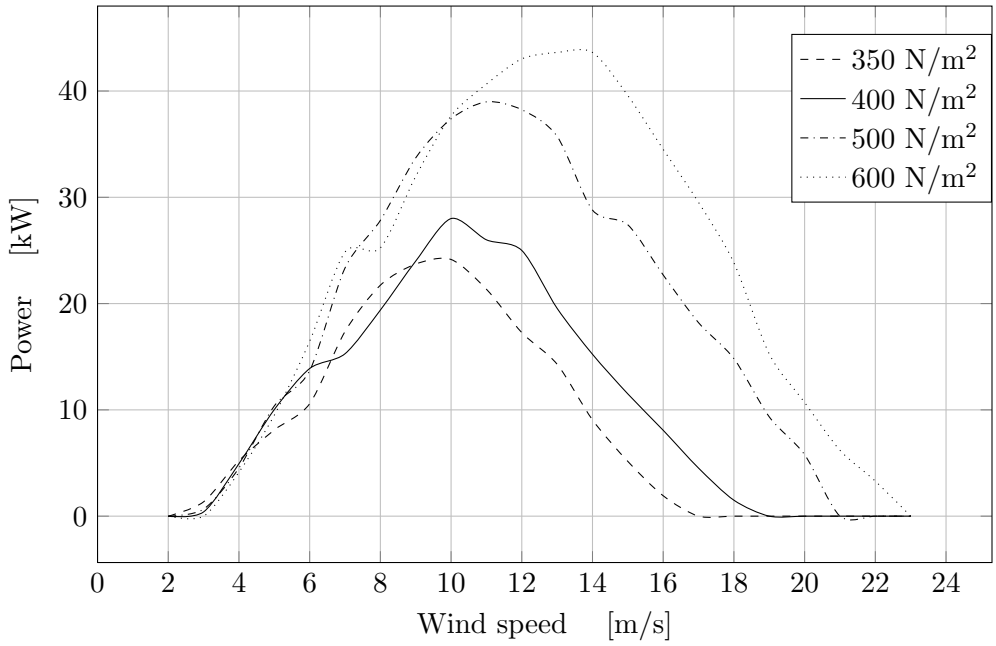

Figure 11.3: Power curves with different kite wing loading

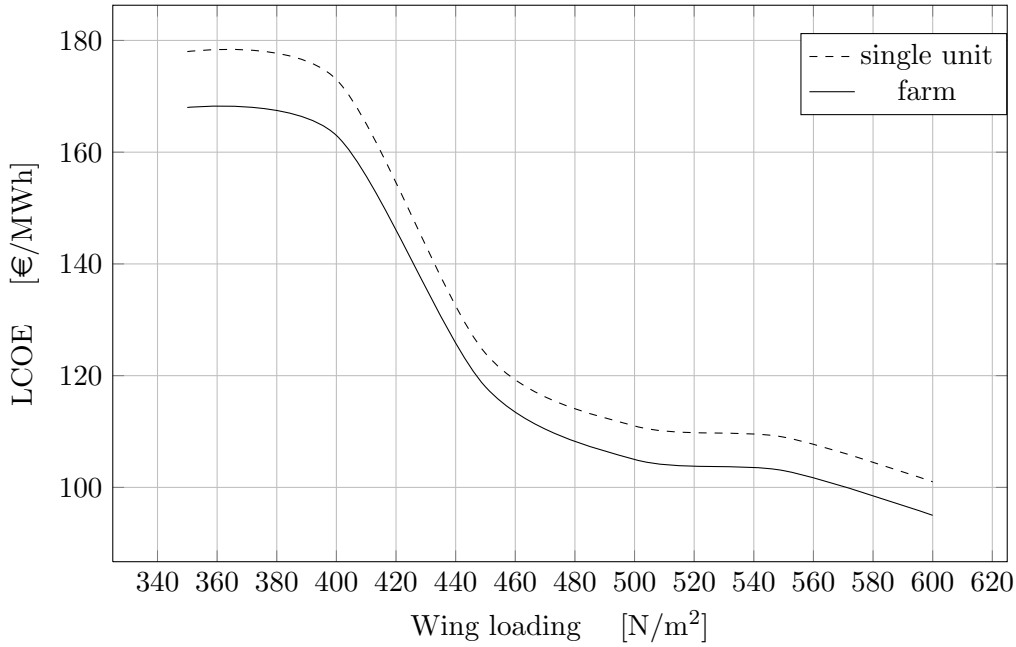

Figure 11.4: LCOE of the farm and of the single unit with different kite wing loading

kite area[m^2]	difference [%]
100	
50	-50
150	50

Table 11.5: Kite area for the sensitivity analysis

of the cost of the ground station due to the more powerful electrical machines, the increase of the energy production makes the LCOE decrease remarkably. The model result very sensitive to the wing loading at low values. For higher values the increase in the costs counterbalance the increase of energy production and the decrease of the LCOE is less steep. This is due to the fact that the increase in energy production is not constant. Even though the peak of the power curve increases, shifting it to higher wind velocities results progressively less effective for the energy production, due to the shape of the probability density function of the wind speed.
Higher values of the wing loading are not investigated because considered non realistic for a LEI kite. To increase even further the wing loading a different type of kite should be considered.

11.3 Kite Size Sensitivity and Rough Optimization

Finally the sensitivity of the model to the kite size is investigated. The importance of this component is out of question and picking the wrong kite size heavily affects the final levelized cost of energy. In this section a sensitivity analysis is carried out on the kite size.
As for the case of the rated speed the variation of the LCOE is investigated taking a lager and a smaller kite area as in Tab 11.5.

The whole unit design has to be carried out from the beginning. First the preliminary optimization is done with the new kite area. The choice of the rated wind speed follows the result of the previous section and the electrical machines is sized according to the highest wind velocity that returns a positive average power over the cycle. In all the cases the value has been found equal to 23 m/s. The results of the preliminary optimization once again show the same trends found before and for the sake of compactness are not presented here. From the preliminary optimization, the other components are chosen following the same procedure of the previous case.
The rated powers of the electrical machines chosen according to the maximum operating wind speed is presented in Tab. 11.6.

The power curve of the three different units with the three different kite areas are compared in Fig. 11.5. As expected the shape of the power curve is affected by the kite size. However the peak of the curve remains in the same range of wind speeds. This because both the maximum allowable tether force and the aerodynamic force on the kite are correlated and both are linear functions of the kite area. The maximum wing loading

kite area [m^2]	Generator Nominal Power [kW]	Motor Nominal Power [kW]
100	280	180
50	106 (-62%)	80 (-55 %)
150	440 (+57 %)	270 (+50 %)

Table 11.6: Nominal generator and motor power picked after the preliminary optimization for the different kite sizes.

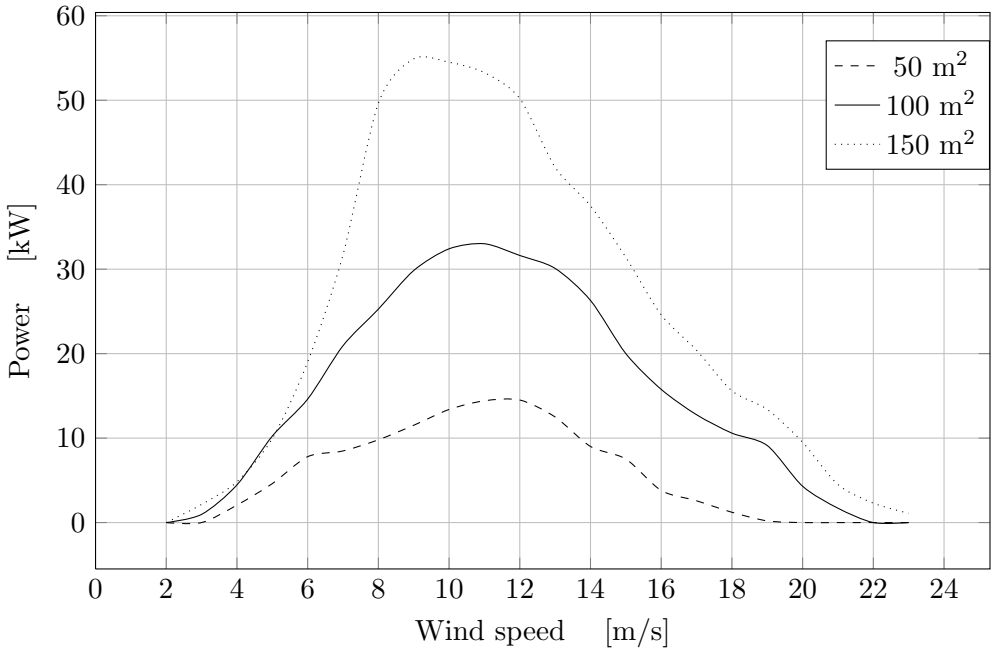

Figure 11.5: Power curves with different kite areas

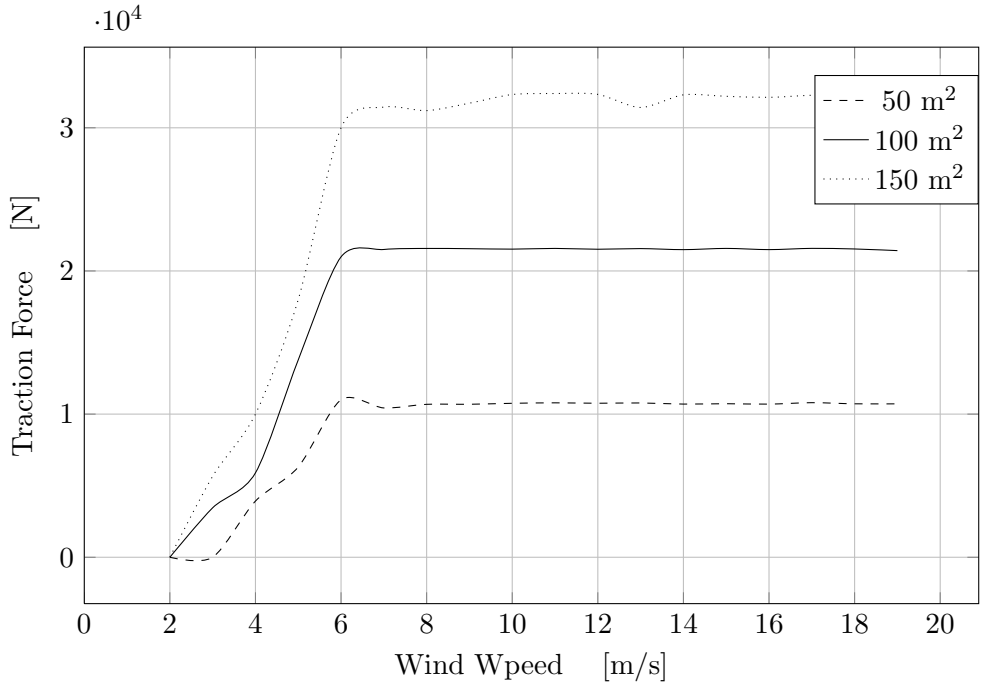

Figure 11.6: Traction tether force for different kite area

kite size [m^2]	AEP [MWh]
100	162
50	58 (-64%)
150	228 (+39%)

Table 11.7: Annual energy production of the unit with the different kite size

is kept constant regardless the change of the kite area. Therefore the maximum tether force is reached approximately at the same wind speed (6 m/s) in the three different cases (Fig. 11.6).

The energy production increases as well as the costs increasing the kite area. In Tab. 11.7 are presented the different annual energy yield for the single unit and the percentage difference with the first case analyzed.

Finally the LCOE of the single unit and the farm with the different kite sizes are compared numerically in Tab. 11.8. In fig 11.7 the LCOE trends obtained with the 150 m^2 kite and the 100 m^2 are plotted as function of the number of units. Even from this analysis it results that it is more convenient to maximize the energy production despite the increase of the installation and the maintenance costs. The cost of energy found for the case of 150 m^2 is more similar to the costs found in previous works [19].

As expected the LCOE shows a strong dependency on the kite area.
Previous works [19] [21] have shown the it decreases to a minimum value and then it starts

kite area [m^2]	LCOE unit [€/MWh]	LCOE farm [€/MWh]
23	120	114
50	245 (+104 %)	234 (+105%)
150	109 (-9%)	102 (-10%)

Table 11.8: Comparison of the LCOE of the units and the farms obtained starting from a different kite size

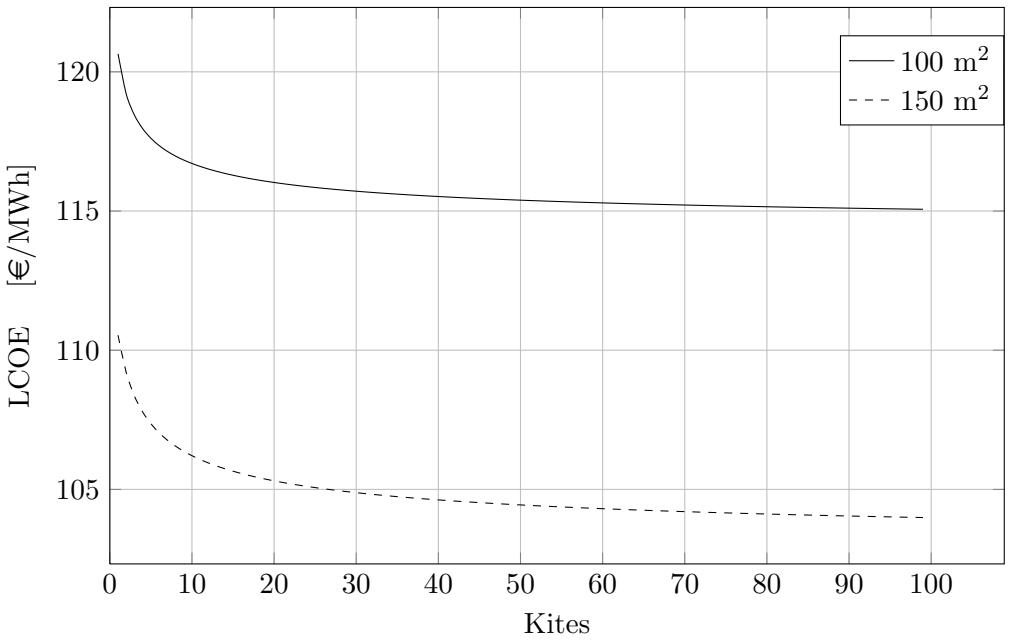

Figure 11.7: LCOE with different kite areas

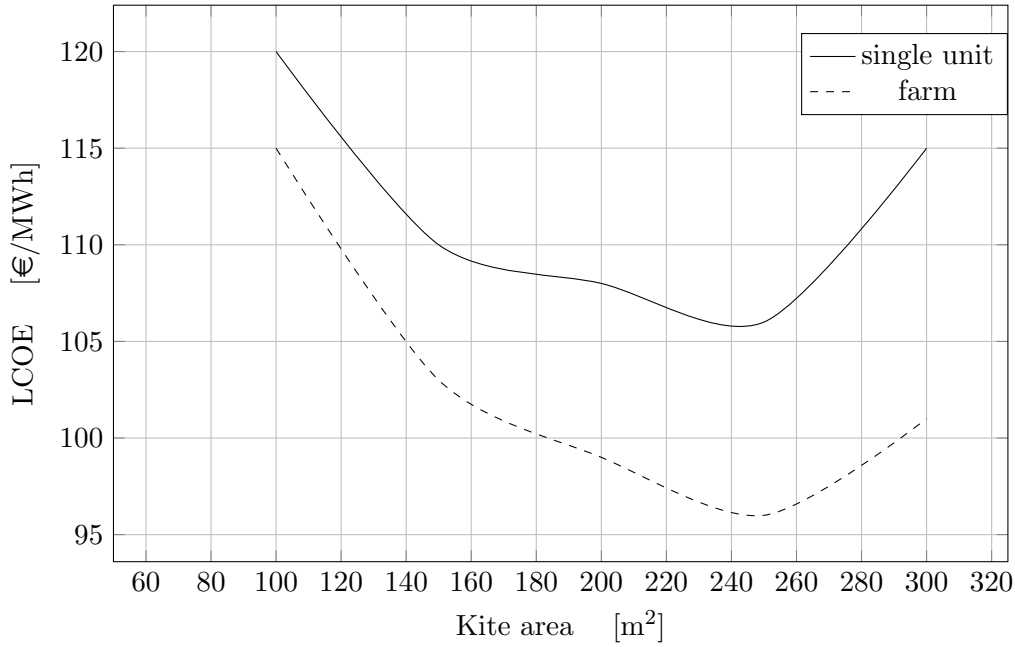

Figure 11.8: LCOE of the single unit and of the farm (24 kites per row) as function of the kite size

to increase again. Expecting this behavior, the kite area is increased further to have an idea of which kite area could lead to the lowest LCOE.
An optimization on the kite area is performed. The kite area is increased in steps of 50 m^2 and for every new kite area a new unit is designed, optimized and the LCOE computed until it keep decreasing.
The minimum LCOE has been found for a kite size of 250 m^2. Then for 300 m^2 cost increases again (Fig. 11.8).

It happens that following always the same design procedure and imposing the same physical constraints (kite wing loading), the operating wind range remains constant while the rated power reaches progressively higher values (it can be already noticed in Fig. 11.6, the power curves found for the larger kite sizes are reported and compared in App. C). The shape of the power curve gets narrower increasing the kite area. This makes the capacity factor decrease. At the same time the rated power increase slower than the necessary rated power of the generator. The index P_{rat}/P_{gen}, which can be considered as a cycle efficiency, is plotted as function of the kite size in Fig.11.9. Regardless the absolute values of this ratio, it is clear that the larger kites perform worse with respect to this indicator. The last index analyzed in the previous chapter, the land power density, happens to decrease increasing the kite size. Apparently the minimum distance between the units increases faster than the rated power when increasing the kite size.
Those negative effects are anyway counterbalanced until a kite size of 250 m^2 by the fast increase of the energy production which makes the LCOE decrease anyway. The lowest value of the LCOE is reported in Tab 11.9

From Fig.11.8 it can also be noticed that the farm configuration becomes progressively

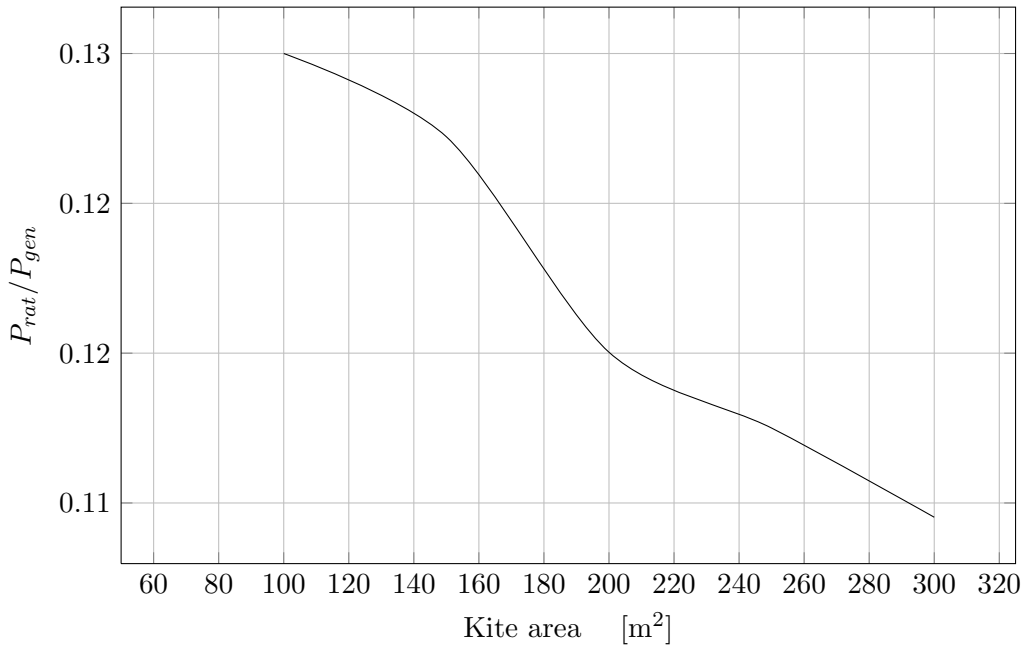

Figure 11.9: Ratio between the rated power and the nominal power of the generator

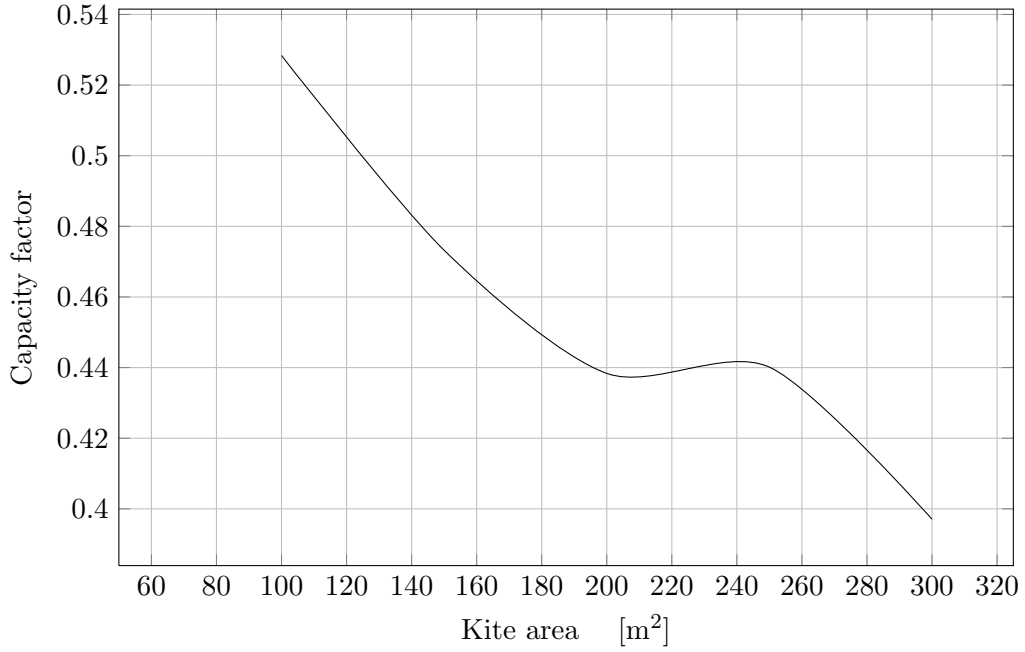

Figure 11.10: Capacity factor

single unit min LCOE [€/MWh]	farm min LCOE [€/MWh]
105	96

Table 11.9: Minimum LCOE found after the sensitivity analysis

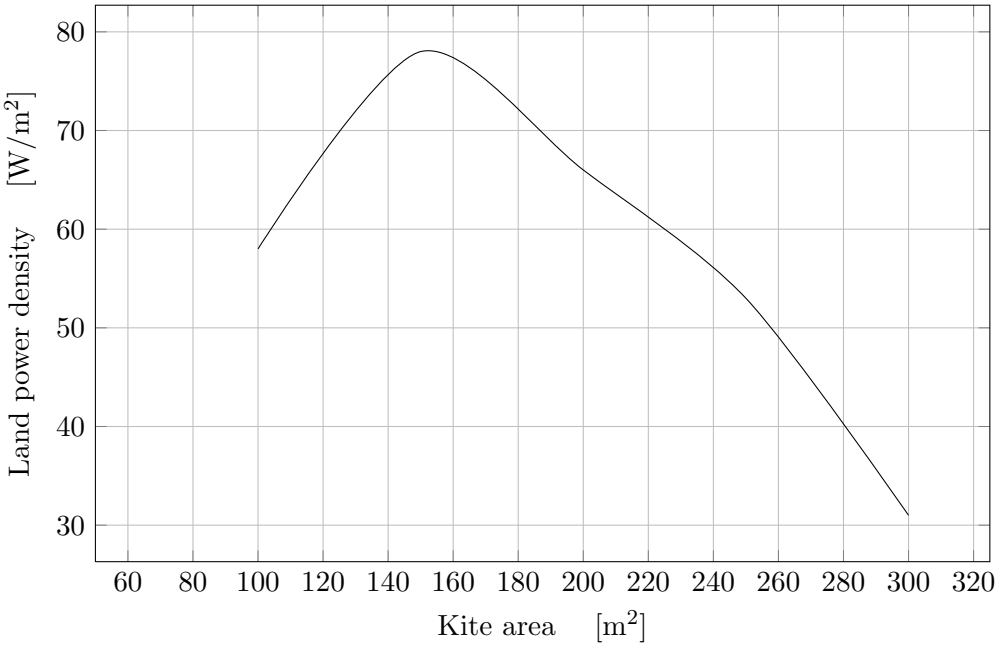

Figure 11.11: Land power density of the farm as function of the kite area

more convenient than the single unit increasing the kite size. The reason for this has been found in the trend of the O&M costs over the total costs. The increase of the O&M cost share increases with the increase of the kite size because of the higher energy production. This enhances the scale effect and makes the the farm progressively cheaper than the LCOE of the single unit.
The same results have been found also in other works on the topic (Heilmann [21], Grete [19]).

Chapter 12

Conclusions and Recommendations

The final objective of the thesis described in the introduction can be considered achieved. The levelized cost of energy (LCOE) of a wind farm of pumping kite power systems has been obtained. The process to get to the final result begins with the choice of a kite size. From it the pumping kite unit is designed through a preliminary optimization (Chap. 4) of the operational parameters to maximize the energy production. The optimal layout of the ground-station for the unit has been studied. This has been done by means of the model of the efficiency of the electrical machines (Chap. 5). The obtained unit is put in a squared array and the cumulative production of multiple units together is analyzed (Chap. 8). Some effort has been put in understanding the layout of the farm, the distance between the units and the characteristics of the cumulative instantaneous power production for different wind conditions. Interesting results regarding the advantages of using multiple units at the same time in a cluster has been presented as well. Finally the annual energy production can be computed and from it and the costs model (Chap. 9) the LCOE of the farm is obtained (Chap. 10).
The result obtained reveals an interesting scale effect. The cost of energy decreases by increasing the number of kites in the farm. At this point the initial choices for the unit design are checked through a sensitivity analysis and optimum for the rated wind speed and kite size is found (Chap. 11). The lowest LCOE is found for a farm of units with a 250 m^2 kite, and it is equal to 96 €/MWh. The value for the single unit was found equal to 105 €/MWh.
The results for the single unit are in line with previous works [19], [21], and the effects of multiple units working together is clearly visible in the LCOE of the farm. The comparison of relevant indexes with wind turbines shows the major strength points of this technology compared to the traditional way of harvesting wind energy. The LCOE has also been compared with the one of other renewable technologies revealing the great potential of the pumping kite system (Sect. 10.4).
The system is far from being fully optimized. The possibility of different kinds of kites,

maybe rigid or semi-rigid, has not been investigated in the work. The drawbacks of having heavier and more expensive kites can be counterbalanced by a higher performing shape, an increase in the lifetime and, probably more important, higher wing loading.
Recommendations for future works can be in the research on the tether design, whose drag heavily affects the power production of the unit. Its heavy drag and weight still limit the optimal operating altitude.
Concerning the farm configuration the grid interface has not been studied in this work. The power coming from the farm shows important oscillations whose amplitude and frequency depends on the wind conditions. Those oscillations have to be leveled out with a fast storage system before the energy can be fed to the grid.
Finally the offshore environment seems very promising. The concept features of low mass and no bending moment at the ground make the system particularly suitable for offshore applications, likely on floating platforms.
The path to get to the scenario described in the work is still long. At the current state of the art there are no fully automated working units producing energy constantly. Smart and skilled research teams are currently competing to get there. Improvements on the concept level can still be done. Nevertheless the high expectations on airborne technology can be certainly shared and should be justified by the results of the present work.

References

[1] U Ahrens, M Diehl, and R Schmehl. *Airborne Wind Energy*. Green Energy and Technology. Springer Berlin Heidelberg, 2013. ISBN 9783642399640. URL http://books.google.nl/books?id=FNVrngEACAAJ.

[2] Alxion. ALXION STK for wind turbines, 2014. URL http://www.alxion.com/products/stk-alternators/.

[3] AMPIX. Ampix Power, 2014. URL http://www.ampyxpower.com/.

[4] Ivan Argatov, Pauli Rautakorpi, and Risto Silvennoinen. Estimation of the mechanical energy output of the kite wind generator. *Renewable Energy*, 34(6):1525–1532, June 2009. ISSN 09601481. doi: 10.1016/j.renene.2008.11.001.

[5] BP. BP Energy Outlook 2030 - Presentation Slides, 2013.

[6] Michael W Brown. A Pilot s Guide to Understanding Restrictions in Today s National Airspace System. *Airspace Obstacles and TFR Trivia*, 1(December):1–12, 2003.

[7] Gro Harlem Brundtland. Our Common Future. Technical report, WCED, 1987. URL http://www.unece.org/oes/nutshell/2004-2005/focus_sustainable_development.html.

[8] David JC MacKay. *Sustainable Energy without the hot air*. San Diego, CA, 2009.

[9] Paul Denholm, Maureen Hand, Maddalena Jackson, and Sean Ong. Land-Use Requirements of Modern Wind Power Plants in the United States Land-Use Requirements of Modern Wind Power Plants in the United States. (August), 2009.

[10] Furkan Dincer. The analysis on wind energy electricity generation status, potential and policies in the world. *Renewable and Sustainable Energy Reviews*, 15:5135–5142, 2011. ISSN 13640321. doi: 10.1016/j.rser.2011.07.042.

[11] Dmitrey L. Kroshko. Open Opt, 2014. URL http://openopt.org/GLP.

[12] Storm Dunker. Ram-air Wing Design Considereations for Airborne Wind Energy. In U Ahrens, M Diehl, and R Schmehl, editors, *Airborne Wind Energy*, chapter 31. Springer Berlin / Heidelberg, Berlin, first edition, 2013.

[13] Michael Erhard and Hans Strauch. Theory and Experimental Validation of a Simple Comprehensible Model of Tethered Kite Dynamics Used for Controller Design. In Uwe Ahrens, Moritz Diehl, and Roland Schmehl, editors, *Airborne Wind Energy*, chapter 8. Springer, Berlin, 2013.

[14] Lorenzo Fagiano, Aldo Zgraggen, and Manfred Morari. On Modeling, Filtering and Automatic Control of Flexible Tethered Wings for Airborne Wind Energy. In Uwe Ahrens, Moritz Diehl, and Roland Schmehl, editors, *Airborne Wind Energy*. Springer Berlin / Heidelberg, Berlin, 2013.

[15] Falko Fritz. Application of an Automated Kite System for Ship Propulsion and Power Generation. In Uwe Ahrens, Moritz Diehl, Roland Schmehl, editor, *Airborne Wind Energy*, chapter 20. Springer Berlin / Heidelberg, Berlin, 2013.

[16] Uwe Fechner and Roland Schmehl. Model-Based Efficiency Analysis of Wind Power Conversion by a Pumping Kite Power System. In Uwe Ahrens, Moritz Diehl, and Roland Schmehl, editors, *Airborne Wind Energy*, chapter 14. Springer, Berlin, 2013.

[17] Uwe Fechner, Rolf Van der Vlugt, and Roland Schmel. Dynamic Model of a Pumping Kite Power System. *Renewable Energy2*, 2014.

[18] Fraunhofer IWES. Workshop: Windpotentiale für Flugwindenergiesysteme (Wind Potential for Airborne Wind System), 2012.

[19] C Grete. *Optimization, Scaling and Economics of Pumping Kite Power Systems*. Msc thesis, TUDelft, 2014.

[20] Sebastien Gros and Moritz Diehl. Modeling of Airborne Wind Energy Systems in Natural Coordinates. In Uwe Ahrens, Moritz Diehl, and Roland Schmehl, editors, *Airborne Wind Energy*, chapter 10. Springer, Berlin, 2013.

[21] Jannis Heilmann. *The Technical and Economic Potential of Airborne Wind Energy*. Msc thesis, Utrecht University, 2012.

[22] IEA. Projected Costs of Generating Electricity. *Atomic Energy*, 118 Suppl:218, 2010. ISSN 16602110. doi: 10.1787/9789264084315-en. URL http://www.iea.org/publications/freepublications/publication/projected_costs.pdf.

[23] IEA. *World Energy Outlook*. 2014 edition, 2014.

[24] Christoph Kost, Jhonannes Mayer, Jessica Thomsen, and Niklas Hartmann. Levelized Cost of Electricity Renewable Energy Technologies. Technical Report November, Fraunhofer institute for solar energy systems, 2013.

[25] Miles L Loyd. Crosswind Kite Power. *Energy*, 4(3):106–111, 1980.

[26] Stefan Lundberg. *Performance comparison of wind park configurations*. PhD thesis, CHALMERS UNIVERSITY OF TECHNOLOGY, 2003.

[27] Makani. Makani Power, 2014. URL http://www.google.com/makani/.

[28] J F Manwell, J G McGowan, and A L Rogers. *Wind Energy Explained*, volume 1. wiley, 2009. ISBN 0470846127. doi: 10.1002/0470846127. URL http://onlinelibrary.wiley.com/doi/10.1002/0470846127.fmatter_indsub/summary.

[29] C. Mayhew. Astronomy Picture of the Day, 2007. URL http://apod.nasa.gov/apod/ap001127.html.

[30] Morse. types CKK and CSK sprnag clutches data sheet, 2014.

[31] J.T.G. Pierik, M. Pavlovsky, J. Bozelie, P. Bauer, and S.W.H. de Haan. Dowec Electrical System Baseline design. pages 1–30, 2002.

[32] Frank F A Van Der Pijl, Gert-jan De Vilder, Peter Tavner, and Henk Polinder. Comparison of Direct-Drive and Geared Generator Concepts for Wind Turbines. pages 543–550, 2005.

[33] Paul Smeets Rigo Bosman, Valerie Reid, Martin Vlasblom. Airborne Wind Energy Tethers with High-Modulus Polyethylene fibers. In *Airborne Wind Energy2*, chapter 33. Springer Berlin / Heidelberg, Berlin, first edition, 2013.

[34] Roland Schmehl. Kite Power and Propulsion exam, 2013.

[35] Roland Schmehl. Kite Power and Propulsion course material, 2014.

[36] Roland Schmehl, Micheal Noon, and Rolf van der Vlugt. Traction Power Generation with Tethered Wings. In Schmehl R. Ahrens U., Diehl M., editor, *Airborne Wind Energy*, chapter Chapter 2. Springer Berlin / Heidelberg, Berlin, 2013.

[37] Michael Schölkopf. Design of a Ground Station for a Kite Power System. 2011.

[38] Kamini N Shelke and Mohini D Duraphe. Magenn Air Rotor System (Mars). 2(6): 1566–1568, 2012.

[39] SkySails. SkySails, 2001. URL http://www.skysails.info/english/.

[40] Anne Staack. SkySails helping Ardmore Shipping to set new standards in fuel and operational efficiency, 2013. URL http://www.skysails.info/fileadmin/user_upload/Presselounge/Dokumente/englisch/130416_SkySails_Ardmore_press_release.pdf.

[41] Roland B. Stull. *Meteorology for Scientists and Engineers*. 2000.

[42] TWingTec. Twing Tec, 2006. URL http://twingtec.ch/.

[43] U.S. Energy Information agency. International Energy Outlook 2013, 2013. URL http://www.eia.gov/forecasts/ieo/pdf/0484(2013).pdf.

[44] D Van Baelen, S Barendswaard, L Espinoza Chavez, D Geleyns, R Van Iwarden, J Knols, J Van Der Meijs, K Thieme, and T Willems. DSA Final report - Automated launch, landing and storage if a kite power system. 2013.

[45] Eric Van der Knaap. *A particle system approach for modelling flexible wings with inflatable support structures.* Unpublished masters thesis, TU Delft, 2013.

[46] Rolf van der Vlugt, Johannes. Peschel, and Roland. Schmehl. Design and Experimental Characterization of a Pumping Kite Power System. In Uwe Ahrens, Moritz Diehl, and Roland Schmehl, editors, *Airborne Wind Energy*, chapter Chapter 23. Springer, Berlin, Heidelberg, 2013.

[47] Rolf van der Vlugt, Johannes Peschel, and Roland Schmehl. Design and experimental characterization of a pumping kite power system. *Green Energy and Technology*, pages 403–425, 2013. ISSN 18653529. doi: 10.1007/978-3-642-39965-7_23.

[48] Rolf van der Vlugt, Roland Schmehl, and Micheal Noon. Quasi-Steady Model of a Pumping Kite Power System. *Renewable Energy*, 2014.

[49] L.J. Vermeer, J.N. Sø rensen, and a. Crespo. Wind turbine wake aerodynamics. *Progress in Aerospace Sciences*, 39(6-7):467–510, August 2003. ISSN 03760421. doi: 10.1016/S0376-0421(03)00078-2. URL http://linkinghub.elsevier.com/retrieve/pii/S0376042103000782.

[50] Michiel Zaaijer. *Great Expectations for Offshore Wind Turbines.* PhD thesis, TU Delft, 2013.

Appendix A

Wake Effects

While computing the distance between the kites the wake effect has been neglected. Some qualitative reasons has been given for this fact. Here some additional consideration with a more quantitative approach are given to support this assumption.

A.1 Areas Ratio

A comparison of the wake that different devices have can be already done by computing the ratio of the actual area of the blades (or of the kite) and the swept area. This index is called solidity. In principle the higher the solidity the higher the wake effect.
For the wind turbines this ratio is easy to compute because the swept area is easily detectable. The value changes depending on the kind of turbine, in principle when high torque power is needed (e.g. for water pumping purposes or similar) turbines with high solidity are used while for higher rotational speed (e.g. for electricity production) low solidity are preferred.
In the work of Vermeer et al. [49] different prototypes of turbines are tested and the wakes are measured. The turbines used have a solidity in the range of $0.14 \div 0.7$.
For a pumping kite system the computation of the swept area is not equally easy. The trajectory of the kite depends on the steering inputs and it is not rigidly set by mechanical bonds as for the case of the turbines. Taking the same assumptions made in work to compute the trajectory of the kite, the swept area results 8900 m^2 (Fig. A.1). Such rough estimation of the swept area does not take into account that while the kite flies the figure of eight it is being reeled out. considering the three-dimensional effect of it would increase even further the swept area. Neglecting this factor can ensure us to be on the conservative side of the computation of the solidity.

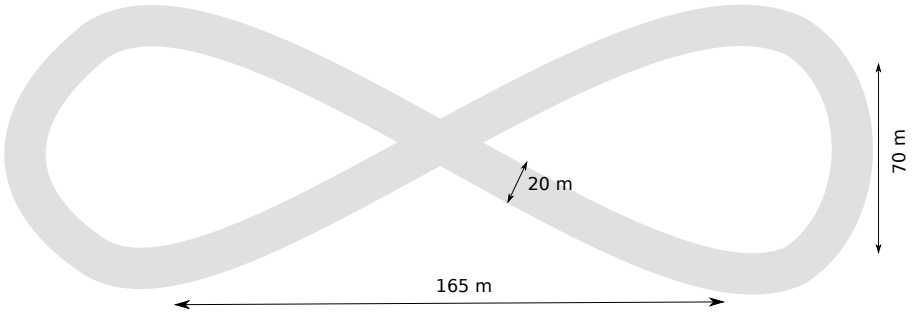

Figure A.1: Trajectory of the kite during one figure of eight.

The solidity for such system result only 0.01, which is one order of magnitude less than the solidity of the normal turbines.

A.2 Induction Factor

To further analyze the problem and justify the assumption of the negligible kite wake, an estimation of how much the wind is slowed down by the system is performed.
Following the Betz theory the power that a harvesting device (actuator disk) extract from the wind is

$$P_{extr} = \frac{1}{2}\rho A v_w^3 4a(1-a)^2 \tag{A.1}$$

where a is the induction factor is a measure of how much the wind is slowed down by the actuator disk. If v_w is the wind velocity at actuator disk the induction factor is computed as:

$$a = \frac{v_w - v_t}{v_w} \tag{A.2}$$

taking the derivative of the P_{extr} for a it is obtained that the maximum power is extracted for $a = \frac{1}{3}$. This is the value for which the turbines are usually designed.

With a reverse engineering process knowing the mechanical power extracted by the kite, it is now possible to compute the induction factor of a kite and compare it to the induction factor of the turbines.
For the 100 m^2 kite the induction factor results in a range between $0.01 \div 0.02$. (the calculus sheet is reported in Fig. A.2)
Such low induction factor justify the assumption of the negligible wake of the kite in the farm and allow to set the spacing according to the minimum distance for safe operation.

	A	B	C	D	E	F
1	wind	Mech power	area	power in wind	4a*(1-a)^2	
2	2.0	0.00	8900	43610	0	
3	3.0	1579.38		147183.75	0.010730656	
4	4.0	7820.26		348880	0.022415321	
5	5.0	17762.05		681406.25	0.026066762	
6	7.0	52342.74		1869778.75	0.027994081	
7	8.0	87551.53		2791040	0.031368782	
8	9.0	114031.05		3973961.25	0.028694556	
9	10.0	142181.84		5451250	0.02608243	
10	11.0	152921.24		7255613.75	0.021076265	
11	12.0	162391.43		9419760	0.017239445	
12	13.0	200522.53		11976396.25	0.016743144	
13	14.0	219744.37		14958230	0.014690533	
14						

Figure A.2: Computations for the induction factor

Appendix B

Distance Between Units

B.1 Small Phase Displacement Between the Units

The distance between two units aligned with the wind direction has been computed assuming perfect synchronization between the two units.
However perfect control on it is rather difficult to achieve, therefore additional investigation is performed on the dependency of the minimum distance between the units when the perfect synchronization is lost and there is a small phase displacement between the units.
Considering again the situation from the side view (Fig. B.1) but now with the two units not perfectly synchronized, the angles and the tether length which are referring to the downwind unit are reported with the 2 subscript and while the one upwind with the 1.

What changes between the two units now is the tether length (L), which changes by

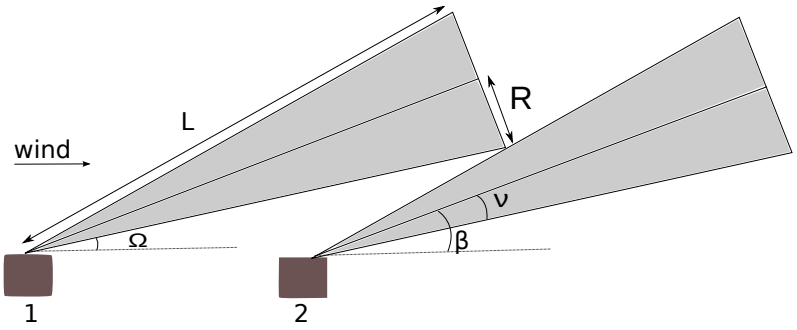

Figure B.1: Side view of two units aligned with the wind direction with a small phase displacement

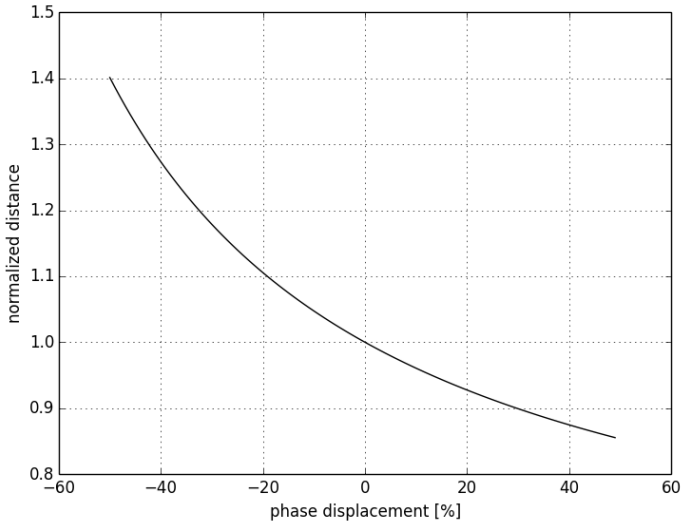

Figure B.2: Normalized minimum distance as function of the phase displacement of the downwind unit respect to the upwind one

consequence the angle ν considering Eq. 8.9.
The minimum distance is computed as function of the phase displacement using the Eq. B.1.

$$d = \frac{L_1}{sin(\alpha - \nu_1)(\frac{1}{tan(\alpha - \nu_1)} + \frac{1}{tan(\nu_1 + \nu_2)})} \tag{B.1}$$

The phase displacement is applied to the downwind unit and is taken into account as percentage difference in tether length between the units. A negative phase displacement means that the downwind unit is delayed with respect to the upwind. The minimum distance is normalized with the distance of the two synchronized units. The result is in Fig. B.2.

It appears that a positive phase displacement can actually reduce the minimum distance, but the risk of entanglement is very high when the downwind unit starts the retraction phase before the upwind unit. A safer displacement is with the downwind unit slightly delayed from the upwind. The most risky moment in this situation would be when the upwind unit starts the traction phase when the downwind one is still in the retraction phase. In this case the tether length is at the minimum and it is smaller than the distance between the units, therefore the situation is assumed to be safe.
A safer control strategy would be to have a small phase shift between aligned units of about 10%, to make sure that, if the control allows a different phase shift between the units, the downwind do not anticipate the upwind one. In this case the minimum distance increases of 5 % from the case of the perfect synchronization.

B.2 Radius of the Trajectory and Kite Size Dependency

Checking the LCOE sensitivity on kite size the minimum distance is made function of the kite size. From the distance between the units important cost items follow, concerning the installation costs and the cable costs. As explained in Sec. 8.1 the distance is function of the radius of the trajectory that the kite can fly.
The curvature radius (R) of the trajectory is made function of the kite area.

Using the same notation and assumptions made in Sec 8.1, the radius can be expressed as:

$$R = \frac{v_{\tau,k}}{\dot{\chi}} = \frac{1}{\frac{C_{st}\delta}{m} + \frac{\mathbf{e}_y^k \cdot \mathbf{g}}{v_a^2}} \tag{B.2}$$

The dot product $\mathbf{e}_y^k \cdot \mathbf{g}$ depends on the direction that the kite is flying and it changes continuously. considering the vectors of interest in spherical coordinates

$$\mathbf{e}_r = \begin{bmatrix} 1 \\ 0 \\ 0 \end{bmatrix} \tag{B.3}$$

$$\mathbf{v}_{k,\tau} = \begin{bmatrix} 0 \\ cos(\chi) \\ sin(\chi) \end{bmatrix} \tag{B.4}$$

$$\mathbf{g} = \begin{bmatrix} -cos(\theta) \\ sin(\theta) \\ 0 \end{bmatrix} g \tag{B.5}$$

The cross product result

$$\mathbf{e}_y^k = \frac{\mathbf{e}_r \times \mathbf{v}_{k,\tau}}{v_{k,\tau}} = \begin{bmatrix} 0 \\ -sin(\chi) \\ cos(\chi) \end{bmatrix} \tag{B.6}$$

and the dot product we are interested in for the computation of the radius

$$\mathbf{e}_y^k \cdot \mathbf{g} = -g\ sin(\chi) sin(\theta) \tag{B.7}$$

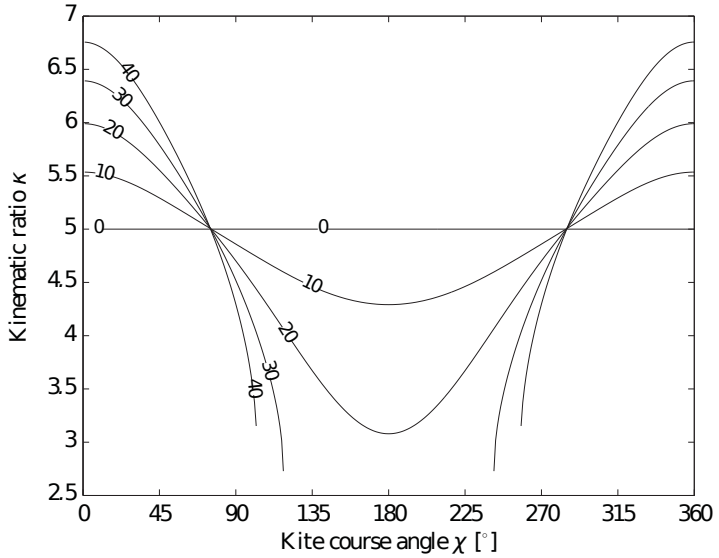

Figure B.3: Kinematic ratio as function of the mass and the course angle for with a same kite size [36]

In the expression of the radius (B.2) this dot product is at the denominator and divided by the apparent velocity squared.
Considering The values of mass (64 kg), the value of the coefficient C_{st} and average values of the course angle, elevation angle and apparent wind velocity, the resultant radius for the 100 m^2 is

$$R = \frac{1}{\frac{8.8 \cdot 0.3}{64} - \frac{9.8 sin(110) sin(75)}{25^2}} = 35m \tag{B.8}$$

When changing the kite size the mass of the kite and the apparent wind velocity are both affected. Since the shape and other characteristics of the kite are assumed to remain the same the value of C_{st} remains the same.

The apparent velocity should be function of the kite area. From the equation of the apparent wind velocity

$$v_a = v_w(sin(\theta)cos(\phi) - f)\sqrt{1 + k^2} \tag{B.9}$$

it is clear the dependency on the kinematic ratio.

The kinematic ratio is strongly dependent on the mass and the course angle. The higher the mass the higher the kinematic ratio if the kite is flying downwards and lower if it is flying upwards (B.3).

However with the mass, the force increases as well, increasing the area of the kite (which

is not taken into account in the Fig. B.3). From the quasi steady model the apparent velocity results more or less stable, with a tendency to decrease. This behavior has not been implemented for instability of the model. For the computation of the radius and the apparent wind velocity is kept constant at 25 m/s.

Appendix C

Results of the Kite Sensitivity

Running the kite and wing loading sensitivity and the rough optimization of the kite area, every time the whole unit has been redesigned and the operational parameters optimized. Some of the results are presented in this appendix to keep the report more easy to read.

The rated power of the electrical machines and the energy production at different values of maximum wing loading is listed in Tab. C.1. The percentage difference which appears besides the values is referred to the 450 N/m^2 case.

The nominal power and the annual energy production of the unit designed and optimized are presented in the table.

The power curves and the consequent annual energy yield are reported as well as the LCOE trend as function of the number of kites.

maximum wing loading [N/m^2]	P_{gen} [kW]	P_{mot} [kW]	E [MWh]
350 (-22 %)	124 (-55%)	77 (-57%)	99 (-38%)
400 (-11%)	260 (-7%)	162 (-10%)	107 (-33%)
500 (+11%)	299 (+6%)	187 (+4%)	187 (+15%)
550 (+22%)	429 (+53%)	268 (+48%)	192 (+18%)
600 (+33%)	478 (+73%)	304 (+68%)	210 (+30%)

Table C.1: Comparison of the characteristics of the unit and the annual energy production with different kites' wing loading

kite size [m^2]	$P_{generator}$ [kW]	P_{motor} [kW]	P_{rated} [kW]	AEP [MWh]
50	106	80	14	58
100	280	180	35	162
150	450	270	55	228
200	625	400	75	288
250	800	570	90	357
300	1000	650	115	401

Table C.2: Power characteristics and annual energy production of the units designed based on the first choice of the kite size.

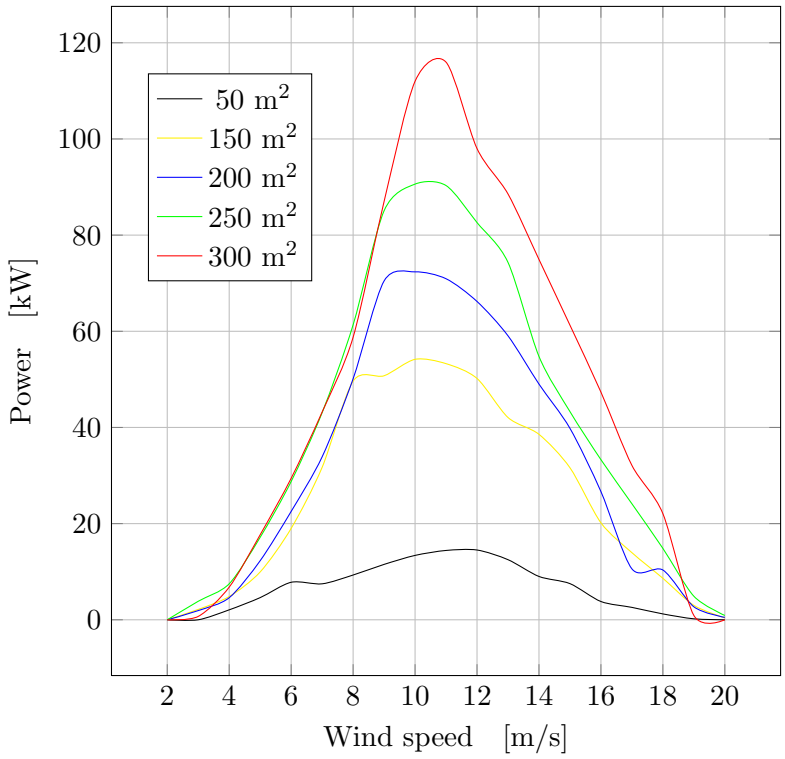

Figure C.1: Power curves obtained with different choices of kite area

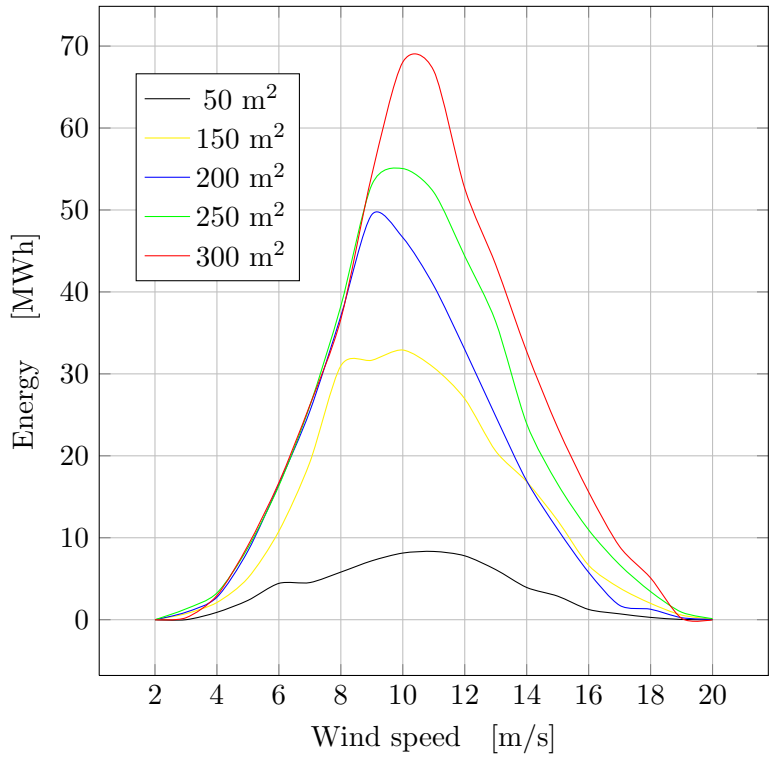

Figure C.2: Energy yield plot for different kite areas

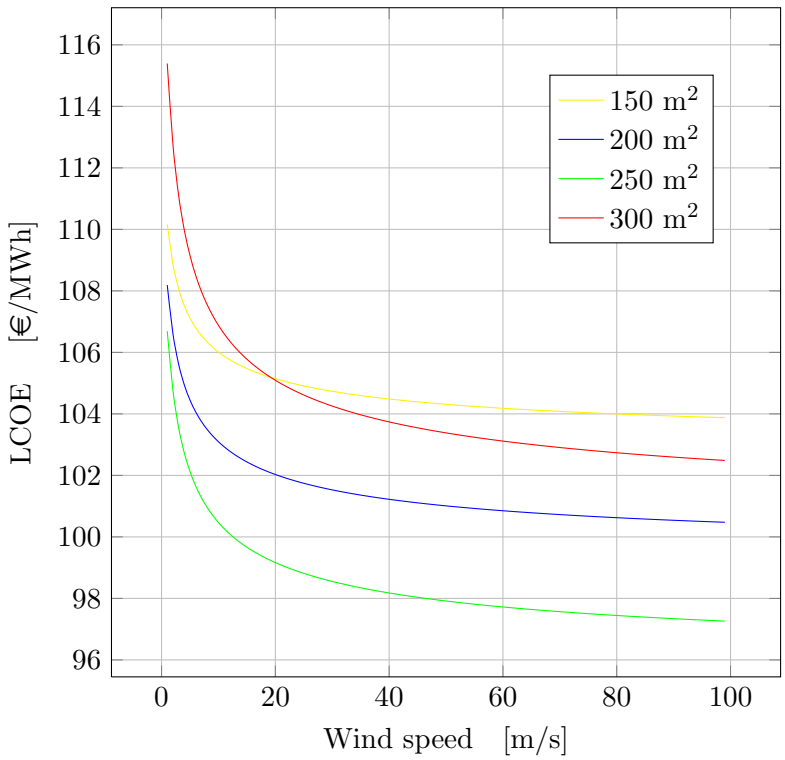

Figure C.3: Power curves obtained with different choices of kite area

Appendix D

Farm Power Production

D.1 Factor for the phase shift

The phase shift has been set equal to the duration of the cycle divided by the number of columns and multiplied by a factor. This factor has been chosen equal to 1 for the case of orthogonal wind direction and 2 for the diagonal wind direction. The graphs refFig face shift factor orto and fig. D.2 prove that the choice made for the phase shift leads to the lowest normalized percentage standard deviation. the phase shift between the columns can be obtained by multiplying the phase shift factor by the cycle duration. Those graphs (refFig face shift factor orto and fig. D.2) justify the choice made in the work. Same shape are found for other numbers of kites and at different wind velocities.

D.2 Effects of the Phase Shift on the Same Column

In the text are presented the patterns of the power production for the case of null phase shift between the units in the same column. This might not be the case in reality when the perfect synchronism is lost.

In the following graphs the power trend is shown for different cases of phase shift of the kites in the same column. For the case of orthogonal wind, the phase shift is beneficial and the power results more constant for the both cases of constant wind speeds and different number of kites in the array (the first graphs) and for the case of fixed number of kites and different wind speeds (latter graphs). For the case of the diagonal wind the

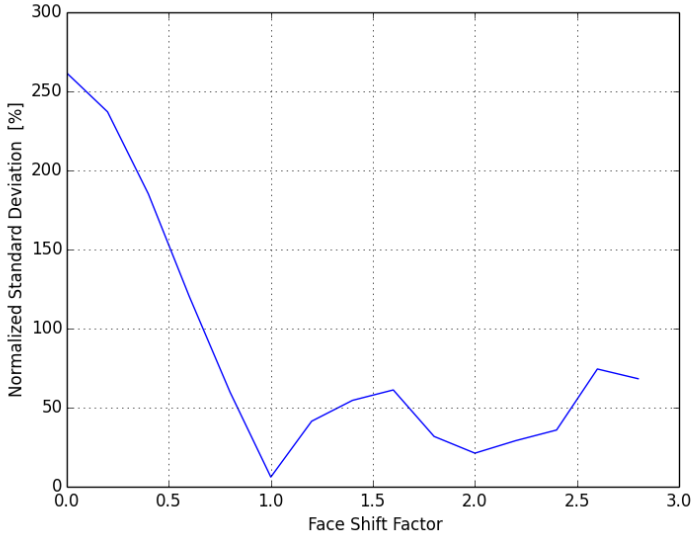

Figure D.1: Normalized standard deviation for the case of orthogonal wind direction as function of the phase shift factor for an array of 8X8 kites and a wind speed of 8 m/s.

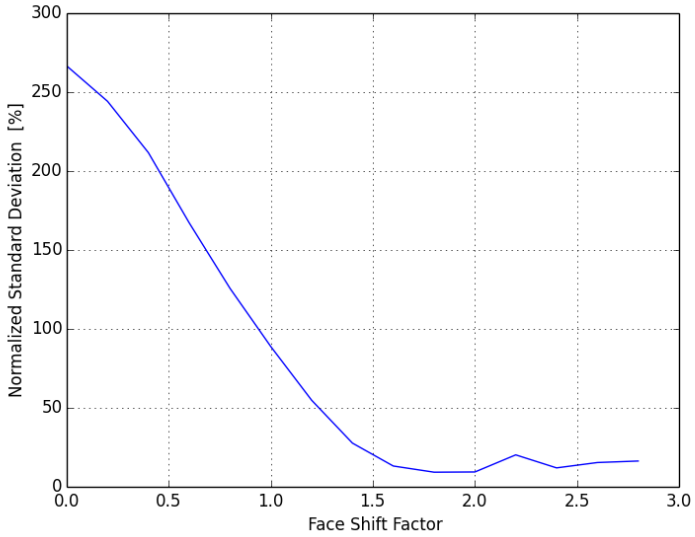

Figure D.2: Normalized standard deviation for the case of diagonal wind direction as function of the phase shift factorfor an array of 8X8 kites and a wind speed of 8 m/s.

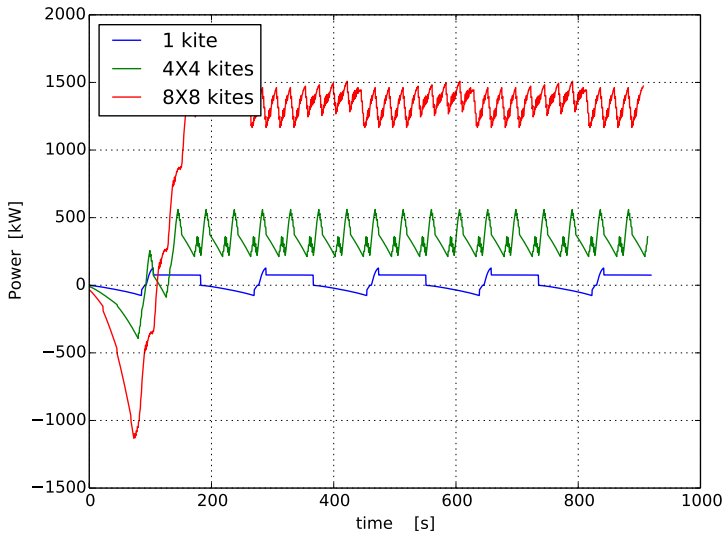

Figure D.3: Power production at 8 m/s of orthogonal wind for different number of kites in the array when there is a phase shift of 1% between the units in the same column

periodic oscillations are enhanced and, increasing the number of kites in the array, lead to a sinusoidal shape of the power production. Also increasing the wind speed the effect of the phase shift results negative for the power production.
Finally the contours of the percentage normalized standard deviation are presented for different phase shift between the units in the same columns. From those graphs is clear that the columns phase shift has a positive effect on the orthogonal case and a negative on the diagonal case.
The normalized percentage standard deviation is computed as

$$\sigma_{\%\ norm} = \frac{\sigma}{P_{avg}} 100 \tag{D.1}$$

with

$$\sigma = \sqrt{\frac{\Sigma_{i=1}^{N}(P(t_i) - P_{avg})^2}{N}} \tag{D.2}$$

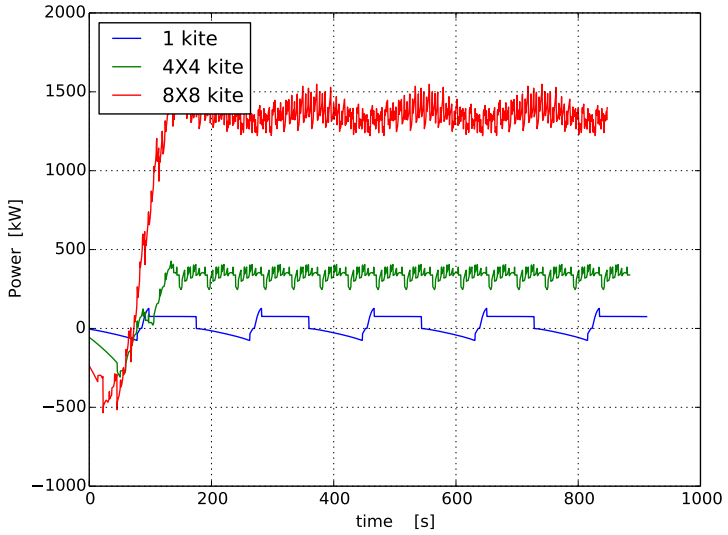

Figure D.4: Power production at 8 m/s of orthogonal wind for different number of kites in the array when there is a phase shift of 5% between the units in the same column

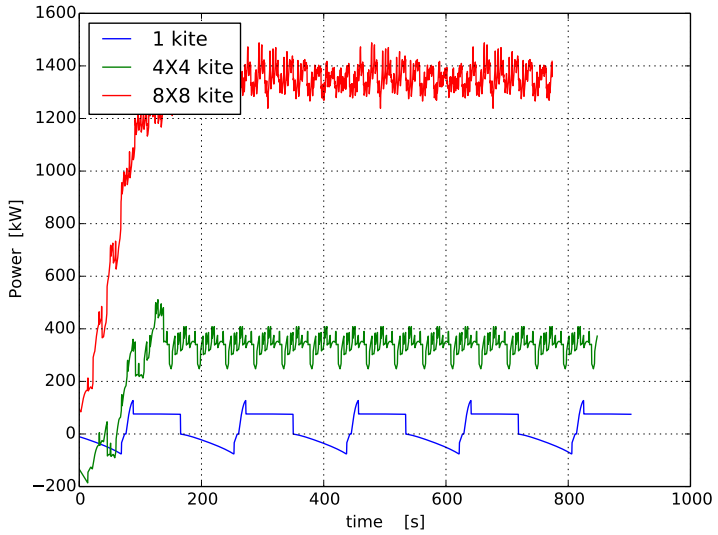

Figure D.5: Power production at 8 m/s of orthogonal wind for different number of kites in the array when there is a phase shift of 10% between the units in the same column

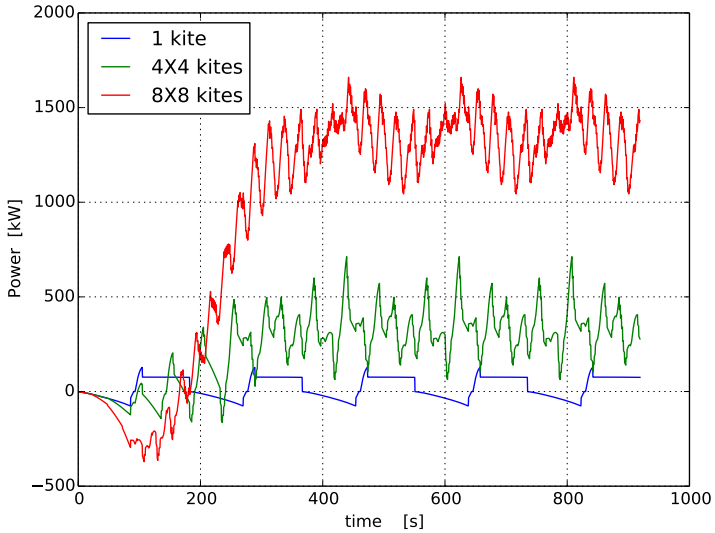

Figure D.6: Power production at 8 m/s of diagonal wind for different number of kites in the array when there is a phase shift of 1% between the units in the same column

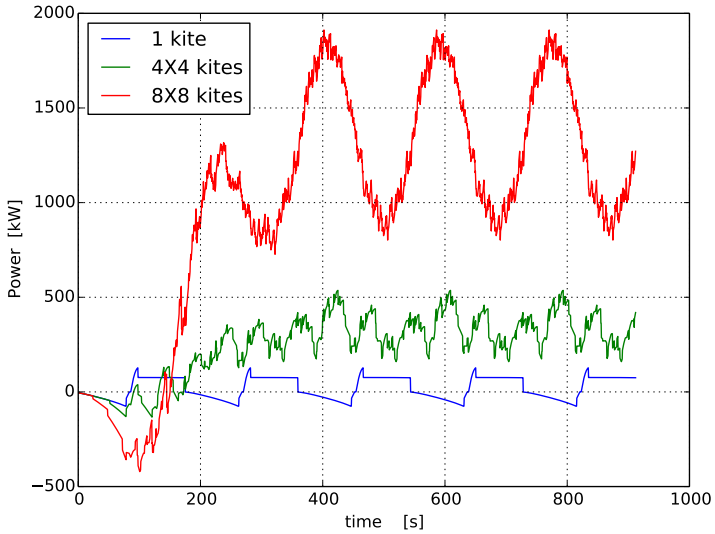

Figure D.7: Power production at 8 m/s of diagonal wind for different number of kites in the array when there is a phase shift of 5% between the units in the same column

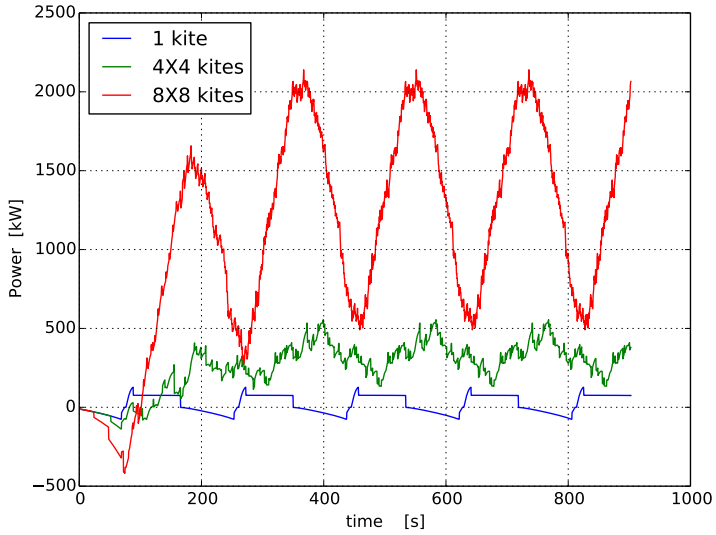

Figure D.8: Power production at 8 m/s of diagonal wind for different number of kites in the array when there is a phase shift of 10% between the units in the same column

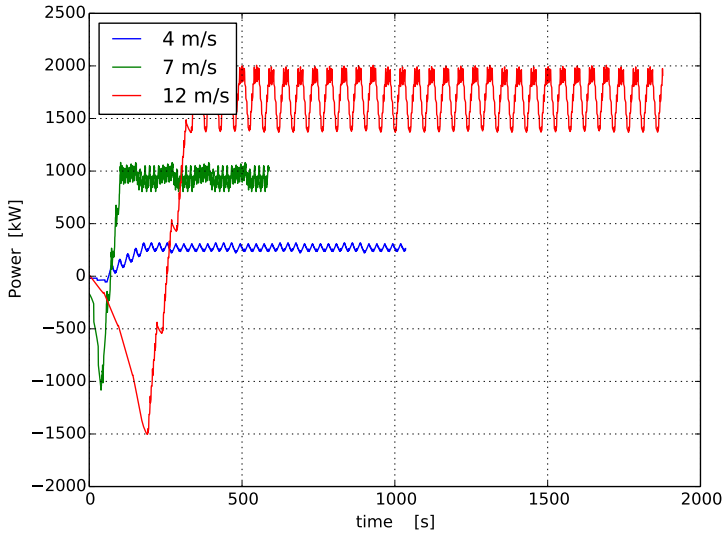

Figure D.9: Power production at different wind speeds of diagonal wind for an 8X8 units array when there is a phase shift of 1% between the units in the same column

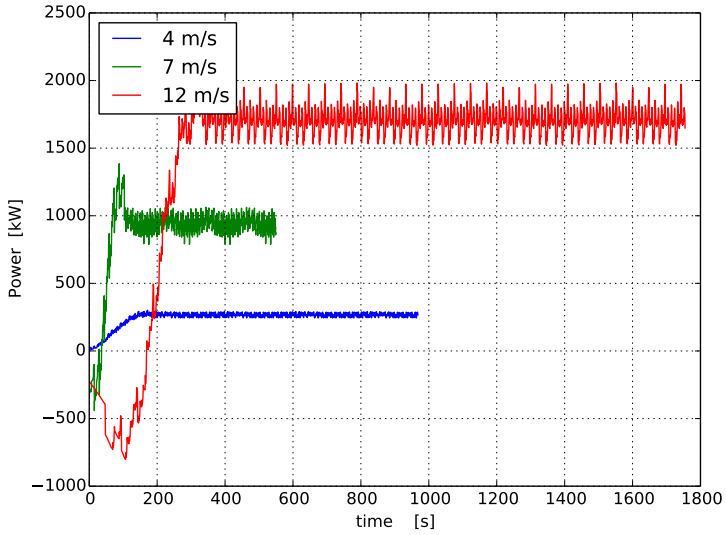

Figure D.10: Power production at different wind speeds of diagonal wind for an 8X8 units array when there is a phase shift of 5% between the units in the same column

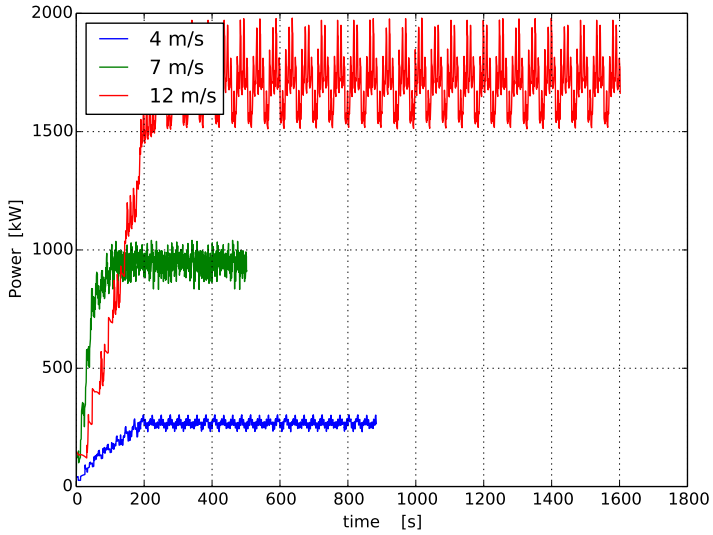

Figure D.11: Power production at different wind speeds of diagonal wind for an 8X8 units array when there is a phase shift of 10% between the units in the same column

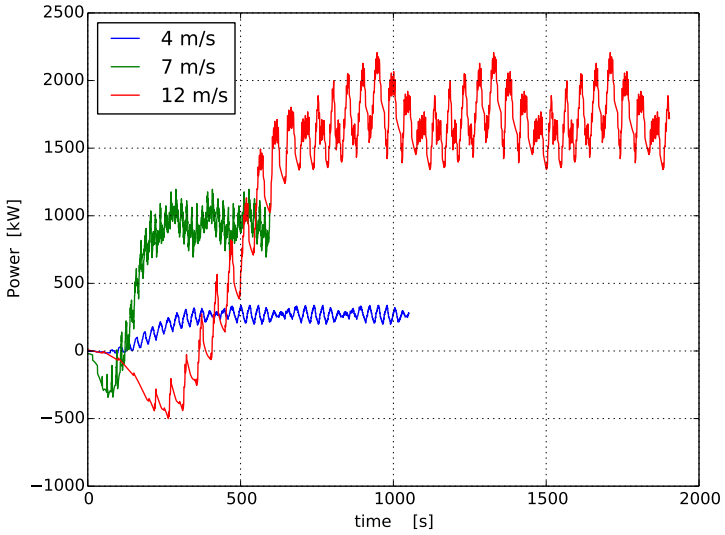

webmail delft

Figure D.12: Power production at different wind speeds of orthogonal wind for an 8X8 units array when there is a phase shift of 1% between the units in the same column

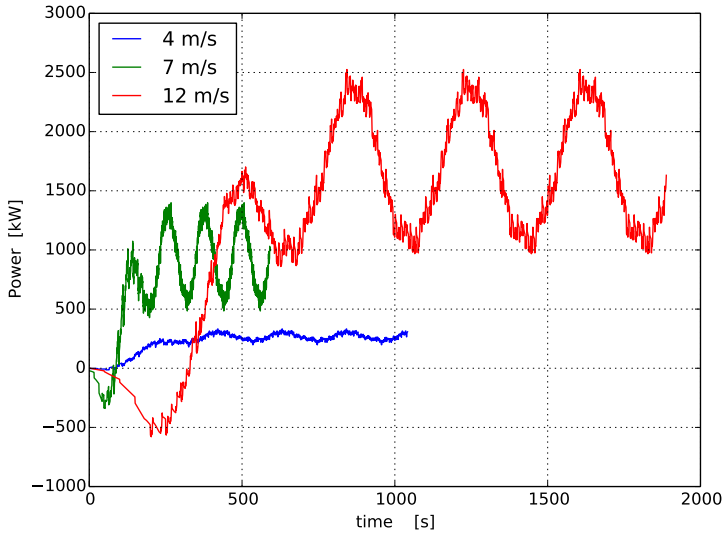

Figure D.13: Power production at different wind speeds of orthogonal wind for an 8X8 units array when there is a phase shift of 5% between the units in the same webmail delftcolumn

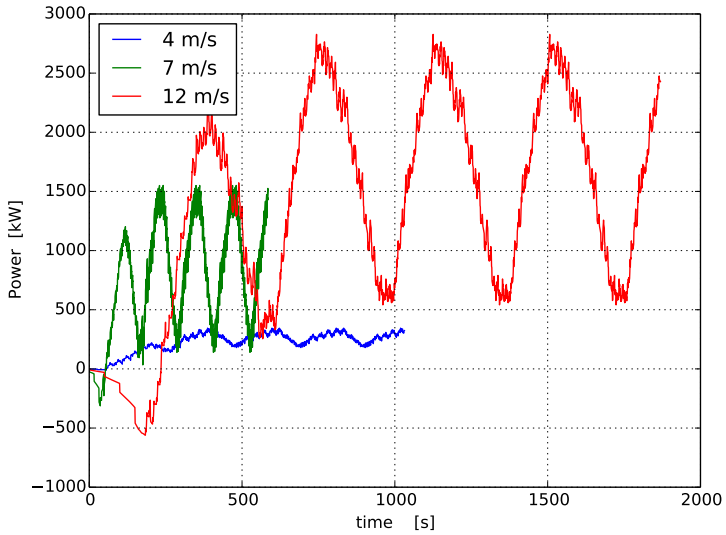

Figure D.14: Power production at different wind speeds of orthogonal wind for an 8X8 units array when there is a phase shift of 10% between the units in the same column

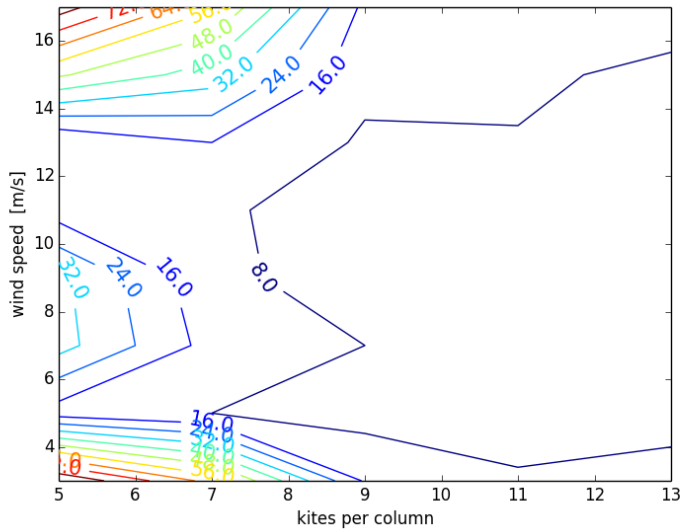

Figure D.15: Normalized percentage standard deviation of the power for different orthogonal wind speeds and number of units per row in the array with 1% of phase shift between the units in the same column

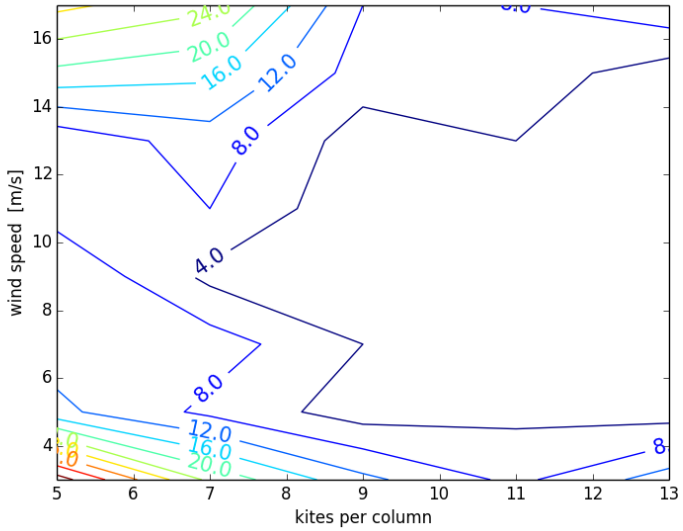

Figure D.16: Normalized percentage standard deviation of the power for different orthogonal wind speeds and number of units per row in the array with 5% of phase shift between the units in the same column

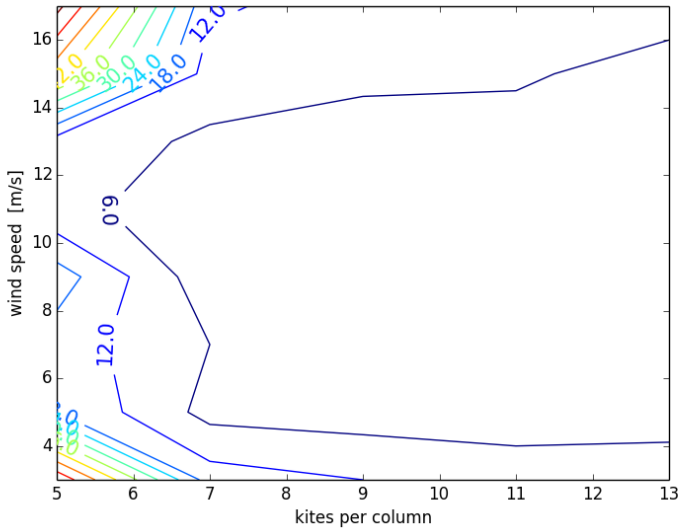

Figure D.17: Normalized percentage standard deviation of the power for different orthogonal wind speeds and number of units per row in the array with 10% of phase shift between the units in the same column

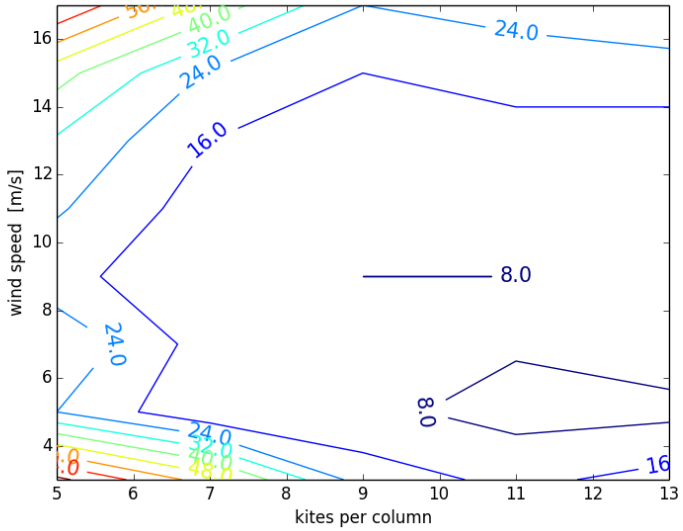

Figure D.18: Normalized percentage standard deviation of the power for different diagonal wind speeds and number of units per row in the array with 1% of phase shift between the units in the same column

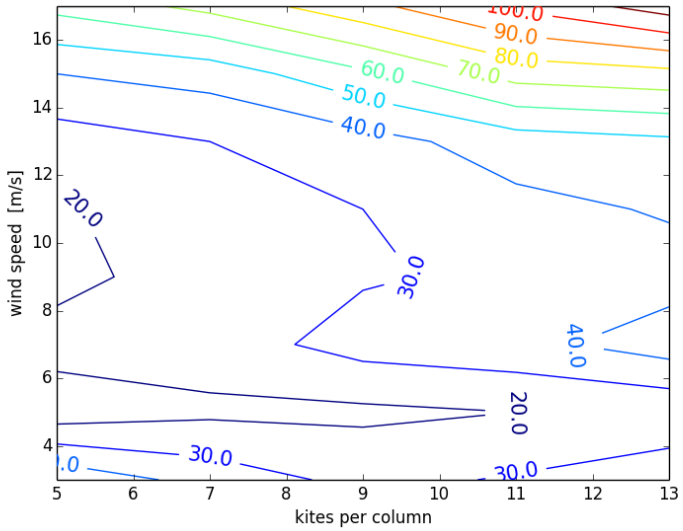

Figure D.19: Normalized percentage standard deviation of the power for different diagonal wind speeds and number of units per row in the array with 5% of phase shift between the units in the same column

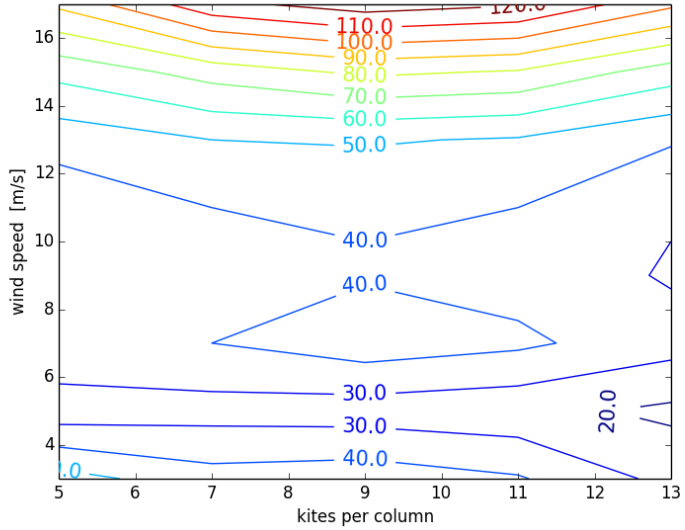

Figure D.20: Normalized percentage standard deviation of the power for different diagonal wind speeds and number of units per row in the array with 10% of phase shift between the units in the same column